THE UNIVERSITY OF CHICAGO

DUODENAL INFLUENCE ON ENDOCRINE PANCREATIC IMMUNITY: A DOMINANT ROLE FOR SHARED LYMPH NODE TONALITY

A DISSERTATION SUBMITTED TO

THE FACULTY OF THE DIVISION OF THE BIOLOGICAL SCIENCES

AND THE PRITZKER SCHOOL OF MEDICINE

IN CANDIDACY FOR THE DEGREE OF

DOCTOR OF PHILOSOPHY

COMMITTEE ON IMMUNOLOGY

BY

HAILEY MURPHY BROWN

CHICAGO, ILLINOIS

JUNE 2021

TABLE OF CONTENTS

LIST OF FIGURES

Novel tool generation for controlling and tracking antigen origin

ACKNOWLEDGEMENTS

My tenure in graduate school has been unimaginably different than what I expected when I first arrived on campus six years ago. There are many individuals I must acknowledge for helping me reach this point.

First, I'd like to thank my mentor, Daria, for taking me in as a fourth year and giving me the opportunity to pursue such interesting science. Your energy and work ethic are contagious, and I am so grateful to have had the opportunity to help you build the lab from the ground up. You taught me to be confident in my ideas and to be willing to take risks. Lastly, thank you for your enthusiastic support to help me further my career in science.

To my thesis committee of Sasha Chervonsky, Justin Kline, and Marisa Alegre, thank you for sticking with me and for all your expertise over the years, I have really enjoyed working with you. To Sasha, I will always remember your kindness when Seungmin left. Thank you for your support to help me find a new lab home. To Tatyana Golovkina, thank you for being a mentor and a friend, Luna and I will miss visiting on the weekends.

Thank you to the new members of the Esterhazy lab for all your help and for making lab a fun environment, even amid a worldwide pandemic. Thank you to the COI community for the insight and collaborations through journal clubs and WIPs over the years. The engagement within the COI community is truly what makes COI a special place. To my fellow classmates, thank you for the discussions, help, and most importantly for all the fun outside of the lab. Every finger I broke during flag football was worth it.

Thank you to all of my close friends, both in grad school and outside. The past six years have been unlike any other time in my life and I can't imagine getting through it all without your love and friendship. To my parents, Marlee and Peter, and my brothers, Colin and Aidan, thank

you for your endless support. Graduate school can often be a test of perseverance, and I know my drive to keep going was instilled by you.

Lastly, thank you to my partner Steven and our dog Luna. It is hard to describe the gratitude I feel for having you by my side during the trials and tribulations of grad school. Thank you for your love, support, and infectious curiosity. Thank you Luna for inadvertently learning how to become an emotional support dog.

ABSTRACT

While it is appreciated that the continual exposure of the intestinal immune system to dietary content, commensal bacteria, and infections can have wide ranging effects on systemic immunity, the mechanism by which distal organs are affected is unclear. Here, I examined the unique effect of common lymph node (LN) drainage between a peripheral organ and the gut on imparting the effects of intestinal modulation to other sites. One organ in particular, the pancreas, shares several immunosuppressive LNs with the upper small intestine, the duodenum. How these tolerogenic pancreatic-duodenal LNs may impact pancreatic disease, such as protection from type I diabetes or pancreatic cancer, respectively, is unknown. I focused on these common LNs in the context of type I diabetes (T1D), as studies in human have linked enteric infection with diabetes onset. Using sequencing-based methods, I systematically characterized migratory dendritic cell (DC) gene expression profiles in the pancreas, liver and duodenum and the shared lymph nodes. These results revealed that while migratory DCs express distinct tissue specific signatures when present in their respective tissue, once in the shared LNs, these DCs become much more homogenous, expressing only remnants of the tissue of origin signature. In parallel, experiments utilizing pancreas-specific T cells demonstrated that upon duodenal infection pancreas-specific $CD8^+$ T cells within these LNs became activated despite an uninfected pancreas, suggesting the fate of autoreactive T cells can be altered by intestinal modulation. Taken together, these results support the idea that the local LN milieu shapes the immune response to any antigen that enters the LN. These data may give mechanistic insight into links between enteric infection and T1D and provide a basis for targeting the pancreatic immune system via manipulation of the duodenal LN milieu. In addition, I generated a number of novel tools for further elucidation of the effects of shared LNs on pancreatic and duodenal immunity.

1. INTRODUCTION

1.1 Immunity of the digestive system

The digestive system is made up of the gastrointestinal tract and the surrounding accessory organs that contribute to its function including the pancreas, liver, and gallbladder. Much like any other organ, the role of immune cells in homeostasis and disease within each digestive organ has been extensively studied, though relatively more attention has been paid to the gastrointestinal (GI) tract. The large interface between the environment and host present within the GI tract necessitates an immune system capable of striking a balance between the promotion of tolerance to food and commensal bacteria while defending against pathogens. This vast interface positions the GI tract, and therefore intestinal immune system to be directly influenced by gut-derived factors such as microbiome and diet. More recently it has been appreciated that these same factors can have wide ranging systemic effects, many times as a result of migratory immune cell populations or systemic molecules such as hormones and metabolites.

Despite the functional and anatomic connections from the GI tract to accessory digestive organs, the potential for immunological crosstalk between these tissues has been largely overlooked. An underappreciated feature of the gastrointestinal system is that several gut draining lymph nodes (LNs) simultaneously collect afferent lymph from multiple digestive organs. Whether this common LN drainage between the gut and other organs, in particular the pancreas, is responsible for imparting the systemic effects of intestinal modulation remains unexplored and is the subject of this thesis.

1.2 Relationship of the pancreas and the gastrointestinal tract

The pancreas is an important digestive organ that sits within the abdominal cavity surrounded by the stomach, small intestine, liver and spleen. The pancreas develops as two separate buds from the duodenal region of the foregut, the embryonic equivalent of the gastrointestinal tract[1]. The dorsal bud gives rise to the neck, tail and body of the pancreas, while the ventral bud gives rise to the head. The head refers to the region of the pancreas connected to the duodenum, while the body and tail refer to the region extending towards the spleen. The dorsal and ventral buds fuse together, generating the definitive pancreas with the main pancreatic duct, also known as the duct of Wirsung, joining the common bile duct to reach the duodenum at the ampulla of Vater (Figure 1.2.1).

Post development, the duodenum and pancreas maintain an intimate connection throughout the life of the organism. In addition to the main pancreatic duct, the pancreas is also connected directly to the duodenum through the auxillary duct of Santorini[2]. Furthermore, shared vasculature as a result of hepatic circulation between the pancreas and the gut serves as a first pass sensing route for the pancreas to react to nutrients and postprandial gut hormones but may also induce pancreatic stress via molecules absorbed in the gut[3]. The majority of the pancreas (~95%) is dedicated to digestive function and composed of exocrine tissue. A much smaller proportion (~5%) is composed of endocrine tissue, responsible for the regulation of blood glucose levels. The exocrine pancreas is organized by acinar units, made up of clusters of polarized acinar cells which contain apically localized zymogen granules consisting of proenzymes or inactivated forms of multiple digestive enzymes such as trypsinogen. Each acinar unit surrounds the duct network made of duct cells that carry pancreatic juices to the main duct[4]. Upon food intake, cholecystokinin (CCK) release by enteroendocrine cells of the duodenum

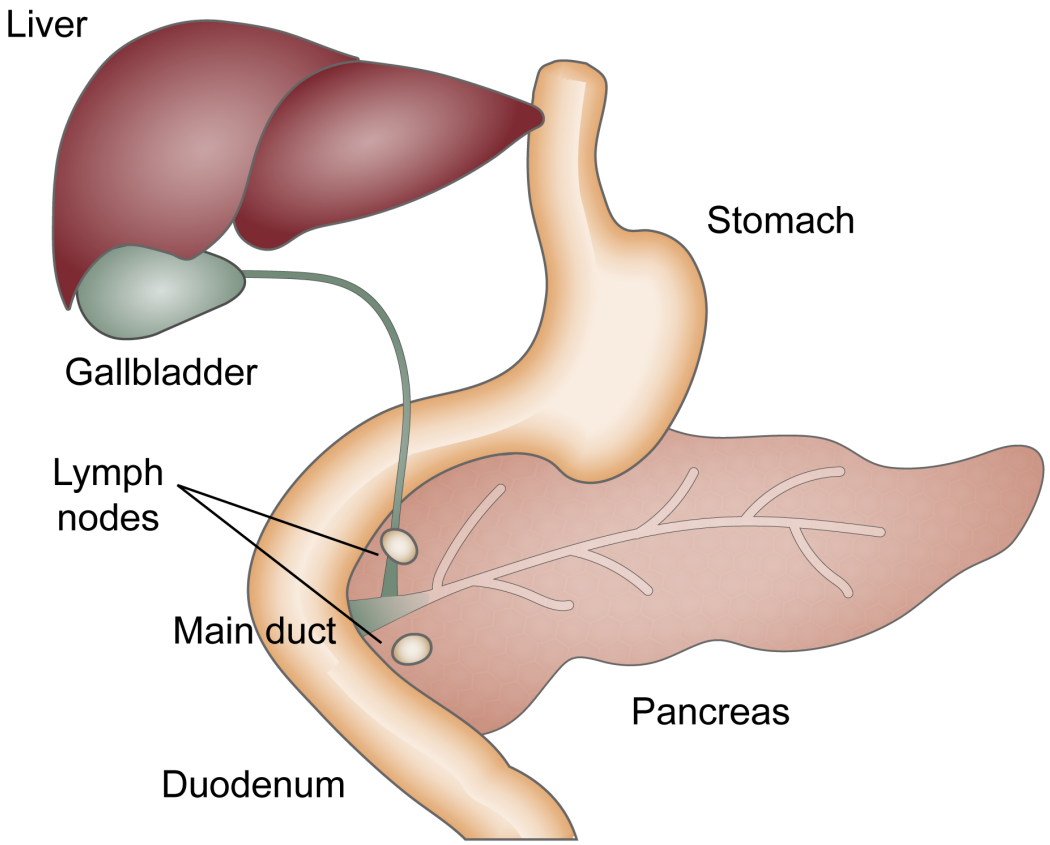

Figure 1.2.1 Connectivity of the pancreas, liver and duodenum.

Schematic demonstrating the connections between the pancreas, liver and duodenum. The head of the pancreas is connected to the duodenum while the tail extends toward the spleen. The duct system of the pancreas converge to release into the duodenum through the main duct at the Ampulla of Vater.

causes release of the zymogen granules within acinar cells, causing pancreatic juices to flow into the duodenum[5]. Local activation of the proenzymes in the duodenum facilitates the breakdown of proteins, carbohydrates and fat in the intestine.

The remaining pancreatic tissue is made up of neuroendocrine islets of Langerhans. These highly vascularized islets are composed of α-, β-, δ-, ε- and pancreatic polypeptide (PP) cells, which produce glucagon, insulin, somatostatin, ghrelin and pancreatic polypeptide respectively[6]. Interspersed throughout the organ, the islets are often spherical, with a β-cell core surrounded by α- and δ- cells. Blood glucose levels are tightly regulated through the coordination of the islet-derived hormones. Insulin is synthesized by β-cells as a precursor known as preproinsulin. Removal of the signal peptide during endoplasmic reticulum translocation to the secretory pathway results in the generation of proinsulin which is further cleaved within the secretory granules by endopeptidases, thereby releasing C-peptide and generating mature insulin[7]. Once secreted, insulin promotes the absorption of glucose, causing blood sugar levels to fall. In contrast, glucagon, produced by α-cells, causes blood glucose levels to rise either through the generation of glucose known as gluconeogenesis, or by breakdown of glycogen. Somatostatin and pancreatic polypeptide have suppressive effects on the release of insulin, glucagon as well as exocrine secretion[8].

Endocrine and exocrine organs are often the target of autoimmune attack, leading to T cell mediated tissue destruction[9]. In the case of the pancreas, dysfunction of pancreatic immunity can result in type 1 diabetes (T1D, discussed in more detail below). A comprehensive understanding of the factors that govern pancreatic immunity is therefore critical for the generation of new therapeutic strategies. While exocrine and endocrine pancreatic tissue appear to have unique modes of vascularization, with individual vascularization for each islet, the

lymphatic vessels of the pancreas are sparser and do not appear distinct for endocrine versus exocrine tissue[10]. Therefore, lymph from both the endocrine and exocrine pancreas can be assumed to drain to the same LNs. The LNs of the pancreas are unique in that they are shared between other digestive organs including some from the duodenum as well as the liver. This feature is even more exaggerated in humans, where the number of pancreatic and gut draining LNs is much greater. In addition, antigens and cells from the peritoneum preferentially localize to the pancreatic LNs[11]. As a result, the pancreatic-duodenal LNs receive both exocrine- and endocrine-derived antigen in addition to self and luminal antigen from the intestine. The impact of common pancreatic-duodenal LNs in linking intestinal perturbations to pancreatic immunity is the subject of this thesis.

1.3 Lymph nodes of the intestine

The pancreatic-duodenal LNs are part of a larger collection of LNs that drain the intestine and are referred to as gut draining LNs (gLNs). These highly organized structures are a critical inductive site of adaptive immune responses within the intestine. Lymph from the lymphatic vessels of the tissue enters the LN via afferent lymphatic vessels, flowing through the subcapsular and medullary sinuses and eventually leaving the LN via efferent vessels which return lymph to the thoracic duct. Specialized niches exist within the LN such as B cell follicles, separated from one another by interfollicular zones, and the T cell zone. The B cell follicles are the site of germinal center reactions and thus the generation of humoral immune responses, while the T cell zone is the primary site of T cell priming (Figure 1.3.1)[12]. These regions are supported by a network of specialized stromal cells, recently identified to be much more heterogeneous than previously thought[13]. One class of stromal cells, fibroblastic reticular cells, form the conduit system, thereby allowing entry of certain sized molecules to flow deeper within the LN from the

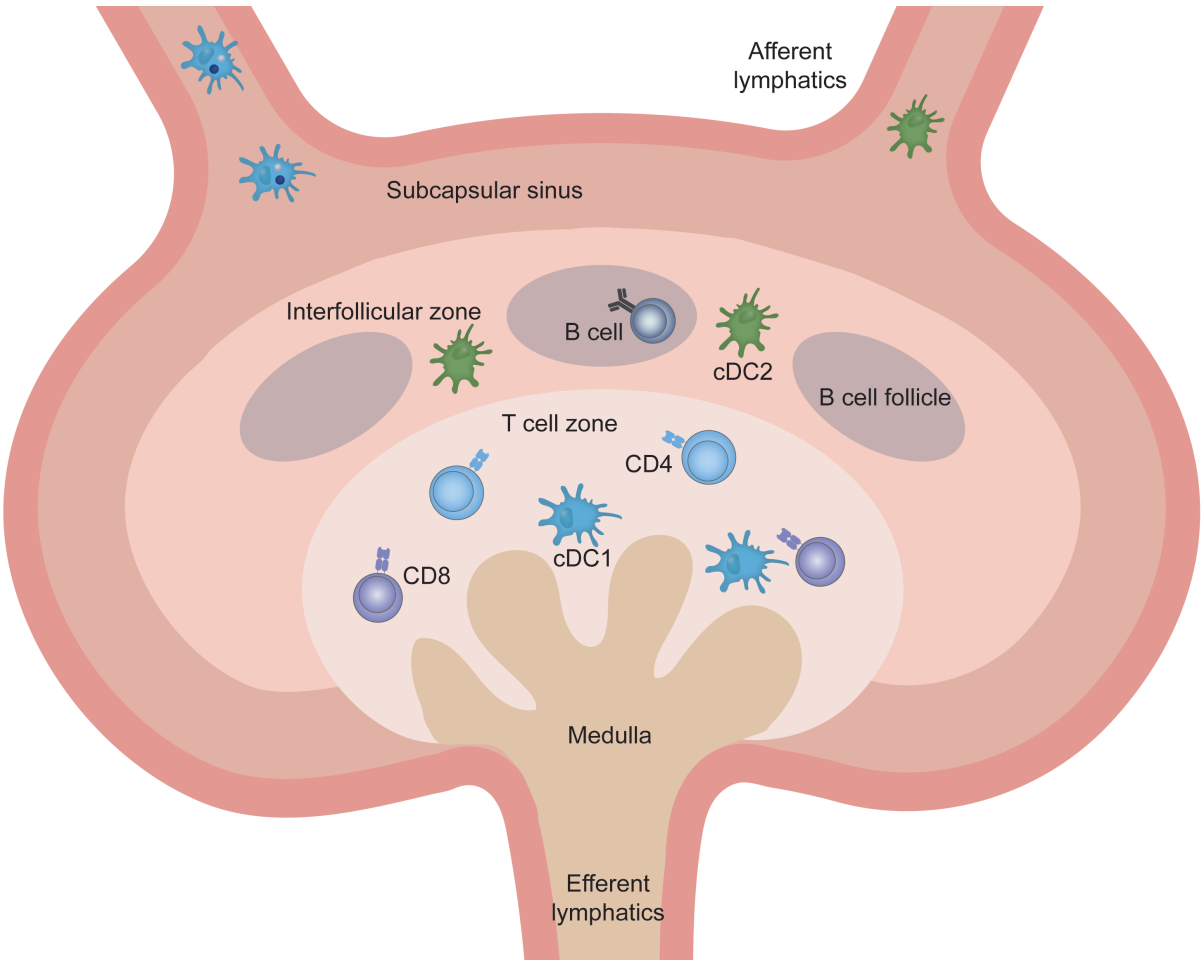

Figure 1.3.1 Lymph node structure and organization.

Adapted from Grant et al[12]. The lymph node includes various sub compartments including the subcapsular sinus, the interfollicular zone, the B cell zone, the T cell zone, the medulla. Lymph flows into the lymph node via afferent lymphatics and leaves via efferent lymphatics. Various cell populations are known to localize to distinct places in the lymph node. CD4 = $CD4^+$ T cell, CD8 = $CD8^+$ T cell, cDC1 = conventional dendritic cell 1, cDC2 = conventional dendritic cell 2.

subcapsular sinus. Moreover, stromal cells can also act as a series of roads to guide the intra-LN migration of cells between regions. The architecture of a LN and the proper distribution of cells among this structure is critical for efficient generation of immune responses. Many of these observations have been made in LNs other than the gLNs, but the principles are still common to all LNs.

Despite their uniform appearance in mice, it has long been appreciated that the gLNs receive lymph from distinct segments of the intestine[14]. The gLNs consist of two pancreatic-duodenal LNs (one being the celiac which in addition drains the liver, the other being the main duodenal LN), ascending and transverse colonic LNs, the main mesenteric LN chain which drains the distal duodenum, jejunum, ileum and cecum and colon, as well as the caudal and iliac LNs which drain the descending colon. Recent studies have expanded on these observations, finding that the gLNs also harbor unique immunological signatures dependent on location[15–17].

All the gLNs are biased toward the generation of tolerance, as evidenced by the lack of inflammatory reactions to ingested material and commensal microbes in the healthy state. However, within the gLNs a dichotomy still exists, where the LNs of the upper small intestine (duodenum) are the most tolerogenic while the LNs of the distal intestine (cecal/colonic) are more inflammatory in nature (discussed in more detail below). Accordingly, tolerance to oral antigens is established in the proximal small intestinal LNs[15,18], however, colonic tolerance is established in the iliac and caudal LNs[16]. It is precisely these tolerogenic LNs of the duodenum that are shared with the pancreas, raising questions about whether properties of a LN apply to all antigen, even from distinct sources. In sum, anatomic separation, coupled with distinct inflammatory thresholds of each LN, allows the intestinal immune system to produce two conflicting immune responses like tolerance and inflammation simultaneously.

The exact mechanisms responsible for generating the immunologic tone of each gLN is not fully understood. Regionalized differences in immune cell composition of the epithelium and lamina propria in combination with the functional demands of each intestinal segment may influence the corresponding LN. In addition, distinctive luminal contents along the length of the intestine may contribute to a unique lymph milieu entering each gLN[19]. For example, the duodenum and jejunum are adapted for efficient absorption of the high concentration of dietary derived nutrients. The regionalized input of pancreas- and gallbladder-derived enzymes and bile acids from the bile duct aid in macromolecule break down and lipid emulsification resulting in the highest lipid absorption by enterocytes in the duodenum and jejunum. Free fatty acids and glycerides are packaged into chylomicrons and released for uptake by lymphatic vessels, being too large for blood capillaries. Lymph from the duodenum and jejunum that drains to the corresponding LNs is enriched for triglycerides, lipid soluble vitamins, such as vitamin A, and dietary antigen compared to distal regions of the gut. As a result, absorption of vitamin A, a key molecule involved in tolerogenic responses (discussed more below), is highest within the LNs of the upper small intestine. In contrast, the colon has little role in the absorption of nutrients and instead houses the majority of commensal microbes within the gut. The colonic lymph is therefore enriched for bacterial derived products and this may impact the basal tone of the LN. Notably, the tolerogenic properties of the duodenal LNs are maintained in germ free mice, suggesting that microbial load alone does not explain differences between the LNs. The tolerogenic properties of the duodenal LNs may be similar impacted by the co-drainage with the pancreas.

Even the same cell type across different gLNs can have distinct gene expression profiles. Migratory dendritic cells and stromal cells of the LN have been shown to have location-dependent gene expression profiles[15,20,21]. Interestingly, the tolerogenic properties of mLNs are maintained

after transplantation to the popliteal fossa in a dendritic cell (DC) dependent manner, underscoring the importance of stromal cells communication with DCs[20]. Moreover, this stromal cell imprinting takes place during the neonatal period, setting the tolerogenic status of the mLNs early in life[21]. Thus, not only is the duodenal LN immunosuppressive at baseline, but the LN environment as a whole likely contributes to these properties actively, supporting the hypothesis that responses to pancreatic antigen present in the same LNs would be similarly tolerogenic.

1.4 Dendritic cells of the gLNs and their antigen uptake

Dendritic cells are one class of professional antigen presenting cells (APCs) that constitute a core component in the initiation of immune responses within the LN. DCs are typically classified into different subsets based on ontogeny; the main T cell priming subsets in the LN belong to conventional, or classical DCs (cDCs), derived from the common DC progenitor (CDP). These can be distinguished from other DC subsets such as monocyte derived DCs or plasmacytoid DCs, which have separate developmental pathways[22]. cDCs can be further subdivided into either type 1 (cDC1s) or type 2 (cDC2s) based not only on differences in development but also functional differences in the types of T cell responses each subtype primes (Figure 1.4.1). cDC1s, marked by XCR-1 and CD8a expression, depend on the transcription factors *Batf3* and *Irf8* and are primarily responsible for priming $CD8^+$ T cell responses via cross presentation of antigen. In contrast, cDC2s, marked by CD11b, depend on the transcription factor *Irf4*, and are known for $CD4^+$ priming[23]. Conventional DCs can be either resident within the LN or migratory which travel from the tissue to the LN based on CCR7 expression. Once in the LN, migratory DCs have an average lifespan of 3-4 days. cDC populations within the gLNs comprise four major groups: two resident MHC^{int} populations ($CD8a^+CD11b^{lo}$ and $CD8a^-CD11b^+$) and two migratory populations ($CD103^+CD11b^-$ and $CD103^+CD11b^+$)[24]. Generally, within the duodenal LNs, there is a higher

frequency of $CD103^+CD11b^-$ DCs compared to $CD103^+CD11b^+$ DCs, though this can vary with mouse facilities. Importantly, different DC subtypes localize to specific niches within the LN and this is essential for the proper induction of multiple immune responses. LN-resident and migratory cDC1s are found deep within the T cell zone while cDC2s are found near the B-T cell border[25].

The type of antigen, dose and route of entry to the LN are all major factors that can impact DC priming of T cells. In general, antigen can reach the LN by two major mechanisms: acellular movement in from the tissue via the lymph or carriage by migratory DCs from the tissue. Free flow of antigen to the LN requires high doses of antigen and additionally the size of antigen will dictate how deep within the LN the antigen can flow[26]. The conduit system acts as a molecular sieve, limiting particles over a specific size. Antigen that reaches the LN acellularly can then be acquired by many different subsets of DCs within the LN, likely the cDC2s which sit closer to the LN entry. Antigen can also be carried to the LN after uptake by migratory DCs. Depending on the relative ratio of migratory cDC1s vs cDC2s within the tissue type the proportion of DC subtypes with antigen may vary. Within the murine intestine, there are far more $CD103^+$ cDC2s compared to $CD103^+$ cDC1s however within the gLNs the ratio is often observed as flipped with increased frequencies of CD103+ cDC1s, though this is dependent on both location and microbial status. Within the pancreas the major migratory subset is $CD103^+$ cDC1s. Therefore, the $CD103^+$ cDC1s in the pancreatic duodenal LNs comprise a heterogeneous population of pancreas and duodenal derived DCs and may possess antigen from each tissue respectively. Thus, the LN positioning of DCs and origin of antigen are important factors that are highly consequential in the induction of immunity. The immunological consequences of different types of antigen or their tissue source is not comprehensively understood. Elucidating how shared LN drainage between tissues may affect

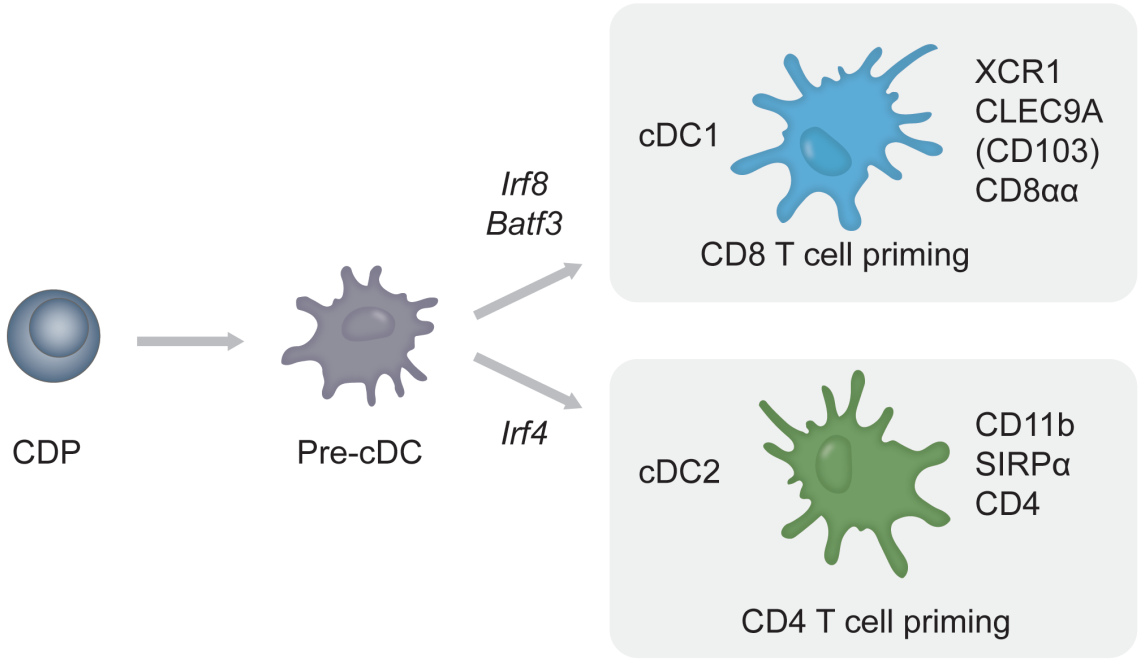

Figure 1.4.1 Dendritic cell ontogeny.

Adapted from Eisenbarth, 2019[22]. The common DC progenitor (CDP) gives rise to the pre-conventional DC (pre-cDC) which then gives rise to the two major subsets of conventional DCs (cDCs): cDC1 and cDC2. cDC1s are dependent on *Irf8* and *Batf3* and are most involved in $CD8^+$ T cell priming while cDC2s are dependent on *Irf4* and are most involved in $CD4^+$ T cell priming. Genes associated with each subtype are listed to the right of each DC type.

these factors will shed light on how a LN can appropriately handle antigen derived from distinct tissue sources during homeostasis and stress.

1.5 T cell tolerance and T cell activation

During the development of B and T cells an enormous diversity of B (BCR) and T cell receptors (TCR) are generated, allowing the immune system to recognize random antigens that may be associated with threats such as pathogens. However, the nearly infinite repertoire of antigen receptors also poses a serious threat to the organism as many receptors may have the capacity to recognize self-antigen. To account for this possibility, the immune system has a number of mechanisms in place to eliminate self-reactive T and B cells, classified as either central or peripheral tolerance. Central tolerance refers to the process of purging autoreactive T and B cells from the repertoire during development in the thymus and bone marrow, respectively[27]. During T cell development, self-reactive T cells can either be deleted by a process known as negative selection or can be diverted into other T cell fates including $Foxp3^+$ regulatory T cells among others[28]. Regulatory T cells generated in the thymus are referred to as natural Treg cells[29].

Central tolerance mechanisms rely on the expression of self antigens within the thymus to remove autoreactive cells, however, a number of antigens are expressed in a tissue specific manner and therefore would not be present in the thymus. Though this problem is somewhat remedied by the expression of the transcription factor Aire, which allows expression of tissue specific antigens within the medullary epithelial cells of the thymus, autoreactive T cells can still escape[30]. Peripheral tolerance, therefore is critical to prevent self antigen recognition. Peripheral tolerance occurs through three major mechanisms: peripheral deletion, induction of anergy, and induction of regulatory T cells[31]. For a productive immune response, DCs must present antigen

to T cells (signal 1) in the presence of additional costimulatory molecules (signal 2) and cytokines (signal 3)[32]. In the absence of inflammatory stimuli, DCs can still interact with autoreactive T cells, thus providing signal 1, however without signal 2 or 3 this results in clonal deletion of T cells or the induction of anergy[33]. Peripheral induction of regulatory T cells, known as pTreg cells occurs as a result of similar conditions except that T cell affinities are generally higher, and the additional presence of TGF-β is required[34]. pTreg differentiation is enriched in mucosal associated tissues, which are often abundant sources of TGF-β and retinoic acid, another pTreg promoting molecule (discussed in detail below).

When a naïve T cell interacts with an activated APC, fulfilling the requirements for signal 1 and signal 2, the T cell will become activated. Decades of research has determined the cytokines required to skew $CD4^+$ T helper cells towards a particular type of effector response. Initially, two major subsets of Th cells were identified based on their production of either IFNg or IL-4 and IL-5 and these were named Th1 and Th2, respectively. Th1 cells, defined by T-bet expression, are induced by IL-12 and are critical in mounting immune responses to intracellular pathogens like bacteria and viruses. Th2 cells contribute to anti-helminth immunity and are marked by expression of IL-4 and Gata-3. An additional subset effective against extracellular bacteria and fungal infections, Th17 cells, was discovered more recently. These cells are induced by IL-6 and TGF-β and express the transcription factor RORgt and cytokines such as IL-17 and IL-22.

During the initial response to inflammation or infection, naïve $CD8^+$ T cells differentiate into effector cells, marked by expression of cytotoxic molecules such as perforin and granzyme as well as cytokines such as IFNG and TNFa. Perforin and granzyme are released from the granules within the cytotoxic T lymphocytes (CTLs) upon formation of an immunological

synapse with an infected cell. Perforin generates pores into the target cell, facilitating the entry of granzyme inside the cell where it can activate caspase 3 and induce apoptosis[35]. Though the programs of activation are very similar for $CD4^+$ and $CD8^+$ T cells, $CD8^+$ T cells seem to require less time with antigen to induce priming and have higher proliferation rates[36]. As the LN is the major inductive site of T cell responses, how shared LNs between multiple tissue types affects T cell activation and T cell tolerance is unknown.

1.6 pTreg induction in the gLNs and oral tolerance

The phenomenon of oral tolerance refers to the process by which an initial oral administration of antigen results in the suppression of local and systemic immune responses to subsequent antigen encounter[37]. Errors in this process are thought to underlie food allergy and celiac disease, where recognition of food products by the immune system results in inflammation and pathology. The induction of oral tolerance is often measured by reductions in delayed type hypersensitivity responses, serum immunoglobulin levels, especially IgE, as well as cytokine levels when animals are challenged with the inducing antigen. There is evidence that orally delivered antigen can be found systemically and may contribute to the induction of oral tolerance[38]. However, it is clear that oral tolerance requires the gLNs, as genetic deficiencies rendering mice without LNs or lymphadenectomy results in loss of oral tolerance[18,39].

The process of oral tolerance is largely driven by $CD103^+$ migratory DCs that carry antigen from the intestine to the gLNs[39]. $CD103^+$ migratory DCs include both the $CD103^+CD11b^-$ and $CD103^+CD11b^+$ populations, belonging to either the cDC1 or cDC2 lineage, respectively[40]. *Ex vivo* studies demonstrated the cDC1 population, $CD103^+CD11b^-$ DCs, have the highest propensity to give rise to $Foxp3^+$ pTreg cells, though all other cDC subtypes within the LN are all capable[24]. Notably, in the absence of all cDCs monocyte derived DCs are unable to

mediate the same functions and a break in oral tolerance is observed. Additionally, mice deficient in *Ccr7* have impaired migration of DCs from the intestine to the draining LNs and are similarly unable to induce oral tolerance, underscoring the importance of migratory DCs in this process[39]. The ability to metabolize vitamin A into retinoic acid (RA) endows $CD103^+$ DCs with unique capabilities to induce the differentiation of pTreg cells as well as induce gut homing receptors for return of activated T cells to the intestine. RA reporter studies have demonstrated that RA levels are highest within the small intestine and that this imprints small intestinal migratory DCs to express higher levels of RALDH2, the enzyme responsible for converting vitamin A to RA, compared to colonic DCs[15,41]. Furthermore, as previously mentioned, retinol levels, a proxy of vitamin A absorption, are highest within the pancreatic-duodenal LNs. Thus, higher levels of RALDH2 generated by DCs within the proximal LNs synergizes with TGF-β to drive differentiation of pTreg cells[42]. RA acid mediates the increased TGF-β driven expression of Foxp3 to promote pTreg differentiation through direct and indirect mechanisms[43,44]. Additionally, RA signaling leads to the expression of α4β7 and CCR9 on $CD4^+$ T cells, $CD8^+$ T cells and B cells[45], allowing cells to traffic back to the small intestine, a feature critical for the successful generation of oral tolerance: local expansion of pTreg cells within the intestine is required for complete oral tolerance[46]. However, there is speculation that the cells also circulate systemically to dampen responses in distal sites from the gut, the basis for oral tolerance also working in systemic antigen re-challenge set-ups[37].

The $CD103^+$ driven differentiation of pTregs is essential for oral tolerance generation. Older studies performed before the discovery of Foxp3 have shown that depletion of $CD4^+CD25^+$ cells which are highly enriched for Treg cells impairs oral tolerance[47]. The same study found that transfer of pTreg cells specific to antigen into a new host is sufficient to prevent

responses to the same antigen. These data indicate that pTreg cells are necessary and sufficient for oral tolerance induction. In the context of pancreatic antigen, rather than oral antigen, the pTreg inducing propensities of the shared pancreatic-duodenal LNs may be critical in maintaining tolerance by enforcing an immunosuppressed state to pancreatic self-antigen.

1.7 Infection induced loss of oral tolerance

In order to maintain homeostasis, the mucosal immune system must respond specifically to pathogenic challenge while maintaining tolerance toward food and commensal microbiota. One way this is accomplished is through anatomical separation of LNs draining distinct regions of the intestine. For example, the induction of oral tolerance as measured by pTreg generation is unaffected in the proximal LNs during concurrent infection of the colon by the bacterium *Citrobacter rodentium*[15]. However, infections with tropism for the upper small intestine pose a serious threat to the ongoing generation of tolerance to oral antigens.

Previous work from our laboratory and others has shown that infection of the duodenum at the same time as oral antigen administration can result in impaired oral tolerance. A number of pathogens capable of interfering with oral tolerance have been identified and include: pan-intestinal pathogens such as type-1 lang (T1L, reovirus), murine norovirus (MNV, calicivirus), *Yersinia pseudotuberculosis* (*Y.p.*, gram-negative bacteria), or duodenal tropic pathogens such as *Strongyloides venezuelensis* (*S.v.*, helminth)[15,48–50]. In each case, infection with these bugs results in severe changes to the tolerogenic properties of the gLNs, leading to compromised pTreg generation. Pan-intestinal infection with T1L, a double stranded RNA virus, or MNV, a positive sense single stranded RNA virus, during simultaneous oral antigen exposure results in a reduction in pTreg generation and a concomitant increase in T-bet^{+} Th1 cells[48,49]. This was correlated with upregulation of IL-12p40 expression within CD103^{+}CD11b^{-} DCs. The helminth

S.v. enters the host subcutaneously in a larval stage but matures into its adult form in the duodenum, reaching peak levels around 7 days post infection. *S.v.* infection leads to significant swelling of LNs associated with structural changes, though unlike viral infection, the worms are confined to the gut and cannot infect the LNs. *S.v.* infection during oral antigen administration leads to significantly reduced frequencies of $CD103^+CD11b^-$ DCs in the duodenal LNs, likely due to an influx of $CD11b^+$ inflammatory monocytes, and this is associated with reduced pTreg induction and the emergence of Gata-3^+ Th2 cells[15]. Similarly, *Y.p.* infection-induced mesentery lymphadenopathy leads to a paucity of $CD103^+$ DCs in the gLNs, instead localizing to the mesentery, resulting in impaired oral tolerance[50]. In all cases major changes to the prominent pTreg-inducing $CD103^+$ DC populations accompany the infection, explaining the inability to induce oral tolerance. Whether this infection-induced disruption in tolerance reshapes the response to other antigen present in the LN, such as pancreatic antigen, is unknown.

1.8 Diseases of the pancreas: Type I Diabetes (T1D)

There are several diseases of the pancreas including pancreatic cancer, pancreatitis and Type 1 Diabetes (T1D), many of which have very limited treatment options. T1D is a chronic autoimmune disorder in which pancreatic β-cells are gradually destroyed by autoreactive T cells[51]. T1D affects over one million Americans, with the peak incidence of disease occurring during childhood. There are strong genetic associations for the development of T1D, the strongest of which maps to the human leukocyte antigen (HLA) or major histocompatibility (MHC) locus: Individuals with the haplotypes HLA-DQ2 and HLA-DQ8 have the highest risk of developing the disease[52]. Interestingly, these alleles are also risk factors for celiac disease, an autoimmune disease resulting in the destruction of the small intestinal epithelium by cytolytic $CD8^+$ T cells in response to dietary gluten[53]. The association of these particular HLA molecules

with disease is thought to be caused by changes to the peptide binding pocket of the MHC molecule. The DQ2 and DQ8 haplotypes possess an amino acid substitution at position β57 of the β chain, replacing a negatively charged residue with a neutral residue[54]. This in turn creates a positive region within the peptide binding groove, leading to an enrichment of acidic peptides found in diabetes associated MHC grooves. However, the peptide binding groove is also able to accommodate neutral peptides, and this results in the expansion of T cells with acidic residues within their CDR3, thereby burying the positive patch associated with the haplotype residue switch, but simultaneously enhancing TCR-MHC binding affinity[55]. Although the HLA loci accounts for the majority of risk alleles, a number of additional SNPs are associated with T1D including IL27, BAD, CD69, PRKCQ, CLEC16A, ERBB3[52].

While it is clear that a break in tolerance to β-cell proteins occurs prior to clinical presentation of symptoms, the specific events that initiate the break in tolerance are not well understood. The process of β-cell destruction in T1D is gradual, often taking years before β-cell mass is reduced enough to impact glycemic levels. Evidence of autoimmunity prior to diagnosis can still be observed by tracking levels of autoantibodies present in serum. Long term studies of genetically susceptible children demonstrated that children with multiple islet-specific autoantibodies had higher likelihood of being later diagnosed with diabetes than children with only one islet autoantibody[56]. The first autoantibodies detected in patients are often specific to insulin, glutamic-acid decarboxylase 65 (GAD65), and IA-2 antigen (IA-2A)[57]. During disease progression, β-cell killing leads to the unmasking of additional epitopes allowing for epitope spreading and thus the acquisition of additional autoantibodies and autoreactive T cells.

A large part of our knowledge about the immune mechanisms of T1D has come from non-obese diabetic mice (NOD) which spontaneously develop diabetes with a similar clinical

presentation to humans[58]. NOD mice harbor the I-A^{g7} MHC II allele, which features an amino acid change at position β57 of the β chain similar to human risk alleles. Disease progresses gradually in these mice, beginning with insulitis around 3-4 weeks old eventually leading to diabetes development in 90% of female mice by 24 weeks. Diabetes incidence and timing of disease development varies and is heavily dependent on colony hygiene status and sex[59]. Lymphadenectomy of the pancreatic LNs inhibits disease development, indicating LNs are essential for priming of autoreactive T cells[60]. Although the importance of the pancreatic LNs in the initiation of type 1 diabetes has already been established, the fact that these LNs simultaneously drain lymph from the gut has been largely unexplored[11].

Both $CD4^+$ and $CD8^+$ T cells are required for diabetes development. Nude NOD mice which lack a thymus, or β_2 microglobulin null mice which lack MHC class one and therefore have impaired $CD8^+$ T cell development do not develop insulitis or diabetes[61]. A number of T cell clones isolated from NOD mice are sufficient to transfer diabetes to NOD.*Rag*$^{-/-}$ mice or NOD.SCID, including both $CD4^+$ and $CD8^+$ clones. Whether $CD8^+$ or $CD4^+$ T cells can transfer disease without the other subset seems to depend on the clone.

Within the islets of Langerhans of mice there are two major APC populations: a macrophage population and a $CD103^+$ DC population[62]. In healthy mice, by absolute number, there are very few APCs in the islets, however in diabetic mice this dramatically increases. The $CD103^+$ DC population increases with age in NOD mice starting from four weeks, correlating with the initial infiltration of autoreactive $CD4^+$ T cells. Notably, crossing NOD mice to *Batf3*$^{-/-}$, and thus eliminating all $CD103^+$ cDC1s completely protects NOD mice from diabetes development[63]. cDC1s are thought to be the major DC population that primes $CD8^+$ T cells and therefore the absence of these cells abrogates CD8 priming, stunting the islet-destructive

response. From previous studies of oral tolerance we also know that the cDC1s are the most tolerogenic DCs within the pancreatic-duodenal LNs and preferentially induce Foxp3^{+} pTreg cells to dietary antigen. It is possible that differences in pTreg generation in NOD and NOD.*Batf3*$^{-/-}$ mice contribute to disease outcomes. There is conflicting evidence about the importance of pTreg cells in diabetes development in NOD mice. Despite a number of checkpoints, self reactive T cells still escape from the thymus and can be detrimental unless held in check by other mechanisms, one of which is pTreg generation. To assess the role of pTreg cells, groups have generated CNS1 deficient NOD mice which lack a specific *Foxp3* enhancer region that is essential for pTreg generation[64]. Two independently generated NOD.CNS1$^{-/-}$ mice were found to have different phenotypes, where one group found that CNS1$^{-/-}$ mice had no differences in insulitis, disease incidence, or time to disease while the other group found CNS1$^{-/-}$ mice had increased insulitis and disease incidence[65,66].

Two diabetogenic CD4^{+} BDC2.5 and CD8^{+} NY8.3 T cell clones are relevant to the work presented here. BDC2.5 cells are CD4^{+} T cells specific for the β-cell antigen chromogranin A (ChgA) and are capable of transferring diabetes when transferred into NOD.SCID mice[67–69]. BDC2.5 transgenic mice have a very reduced incidence of diabetes unless on a Rag-/- background[70]. In the absence of Rag, escapees from allelic exclusion that typically differentiate into immunosuppressive Treg cells are lost, enabling the BDC2.5 T cells to exert their diabetogenic effect. NY8.3 cells are CD8^{+} T cells specific for islet-specific glucose-6-phosphatase catalytic subunit related protein (IGRP) and similarly transfer diabetes when transferred into NOD.SCID mice[71,72]. However, unlike BDC2.5 mice, NY8.3 mice do develop an accelerated form of diabetes that is prevented by breeding to a Rag$^{-/-}$ background[73]. The inability of CD8^{+} T cells of NY8.3 to cause diabetes in the absence of Rag points to the requirement of

$CD4^+$ T cells in the progression of disease. Given the importance of cDC1s in the shared LNs in mediating $CD4^+$ and $CD8^+$ T cell outcomes, both of these T cell clones are useful tools for investigating consequences of duodenal infection on pancreatic immunity.

1.9 Microbial associations with T1D

Increasing evidence has linked T1D and intestinal perturbations such as microbiome changes or infection. As the rate of T1D continues to rise faster than predicted by genetic variation alone, more focus has shifted towards understanding the environmental factors that contribute to disease progression[74]. Studies in monozygotic twins have shown that disease concordance is around 40% indicating possible environmental influence[75]. Viral infections including mumps virus, rubella virus, cytomegalovirus, retroviruses, rotavirus, and most convincingly enteroviruses have been associated with human T1D[76]. In a few notable cases, coxsackie virus has been isolated from the pancreatic islets of a recently deceased T1D patient[77]. Not all diabetes-inducing pathogens have a tropism for β cells however. Infection of Diabetes-Resistant Biobreeder (BBDR) rats with Kilham rat virus (KRV), which does not infect β cells, leads to diabetes development in around 30% of rats as a result of increased serum inflammatory cytokines[78]. A variety of these infections have been tested in NOD mice in attempts to understand the mechanism behind the association. The majority of infections given to NOD early in life (less than 6 weeks old) actually lead to delay or complete inhibition of diabetes across a number of different pathogens including viruses, bacteria and helminths[79,80]. However, for some pathogens, infection of NOD mice later in life (8 weeks or older) leads to acceleration of diabetes progression[81,82]. Thus, a combination of pathogen and infection timing may be critical in determining whether infection precipitates diabetes. This may have to do with the dynamics of β-cell proliferation; β-cell proliferation rates peak several months after birth, and then continue to decline throughout life[83]. Thus, β-cells from

a young pancreas may be more capable of recovering from autoimmune attack. This is supported by the existence of a honeymoon period in almost half of children diagnosed with T1D characterized by improved glycemic control and reduced exogenous insulin requirements[84].

Links between the microbiota and T1D have been more well characterized in mouse models, in particular in NOD mice, than in humans. As previously mentioned, colony hygiene status heavily influences diabetes progression within NOD mice, with "dirtier" mice being more protected from disease incidence[59]. Work by Chervonsky and colleagues has demonstrated that crossing NOD mice to a *Myd88*$^{-/-}$ background prevents diabetes development in SPF conditions. However, NOD.*Myd88*$^{-/-}$ raised in GF conditions are not protected, suggesting that the microbiota is required for the protective effects of *Myd88* knockout[85]. T1D has been associated with increased intestinal permeability, or a "leaky gut," pointing to a connection of microbiome and T1D[86,87]. In support of this, treatment of BDC2.5 transgenic mice with the colitis inducing agent dextran sodium sulfate (DSS) leads to the activation of islet-specific T cells within the intestine and development of diabetes[88].

In humans, the effect of infection and microbiome is somewhat less clear. While research by the Environmental Determinants of Diabetes in the Young (TEDDY) study did not find any significant taxonomic changes associated with diabetic children, they did find by metagenomic functional analysis that the microbiota of healthy children was associated with increased short chain fatty acid synthesis as compared to children with T1D[89]. Through the fermentation of mucus and dietary fiber, the colonic microbiota generates a number of immunomodulatory SCFAs such as butyrate, propionate and acetate. SCFAs are mostly restricted to the colon where the microbial load is highest, though through their absorption via the portal vein they may have wide ranging effects throughout the body. Butyrate has a number of stimulatory properties, resulting in enhanced

generation and expansion of IL-10 producing pTreg cells [90]. NOD mice fed specialized diets that cause high levels of the SCFAs acetate and butyrate were protected from diabetes and this was associated with increased levels of regulatory T cells[91].

1.10 Unknown immunological consequences of shared pancreatic-duodenal LNs

Whether the propensity of the pancreatic-duodenal LNs to induce tolerance extends to all antigens i.e. pancreatic antigen, present in the LN is unknown. This question becomes especially important during infection or tissue stress in which only one of the connected organs is disrupted, for example during duodenal infections in which the properties of the duodenal LNs to oral antigen switch from tolerogenic to inflammatory. How the LN adjusts to meet the demands of one organ without jeopardizing the homeostasis of the other organ is unknown. Are responses to antigen from an unperturbed pancreas in the shared LNs changed as a result of intestinal perturbation? The central hypothesis of this thesis is that common LN drainage between the intestine and the pancreas results in immunological crosstalk between both sites in a reciprocal manner.

Previous studies examining the disruption of the immunosuppressive properties of the duodenal LNs have all been in response to oral antigens, in which the antigen and infection are derived from the same place: the duodenum. In these scenarios, it becomes difficult to separate the effect on the LN from the effect on cells in the local tissue that could migrate to the LN. During intestinal infection, one possibility is that the response to pancreatic antigen may be changed due to changes to the local milieu of the LN that alter the response to any antigen that enters the LN, whether it be from the gut or the pancreas. In this case, we would predict duodenal or intestinal infection would facilitate inflammatory responses to pancreatic antigen. Alternatively, the LN may function more passively as a collecting place for DCs that have been pre-conditioned in the tissue and ultimately dictate T cell response types. In this case, a LN with two sources of antigen may

keep responses to each source of antigen isolated. This latter scenario would make DC tissue of origin a critical factor in directing T cell responses. Accordingly, intestinal infection may only have an effect on pancreatic responses if pancreatic antigen is presented on gut-imprinted DCs. Moreover, the source, subcellular localization, and dose of antigen may also skew these outcomes.

The ability to investigate potential differences within dendritic cells based on tissue of origin was previously hindered by the inability to identify DCs trafficking from each site of interest. Prior to this thesis, there were not any unique markers to distinguish migratory DCs derived from the pancreas versus the gut versus the liver—another organ co-drained with the pancreas—once they are in the common LNs. Previous approaches used in other sites such as injection of labeled antigen or photoactivation of DCs are not feasible for these internal tissues without surgery. The work presented here addresses this gap in the field by utilizing several sequencing based approaches to identify tissue of origin markers to understand migratory DC dynamics within the shared LNs. Further, the generation of novel mouse models of antigen improve our ability to probe consequences of shared LNs in a temporal and tissue specific manner.

In summary, we are investigating the unique relationship between the pancreas and the intestine from a LN centric perspective. By appreciating the crosstalk between these organs, we may better understand how intestinal perturbations are linked with pancreatic disease outcomes. Finally, these experiments may provide a potential therapeutic approach for pancreatic diseases through manipulation of the intestine.

2. METHODS

2.1 Adoptive T cell transfer

Naïve T cells were isolated from pooled lymph nodes and spleens by negative selection using biotinylated antibodies against NK1.1, B220, CD11c, CD11b, TER119, CD8α or CD4, and CD45 and anti-biotin MACs beads (Miltenyi Biotec). Purity of transgenic cells was validated by flow cytometry ($CD45.1^+V\alpha2^+V\beta5^+CD25^-$ for OT-II cells, $Thy1.1^+V\beta8.1^+$ for NY8.3 cells, $Thy1.1^+V\beta4^+$ for BDC2.5 cells). Fluorophores used were PE-Cy7: CD45.1, PerCP-eFluor710: Vβ5, eFluor450: Vα2, PE-Cy7: Thy1.1, FITC: Vβ8.1, BV421: Vβ4. T cells were labeled with Cell Trace™ Violet or CFSE Cell Proliferation Kit (Life Technologies). In general, between 500k to $1x10^6$ cells were transferred by retro-orbital injection under isoflurane gas anesthesia.

2.2 T cell stimulation

Lymph nodes were dissected into RPMI containing 2% FBS and 1% penicillin/streptomycin. Lymph nodes were smushed between frosted glass slides and transferred to 96 well plates for centrifugation. Pellets were resuspended in the RPMI containing 10% FBS and 1% penicillin/streptomycin as above containing Ebioscience Cell Stimulation Cocktail ((Cat.no 00-4970-93) at 1:500 and incubated at 37°C for 4 hours. After incubation cells were spun down and washed once with fresh media before proceeding to cell staining.

2.3 Mice

C57BL/6J, NOD/ShiLtJ, RIPmOVA (B6.Tg(Ins2-TFRC/OVA)296Wehi/WehiJ), *Ptf1a*^{CreERT} (*Ptf1a*$^{tm2(cre/ESR1)Cvw}$/J), *Ins1*^{CreERT2} (B6.Cg-*Ins1*$^{tm2.1(cre/ERT2)Thor}$/J), Ins1^{Cre} (B6.Cg-*Ins1*$^{tm1.1(cre)Thor}$/J), *Villin*^{CreERT2} (B6.Cg-Tg(Vil1-cre/ERT2)23Syr/J), *Rosa26-LSL-Tdtomato* (B6.Cg-*Gt(ROSA)26Sor*$^{tm14(CAG-tdTomato)Hze}$/J), BDC2.5tg (NOD.Cg-Tg(TcraBDC2.5,TcrbBDC2.5)1Doi/DoiJ), NY8.3tg (NOD.Cg-Tg(TcraTcrbNY8.3)1Pesa/DvsJ),

NOD Thy1.1 (NOD.NON-*Thy1*^{a}/1LtJ), NOD *scid* gamma (NOD.Cg-*Prkdc*^{scid} *Il2rg*^{tm1Wjl}/SzJ) were purchased from the Jackson Laboratories. CD11c-YFP (B6.Cg-Tg(Itgax-Venus)1Mnz/J) mice were provided by M. Nussenzweig (The Rockefeller University). OT-II TCR-transgenic were provided by M. Nussenzweig (The Rockefeller University). Mice were used between 6-12 weeks of age. Mice were maintained at the University of Chicago animal facilities under specific pathogen-free conditions.

2.4 Infections

Purified T1L and T3SA+ were provided by the Dermody Lab (University of Pittsburgh). Both viruses were generated by a reverse genetic system, plaque purified and titered by plaque assay. Mice were infected with $2x10^{8}$ T1L, or T3SA+ diluted in PBS by oral gavage. MNV CW3 was provided by the Randall Lab (University of Chicago). CW3 was generated by a reverse genetic system by transfection of 293T cells and then further amplified in BV2 cells. After removing cell debris, supernatants were ultracentrifuged to concentrate MNV and the titer was assessed by $TCID_{50}$. Mice were infected with $5x10^{7}$ $TCID_{50}$ units of MNV CW3 diluted in plain RPMI by oral gavage. *Strongyloides venezuelensis* was maintained in NOD *scid* gamma (NSG) mice by subcutaneous injection with 10,000 larvae. For subsequent experiments, fecal pellets were collected from infected NSG mice and spread onto Whatman paper. Rolled Whatman paper was then placed into a beaker of water at 28°C for three days. The hatching larvae were collected and concentrated by gravity and counted. Mice were infected subcutaneously with 700 larvae/mouse. *Yersinia pseudotuberculosis* (*Y.p*) was provided by Igor Brodsky (University of Pennsylvania). *Y.p.* was streaked onto 2xYT plates containing 2ug/ml Irgasan and incubated overnight at 25°C with shaking at 250rpm. A single colony was then grown overnight in 3ml 2xYT buffer + 2ug/ml Irgasan. The morning of the infection, the dose was calculated by first checking the OD600 of a

1/10 dilution of the overnight culture. Based on a growth curve, the OD600 was converted to CFU and diluted in PBS for the desired dose. Mice were infected with 10^6 and 10^7 CFU by oral gavage and the inoculum was plated for confirmation of the dose.

2.5 Cloning

For all cloning steps, In Fusion (Takara) was used for assemblies and transformed into NEB competent cells. Resulting colonies were checked by restriction digest and then confirmed by sequencing. For the generation of OVA expression constructs, a pcDNA3 construct (provided by Hwang lab) containing a 3xFLAG tag was generated first. pcDNA3 was linearized with XhoI and assembled with a PCR fragment of 3X-FLAG tag from the pTAG expression construct (provided by Hwang lab), transformed and selected on LB ampicillin plates. The resulting vector was linearized with NotI and the respective OVA types were amplified by PCR from Addgene constructs #64600 and #64599 and a cytosolic OVA (COVA) lentiviral construct provided by the Hwang lab. Each DNA fragment was assembled with the pcDNA3-3XFLAG backbone and transformed. Colonies were midi prepped for use in transfections. For the generation of *Rosa26* targeting constructs, each OVA type was amplified including the FLAG tag from the respective OVA-3XFLAG expression constructs and inserted into the MluI/AsiI lineared pR26 vector. To generate BirA expression constructs, BirA-HA was amplified from the Addgene plasmid #36047 using flanking primers including a Kozak sequence (GCCACC) and an ATG and inserted into BamHI linearized pcDNA3. For the *Rosa26* targeting construct, BirA-HA was amplified by PCR from the Kozak containing vector and inserted into the MluI/AsiI lineared pR26 vector. PC3-BirA constructs were generated by nested PCR to amplify BirA-HA with flanking primers to add an N-terminal signal peptide from insulin and the transmembrane domain (TMD) of rat prohormone convertase (PC1/3). PC1SP-BirA-link-mPC1-667 and PC1SP-BirA-link-mPC1-711

were generated by first amplifying either 667-713 or 711-753 from the cDNA for mouse *Pcsk1* (Horizon Discovery) and inserting into pcDNA3 using XhoI. The resulting constructs were then linearized by NotI and BirA-HA including a linker was inserted into each construct.

2.6 Mouse knock-ins

Single colonies from pR26 targeting constructs were grown overnight for no more than 12 hours and then midi-prepped using anion-exchange columns (Invitrogen K210014). Midi-prepped DNA was ethanol precipitated and then resuspended in nuclease free water. On injection day, the injection mix was prepared two hours before injection. First, 5ul crRNA(ACTCCAGTCTTTCTAGAAGA, 1ug/ul, IDT) and 10ul tracrRNA(1ug/ul, IDT #1072533) were annealed in a thermocycler at 95°C ramping down to 25°C at 5°C/min. Next, 10ul of Cas9 (1ug/ul, IDT) was then complexed with 10ul of annealed crRNA:tracrRNA and 30ul of water for 15 min at 25°C. Midi-prepped DNA was then mixed with the complexed Cas9:crRNA:tracrRNA to a final concentration of 15ng/ul in a total volume of 100ul. The entire mixture was spun at 20,000 x g and the top 65ul was moved to a new tube for the Transgenic core. Fertilized eggs from C57BL/6 female mice were then microinjected and reimplanted into pseudopregnant CD-1 females. Tail biopsies were collected at 2 weeks old for genotyping and boiled in 25mM NaOH for 20 minutes and then neutralized with 40mM Tris-HCl. First, the presence of the knock-in construct was assessed using primers sitting within either OVA or BirA*. Mice positive for the presence of the knock-in were then checked for 3' targeting reactions using primers that span from within the construct to outside of the junction of the homology arm. Presence PCR was performed using Jumpstart Taq (Sigma #P0982) and targeting PCR was performed using Q5 (NEB #M0492S) or Phusion (Thermo Fisher #F530S) polymerase. Successful founders were isolated in quarantine for SFB removal and bred to C57BL/6 mice.

Water bottles containing 2mg/ml Truvia and 1mg/ml amplicillin were placed in the cage of pregnant mothers several days before giving birth and maintained until weaning. Presence of SFB was checked at 3 and 6 weeks by qPCR using SFB specific 16S primers.

2.7 APC isolation from lymph nodes

Lymph nodes were dissected into RPMI containing 2% FCS, 1% Hepes. Lymph nodes were finely chopped and digested with 2.5mg/ml Collagenase D (Millipore Sigma #11088882001) for 30 minutes at 37°C. Cells were used for downstream staining immediately. Alternatively, for intracellular cytokine production, pellets were resuspended in RPMI containing 10% FCS, 1% Hepes and Golgi Plug (Biolegend) at 1:500 and incubated at 37°C for 4 hours and then subjected to staining.

2.8 Cell isolation from small intestine

The small intestine was removed from the mesentery and Peyer's patches and feces were removed. The small intestine was roughly divided into four quarters and the proximal ¼ was taken as duodenum. Intestines were cut longitudinally and washed in three times in PBS containing 1uM DTT to remove mucus. The tissue was cut into 1cm pieces and incubated in PBS with 30 mM EDTA for 10 min at 37°C at 230 rpm with vigorous shaking after the incubation. Tissues were transferred to a new tube containing PBS and incubated for 10 min at 37°C at 230 rpm. Tissues were washed with PBS on a metal sieve, finely chopped and digested in RPMI containing 2%FCS, 1% Hepes, and 2mg/ml Collagenase 8 (Sigma # C2139), 200 µg/ml DNaseI (Millipore Sigma # 10104159001) for 30min at 37°C at 80 rpm. Digests were quenched in cold RPMI with 10% FCS. Pellets were resuspended in 40% Percoll and separated by centrifugation in a discontinuous Percoll gradient (80%/40%) at 2300rpm. APCs and lymphocytes were isolated from the interphase, washed, and stained for FACS analysis.

2.9 Cell isolation from pancreas and liver

The pancreas was perfused via the bile duct with 2.5ml HBSS containing 1mg/ml collagenase IV (Thermo Fisher #17104019) and 20ug/ml DNaseI (Millipore Sigma # 10104159001). Lymph nodes were removed and the pancreas was placed into a conical tube with remaining collagenase mixture. The liver was perfused via the portal vein with RPMI containing 2.5mg/ml collagenase D and 20ug/ml DNaseI. Several lobes of the liver were removed, chopped into small pieces and placed into a conical tube with remaining collagenase solution. Pancreas and liver samples were then incubated in a water bath at 37C for 25 min. The digestion was quenched with 20ml RPMI with 10% fetal calf serum (FCS) and tubes were shaken vigorously for one minute before passing each sample through a mesh filter. Liver samples were spun for 1 min at 75 x g, discarding the pellet to remove parenchymal cells. Samples were passed through a mesh filter and spun at 800 x g for 2min. Cells were washed with 20ml RPMI with 10% FCS and spun once more at 800 x g for 2 min. Pellets were resuspended in 5ml Histopaque 1077 and 10ml of plain RPMI was carefully laid over the top. Samples were then spun at room temperature at 900 x g for 18 min without brakes. The white layer of the gradient was transferred to a new tube and washed with 35ml RPMI with 10% FCS. Cells were spun at 800 x g for 2 min and then transferred to an Eppendorf tube for downstream staining.

2.10 Bulk RNAseq library preparation

Library was prepared as previously described[15]. Cells were sorted into TCL buffer (Qiagen) containing 1% beta-mercaptoethanol. RNA was isolated using RNAClean XP beads (Agentcourt) on a magnetic stand. Reverse transcription primers were: P1-RNA-TSO: Biot-rArArUrGrArUrArCrGrGrCrGrArCrCrArCrCrGrArUrNrNrNrNrNrNrGrGrG, P1-T31: Biot-AATGATACGGCGACCACCGATCG31T, P1-PCR: Biot-

GAATGATACGGCGACCACCGAT. RNA was eluted for 1 min in RT- cDNA synthesis mix 1 (0.5µl P1-T31 (20uM), 0.3µl RNasin plus (Promega), 1.5µl 10mM dNTP, 3.5µl 10mM Tris pH 7.5-0.5% IGEPAL CA-630 (Sigma) and 1.7µl RNase free ddH_2O) and pipetted up and down to mix. The eluted sample was then incubated for 3 min at 72°C, followed by 1 min on ice, then 7.5µl of mix 2 was added (3µl 5X RT Buffer, 0.375µl 100mM DTT, 0.375µl RNasin plus, 0.5µl P1-RNA-TSO (40uM), 0.75µl Maxima RT Minus H (Thermo Scientific), 1.8µl 5M Betaine (Sigma), 0.9µl 50mM MgCl2 and 0.175µl RNase free ddH_2O and mixed well. Samples were placed in a thermocycler and subjected to the following protocol: 42°C for 90s, (50°C for 2 min, 42°C for 2 min)x10 cycles, 70°C for 15 minutes. The cDNA was then amplified using 13.5ul cDNA, 20ul KAPA HiFi 2x Mix, 1.5ul P1-PCR, and 5ul H2O. Samples were subjected to the following protocol: 98°C for 3 min, (98°C for 15s, 67°C for 20s 72°C for 6min) x12 cycles, 72°C for 5 min. cDNA was cleaned up using RNA Clean XP beads and eluted in water. The concentration was calculated using a Qubit fluorometer and the average fragment length of 1500-1800 was determined by Bioanalyzer. Samples were normalized to 0.1ng/ul using ddH_2O, and 2.5µl cDNA were tagmented using Nextera XT Index Kit according to the manufacturer's protocol, except that all volumes were used at 0.5x of the indicated volumes. The concentration of the eluted samples was calculated by Qubit. Samples were pooled at 10nM and handed off to the UChicago Genomics Core for sequencing using paired end 50bp reads on a Novaseq S2 flowcell.

2.11 Single cell RNA sequencing library preparation

Between 30,000-100,000 YFP^+ cells were sorted from the liver, celiac and duodenal LNs of *CD11c*^{YFP} mice (n=3, 10 mice pooled per replicate). Cells were handed off to the UChicago Genomics Core for library preparation and sequencing. In brief, cells were loaded onto

Chromium NextGEM Chip (10x Genomics) for 3' end library preparation using dual indexes according to manufacturer's protocol (10x Genomics). The single cell RNAseq libraries were sequenced on a Novaseq SP100 flowcell.

2.12 Bulk RNA sequencing analysis

Raw fastq files were pseudo-aligned to the mouse reference transcriptome M26 (GRCm39) using Kallisto[92]. The resulting gene counts were input to R and transcripts per million (tpm) was scaled by gene length. Initial filtering removed genes with expression under 3 counts per million (cpm). The un-normalized filtered gene counts were then used as input for the R package DESeq2 using the default parameters (Wald test) to compare genes differentially expressed across locations, correcting for replicate and isolation day batch effects[93]. The apeglm method was used for log fold change shrinkage to better visualize effect sizes[94]. Genes with log2 fold changes greater than 2 or less than -2 and a false discovery rate (FDR) of 0.05 were considered significant for downstream studies. To generate tissue specific gene sets the significant genes for both pairwise comparisons (ex: Duodenum vs liver, duodenum vs pancreas) were overlapped in a Venn diagram using the R package Venn Diagram. The overlapping genes were extracted and used to generate heatmaps using the R package pheatmap. Volcano plots were generated using the R package Enhanced Volcano. Principle component analysis (PCA) plots were generated using transcript per million (tpm) values using the R package PCAtools.

2.13 Single cell RNA sequencing analysis

Gene counts were calculated by aligning raw fastq files to the mm10 genome using CellRanger (10xGenomics). The counts were used as input to the R package Seurat[95]. Cells were initially filtered to remove doublets and poor-quality cells based on the unique molecular identifiers (UMIs), number of features, and percentage of mitochondrial genes (<0.25). To normalize gene

counts, Seurat's LogNormalize function was used with default parameters (scale factor = 10,000). Variable genes were then identified using the Seurat function FindVariableFeatures with default parameters. At this point, samples were integrated into one object using the function FindIntegrationAnchors for all further downstream analysis. The data was scaled using ScaleData and then subjected to dimensionality reduction by PCA using RunPCA. The cells were clustered using Seurat's FindNeighbors followed by FindClusters prior to visualization by RunUMAP. Clusters were identified using FindAllMarkers and the resulting gene lists defining each cluster were used as input into ImmGen database to identify the highest correlating cell type. For identification of APC clusters, gene expression data from the published dataset[24] was used to correlate defining gene lists with known identities of resident and migratory cDC1 and cDC2 populations. Additionally, dot plots of canonical cell type surface markers were used to call cluster identities. The steps from FindVariableFeatures through FindAllMarkers was repeated each time data was subsetted. Signature scores from the bulk RNAseq were added to the scRNA dataset using the Seurat function AddModuleScore and projected onto the UMAP using FeaturePlot. The duodenal tissue signature consisted of (*Aldh1a2*, *Il1b*, *Slc38a1*, *Ptp4a1*, *Ifitm6*, *Cybb*, *Stt3b*, *Dusp1*, *Hic1*), the pancreatic (*Anxa2*, *Fcer1g*, *Axl*, *Ccl6*, and *Klrb1b*), the liver (*Id3*, *Ly6a*, *Cd34*, *Sema4c*, *Apoa1*, and *Fabp1*) and the shared liver pancreatic signature (S*ema4a*, *Il15ra*, *Cd63*, *Fcgr2b*, *Il12b*, *Alox5ap*, and *Emp3*).

2.14 Western blot

For cell culture samples, cells were lysed directly in 2x Laemmli Buffer (0.1M Tris [pH 6.8], 4% SDS, 4mM EDTA, 286mM 2-mercaptoethanol, 3.2M glycerol, 0.05% bromophenol blue) and proteins were resolved by SDS-PAGE. Proteins were transferred onto PVDF membranes using a semi-dry transfer. Membranes were blocked in 5% milk/0.1%Tween/TBS (TBST) and probed

overnight at 4°C in 5% milk/TBST with primary antibody. Generally, primary antibodies were used at 1:1000. The next day membranes were washed 3x for 10 min and then incubated with secondary antibody in 5% milk/TBST with HRP-linked secondary antibodies at 1:5000 for two hours at room temperature. Membranes were washed 3x before incubating for 3 min with ECL solution to develop bands. Membranes were exposed on BioRad Chemidoc MP. For streptavidin blots, membranes were blocked in 2.5% BSA in PBS with 0.4% TritonX-100 and then incubated with HRP-conjugated streptavidin at 1:40,000 in the same buffer.

2.15 Cell culture

All cell lines were cultured at 37°C in 5% CO_2 in their respective media. 293T media: Dulbeco's Modified Eagle Medium containing 10% fetal bovine serum, 1x MEM nonessential amino acids, 100U/ml penicillin streptomycin and 10mM Hepes. Ins1 media: RPMI containing 10% FCS, 1% Hepes, 100U/ml penicillin/streptomycin, 2mM glutamine, 1mM sodium pyruvate and 55uM 2-Mercaptoethanol. 293T cells were provided by the Hwang Lab. Ins1 cells were provided by the Oakes Lab. For Ins1 transfection experiments, cells were transfected with 2-5ug of plasmid using Lipofectamine 3000 or Lipofectamine LTX (Invitrogen). For 293Ts, calcium phosphate transfection was used with 2ug of DNA.

2.16 qPCR

One thousand migratory cDC1s were sorted into TCL buffer (Qiagen) containing 1% 2-Mercaptoethanol. cDNA was prepared as described above for the RNAseq library preparation except without tagmentation and with minor changes: cDNA was amplified for 25 cycles at the amplification step, and samples were eluted in 60ul after bead cleanup. Samples were normalized to 1ng/ul and 1ul was used as input for qPCR. Master mixes were prepared using Power Sybr Green (Invitrogen) containing 7.5ul Sybr, 0.15ul 10uM forward and reverse primer mix, and

water up to 14ul. Samples were multichanneled into 384 well plates in duplicate and run on an Applied Biosystems QuantStudio 6 Flex machine. Delta Ct was calculated by subtracting the average of duplicate values for each gene from the average duplicate values for the housekeeping gene 36B4 for each sample. Relative expression values were then calculated by the equation: $2^{-\Delta CT}$. Data are presented as $2^{-\Delta CT}$x10,000.

2.17 Immunofluorescence Microscopy

For immunofluorescence analysis, Ins1 cells were seeded on coverslips in 24-well plates and transfected with constructs as indicated. Cells were fixed, permeabilized and stained as previously described[96]. The images were acquired using the EVOS FL Cell Imaging System. Images from each channel were merged using ImageJ/Fiji.

2.18 Antibodies and flow cytometry

Fluorescent-dye-conjugated antibodies were purchased from Fisher (anti CD25 (501129526); anti CD11c (501129650); anti Foxp3 (50-112-9663); anti-Gata3 (46-9966-41); anti Vβ5.1 (46-5796-82); anti-CD45.1 (501129620); anti-I-A/I-E (MHCII) (50-169-18); anti-CD69 (50-158-11); anti-IL12p40 (25-7123-80),), Biolegend (anti CD11b (101218); anti-CD8□ (100744); anti-TCRβ 109220; anti-B220 (103255); anti-NK1.1 (108724); anti CD90 (202507); anti T-bet (644832); anti-Vβ8.1/2 (118406); anti-CD4 (100510); anti-V□2 (50-246-014); anti-Sca-1 (108113); anti- Granzyme B (372204); anti-IFNγ (505839); anti-CD44 (103024); anti-F4/80 (123121)), or BD (anti CD103 (566297); anti CD45 (564225); Vβ4 (743024)). Additional antibodies were purchased from Cell Signaling (anti HA (3724S)), Santa Cruz Biotechnologies (anti-actin horseradish peroxidase (sc-47778 HRP)), Abcam (anti-insulin (ab7842)), Fisher (Donkey anti-Mouse IgG horseradish peroxidase (A16011)), and Sigma (anti FLAG (F7425)). Biotinylated antibodies were purchased from BD Pharmigen (anti-B220, 553086; anti-CD8□,

553029; anti-CD11b, 553309; anti-CD11c, 553800; anti-CD25, 553070; and anti-NK1.1, 553163; anti-TER-119, 553672). Horseradish peroxidase conjugated Streptavidin, Donkey anti-rabbit IgG horseradish peroxidase was purchased from Jackson ImmunoResearch Laboratories, Inc. Aqua LIVE/DEAD® Fixable Aqua Dead Cell Stain Kit, L-34965, Cell Trace CFSE and Violet Cell Proliferation kits (C34554 and C34557) were purchased from Life Technologies. For intracellular staining, cells were first stained for surface epitopes and then fixed, permeabilized and stained according to the manufacturer's protocol (eBioscience 00-5123-43 or BD 554714). Flow cytometry was performed on an LSRII (BD Biosciences) and analyzed using FlowJo Software (Tree Star). Cell division index was calculated using the FlowJo formula (http://www.flowjo.com/v765/en/proliferation.html), whereby the index represents the fraction of total cell divisions over the calculated total starting cells.

2.19 Statistical analysis

All data were analyzed with Prism software (GraphPad). Data is presented as average ± SEM. Multivariate data was analyzed by applying one-way ANOVA and Tukey's multiple comparison *post hoc* test, comparison between two treatment conditions by one-tailed unpaired Student's t-test. Survival curve was analyzed by Mantel-Cox, Gehan-Breslow-Wilcoxon and Logrank. All differences not specifically indicated to be significant were not significant (n.s., $p > 0.05$). *$p < 0.05$, **$p < 0.01$, *** $p < 0.001$, ****$p < 0.0001$.

3. RESULTS

3.1 Characterization of effects of tissue of origin on migratory DCs in shared lymph nodes

Recent studies from our lab and others have distinguished the gLNs with higher resolution, prompting us to re-establish which gLNs also drain the pancreas (Figure 3.1.1A). Due to the soft consistency of the pancreas, it is technically very difficult to inject dye and follow its trajectory through the lymphatics. Instead, to functionally assess which LNs receive pancreatic antigen and are capable of initiating $CD4^+$ T cell responses I employed two different systems of transgenic T cells specific for pancreatic β cell antigen (Figure 3.1.1A). The first model, RIPmOVA mice, express membrane bound ovalbumin (OVA) under the control of the rat *Ins2* promoter and accordingly express OVA in the pancreatic β cells. These mice are on the B6 background offering flexibility in genetic approaches; however, they have the major caveat that OVA is also expressed in the kidney tubule and at low levels in the thymus. Upon transfer of CFSE-labeled OT-II cells, $CD4^+$ T cells specific for OVA, into RIPmOVA hosts, proliferation was measured by CFSE dilution in the liver LN, gLNs, and inguinal LN as a control. T cell proliferation was only observed in the liver, celiac and duodenal LNs (Figure 3.1.1B, C). To test if this pattern was the same for a natural β cell antigen we used BDC2.5 transgenic $CD4^+$ T cells on the NOD background. Transfer of CFSE labeled BDC2.5 cells into NOD mice resulted in the same pattern of proliferation in LNs: proliferation of BDC2.5 cells was observed in the liver, celiac and duodenal LNs (Figure 3.1.1B, C). Further, proliferation was enhanced with β cell death by streptozotocin (STZ), suggesting increased antigen availability in the LNs upon cell death (Figure 3.1.1B, C). Since both of these models utilize only β cell antigen, I concluded that these three LNs drain the endocrine pancreas.

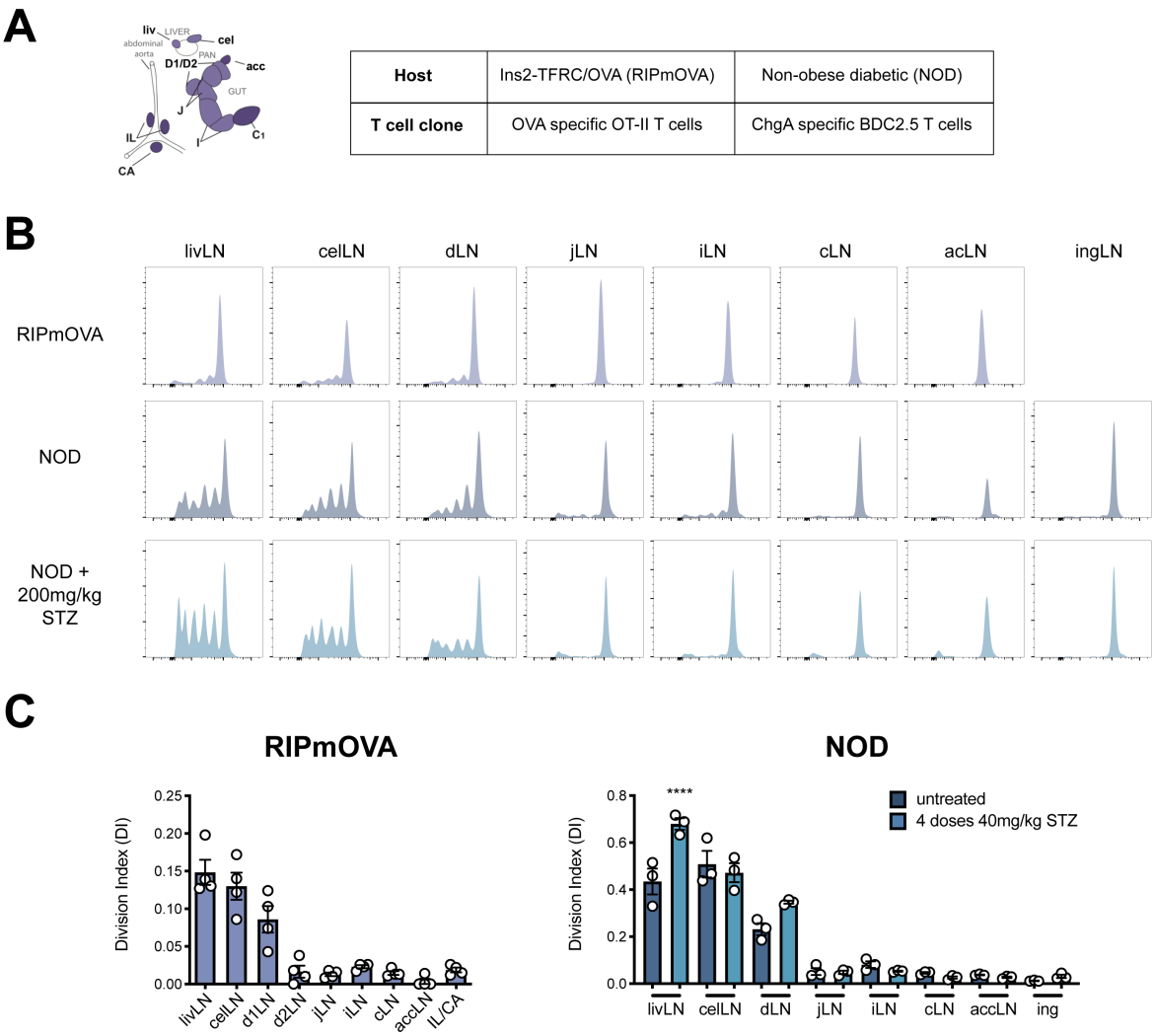

Host	Ins2-TFRC/OVA (RIPmOVA)	Non-obese diabetic (NOD)
T cell clone	OVA specific OT-II T cells	ChgA specific BDC2.5 T cells

Figure 3.1.1 Mapping the shared pancreatic-duodenal lymph nodes in mice.

a) Left: Schematic of gut draining lymph nodes in the mouse. Right: Table of transgenic T cell reactivities and the respective T cell adoptive transfer hosts. **b)** Representative flow cytometry plots for CFSE dilution in indicated lymph nodes 4 or 6 days post adoptive transfer of $1x10^6$ CFSE labeled BDC2.5 or OT-II T cells into of NOD or RIPmOVA hosts, respectively. NOD mice were treated with 200mg/kg streptozotocin four hours prior to T cell transfer. **c)** Division index of $CD45.1^+$ cells in indicated lymph nodes as in **b**, (RIPmOVA n=4, NOD n=3 per group). ****$p < 0.0001$ (Student's t test). LivLN = liver lymph node (LN), celLN = celiac LN, dLN = duodenal LN, jLN = jejunal LN, iLN = ileal LN, cLN = cecal-colonic LN, acLN = ascending colonic LN, ingLN = inguinal LN.

Efforts to confirm the LNs that drain the exocrine pancreas are discussed in more detail below in section 3.3.

All three LNs that drain the pancreas are shared with other nearby organs: the celiac and duodenal LNs are the major LNs of the duodenum and are highly tolerogenic, while the liver LN is shared by the liver but does not drain the intestine. As a note, the celiac LN also drains the liver, giving this LN three different input sources. The patterns of co-drainage between the pancreas, duodenum and liver raise interesting questions about how common LNs handle antigen derived from very distinct origins, and how this may affect tissue specific immunity. Appropriate handling of these antigens is highly dependent on the signals received by DCs which ultimately instruct T cell priming and differentiation. However, whether the signals received by DCs are predominantly imparted by their tissue of origin or the LN environment to which they drain was unknown. Thus, to better understand the contribution of DC tissue of origin on the dynamics of shared LNs, I focused on characterizing migratory DCs within the tissue and shared LNs.

The major migratory DC population common to all tissues is the $CD103^{+}CD11b^{-}$ subset (Fig 3.1.2A), suggesting that within shared LNs the $CD103^{+}CD11b^{-}$ subset comprises a heterogeneous mix of cells derived from each tissue (Fig 3.1.2B). From previous RNAseq experiments it is known that migratory DCs in distinct gLNs can have different gene expression profiles, likely reflective of which segment of the intestine they drained from[15]. Furthermore, many phenotypic features of migratory DCs such as RALDH production or IL-12p40 expression are heterogeneous in LNs. Therefore, it was possible that multiple tissue sources contributed to the heterogeneity seen. Prior to this thesis, however, there were no unique markers to distinguish migratory DCs derived from the pancreas versus the gut versus the liver once they are in the common LNs. Therefore, in order to understand potential tissue of origin effects on DCs I first

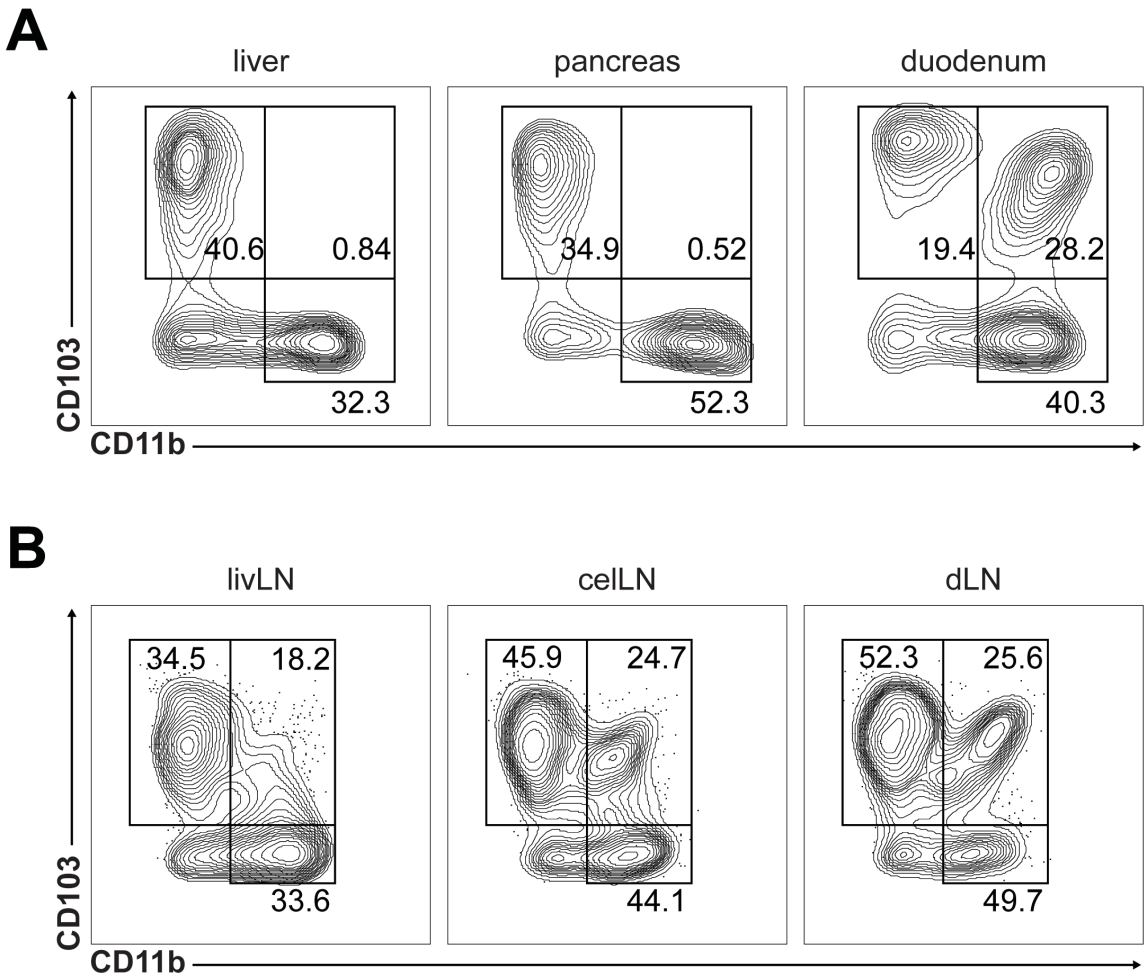

Figure 3.1.2 Dendritic cell frequencies in the duodenum, pancreas and liver and the corresponding lymph nodes.

a) Representative flow cytometry of CD103 and CD11b expression among dendritic cells within the indicated tissues. Cells are pre-gated on live, Dump^{-}(NK1.1, TCRβ, B220, CD90), CD11c^{int}, MHC^{+}, F4/80^{-}. **b)** Representative flow cytometry of CD103 and CD11b expression among dendritic cells within the indicated lymph nodes. Cells are pre-gated on live, Dump^{-}(TCRβ, B220), CD11c^{int}, MHC^{hi}, F4/80^{-}. LivLN = liver LN, celLN = celiac LN, dLN = duodenal LN.

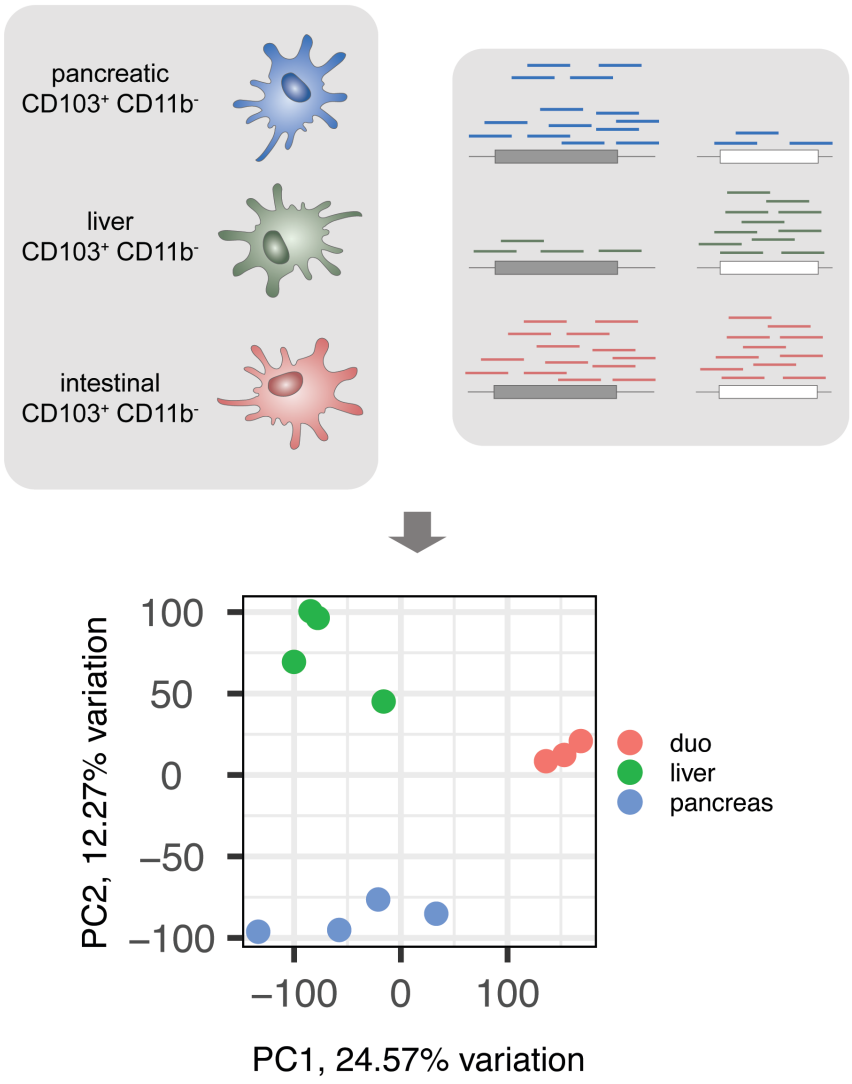

Figure 3.1.3 RNA sequencing of tissue-derived migratory dendritic cells.

$CD103^{+}CD11b^{-}$ migratory DCs were sorted from the pancreas, liver and duodenum and subjected to bulk RNA sequencing. Cells are pre-gated on live, $Dump^{-}$(NK1.1, TCRβ, B220, CD90), $CD11c^{int}$, MHC^{+}, $F4/80^{-}$. Principle component analysis (PCA) of sorted migratory DCs (n=4, pooled from 4 mice each). Duo = duodenum.

needed to establish a DC imprint signature for each tissue. One thousand $CD103^{+}CD11b^{-}$ DCs were sorted from the pancreas, duodenum and liver and subjected to bulk RNA sequencing to identify expression profiles unique to each tissue. As shown in Fig 3.1.3, the DCs clustered strongly based on tissue of origin and each tissue separated well by principal component analysis (PCA). Differential gene expression revealed a number of genes specifically enriched in DCs from each tissue relative to the other tissues (Fig 3.1.4A). Overlapping each set of pairwise comparisons from differential gene expression in a Venn diagram generated a list of genes unique to each tissue (Fig 3.1.4B). From these analyses, 16 liver specific, 11 pancreas specific, and 42 duodenal specific migratory DC genes were identified. Heatmaps of the tissue specific genes highlighted the range in expression level of these genes while confirming enrichment within the respective tissue derived DC (Fig 3.1.4C). A number of these genes are highlighted in Figure 3.1.5. Some identified genes have a known function within DCs such as *Aldh1a2*, the gene encoding the RA producing enzyme RALDH, while other tissue specific genes have more obscure roles within DCs, such as *Ly6a*. Notably, the liver and pancreas derived DCs displayed much less distinct gene expression profiles, in terms of number of differentially expressed genes. However, compared to the duodenal derived DCs, a large number of genes were upregulated in both liver and pancreas derived DCs including *Il12b*, *Ccl5*, *Sema4a*, *Tnfrsf4*, *Emp3*, and *Il15ra* (Figure 3.1.6A, B).

In parallel, to establish subsets of migratory DCs within the LN, I sorted YFP^{+} cells from the liver, celiac, and duodenal LNs of *CD11c*^{YFP} mice for single-cell RNAseq (scRNAseq) using the 10x Genomics platform (Fig 3.1.7A). Cells that passed QC-filters were subjected to dimensionality reduction by uniform manifold approximation and projection (UMAP), yielding 38 unique clusters (Fig 3.1.7B). Identifying markers were computed for each cluster and the top 10 genes per clusters were input into the Immgen database for cell type calling. The resulting

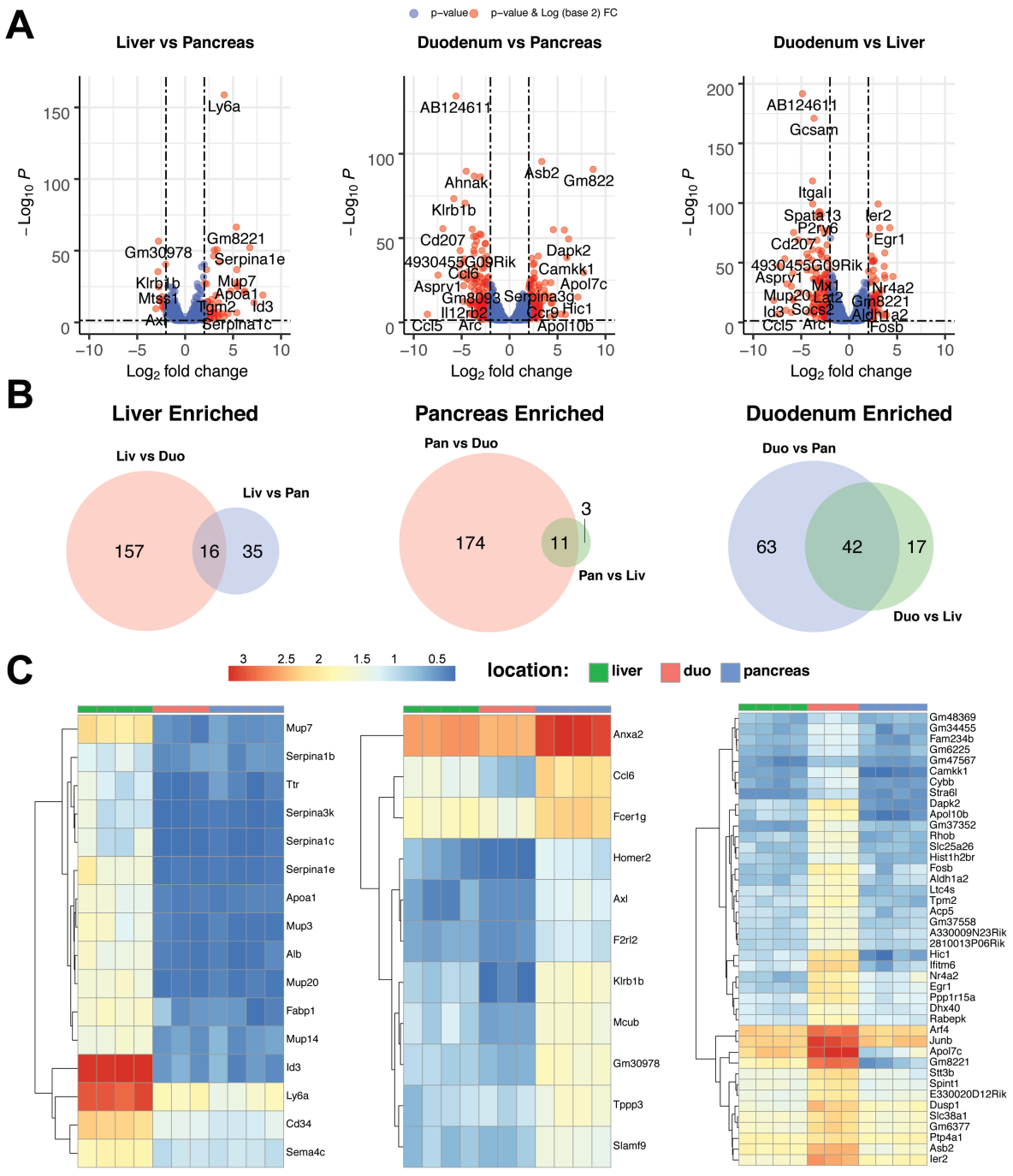

Figure 3.1.4 Migratory DCs display tissue specific gene expression profiles.

a) Volcano plot of differentially expressed genes between migratory DCs from liver vs pancreas (left), duodenum vs pancreas (middle), and duodenum vs liver (right). **b)** Venn diagrams displaying the number of tissue-enriched genes, based on overlap from the indicated comparisons. Genes with log fold changes greater than 2 and adjusted p values less than 0.05 were used for comparison. **c)** Heatmaps of gene expression for each tissue-enriched gene across each tissue type. Duo = duodenum, pan = pancreas, liv = liver.

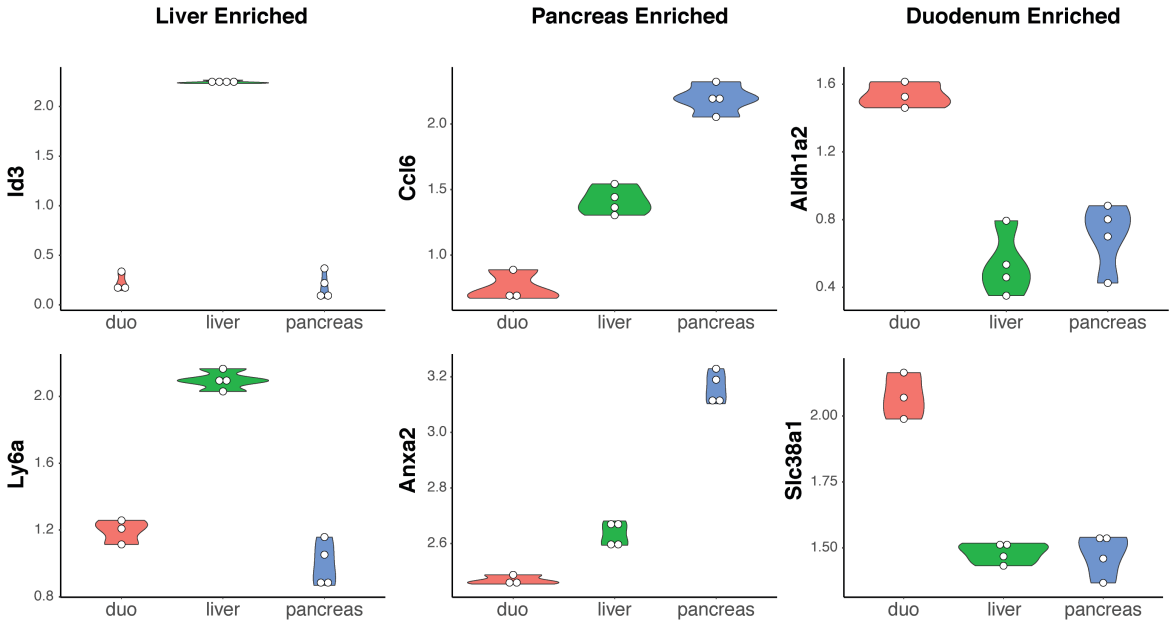

Figure 3.1.5 Representative tissue specific genes within migratory DCs.

Violin plots displaying log(transcript per million values) for representative genes that show a tissue specific expression pattern from differentially expressed genes between migratory DCs from liver, pancreas and duodenum. Duo = duodenum.

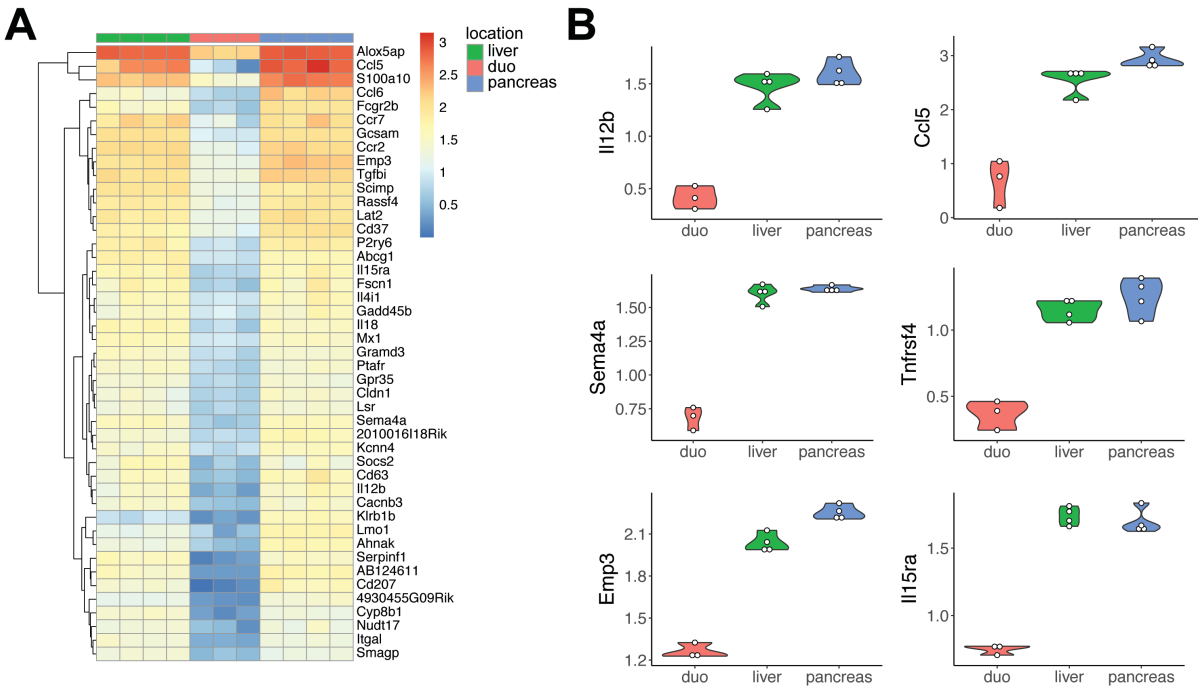

Figure 3.1.6 Liver and pancreas migratory DCs share a number of differentially expressed genes compared to duodenal migratory DCs.

a) Heatmap of gene expression of liver and pancreas DC-enriched genes compared to duodenal DCs. Heatmap only includes the top 45 highest expressed genes upregulated in pancreas and liver. **b)** Violin plots displaying log(transcript per million values) for representative genes upregulated in pancreas and liver, but not duodenum. Duo = duodenum.

clusters were relabeled by their cell type yielding three major populations of T cells, B cells, APCs, as well as minor clusters of plasmacytoid DCs, NK cells/ILCs, developing lymphocytes, macrophages and stromal cells (Fig 3.1.7C). The cell type clusters correspondingly expressed key cell type specific genes such as *Cd3d*/*Cd3g* for T cells, *Ncr1* for NK cells, *Siglech* for pDCs, and so on (Fig 3.1.7D).

To focus on migratory DCs, I first subsetted the dataset to include only APCs, removing the major contaminating B and T cells. Reclustering of the cells yielded 16 unique clusters (Fig 3.1.8A). Interestingly, cluster 9, 12 , parts of 13, 4, and 8 displayed location specific signatures in that they were present only in celiac and duodenal LNs, the two draining LNs of the duodenum, but not the liver LN (Fig 3.1.9B). To identify specific APC subsets, I took advantage of a previously published sequencing dataset from the four major subsets of DCs within the gLNs: mig cDC1s ($CD103^+$, $CD11b^-$), mig cDC2s ($CD103^+$, $CD11b^+$), res cDC1s ($CD8\alpha^+$) and res cDC2s ($CD11b^+$)[24]. The top 20 genes for each APC cluster were used to generate heatmaps displaying the log of transcripts per million (tpm) for each DC type using the published dataset (Fig 3.1.8C). Using the respective heatmaps, cell types were assigned to each cluster based on which DC subtype correlated most closely with the defining genes for each cluster. For some migratory cDC populations, identification of cDC1 vs cDC2s was very difficult since many classic surface markers are not expressed strongly enough to differentiate the cell type. Relabeling of the UMAP revealed five major clusters of migratory cDC1s, migratory cDC1/2s, resident cDC2s, resident cDC1s, and macrophages along with two small contaminating clusters of B and T cells (Fig 3.1.8D). The expression of several DC subset specific genes described previously[97] correlated strongly with the cell types (Fig 3.1.8E), indicating accurate cluster identification.

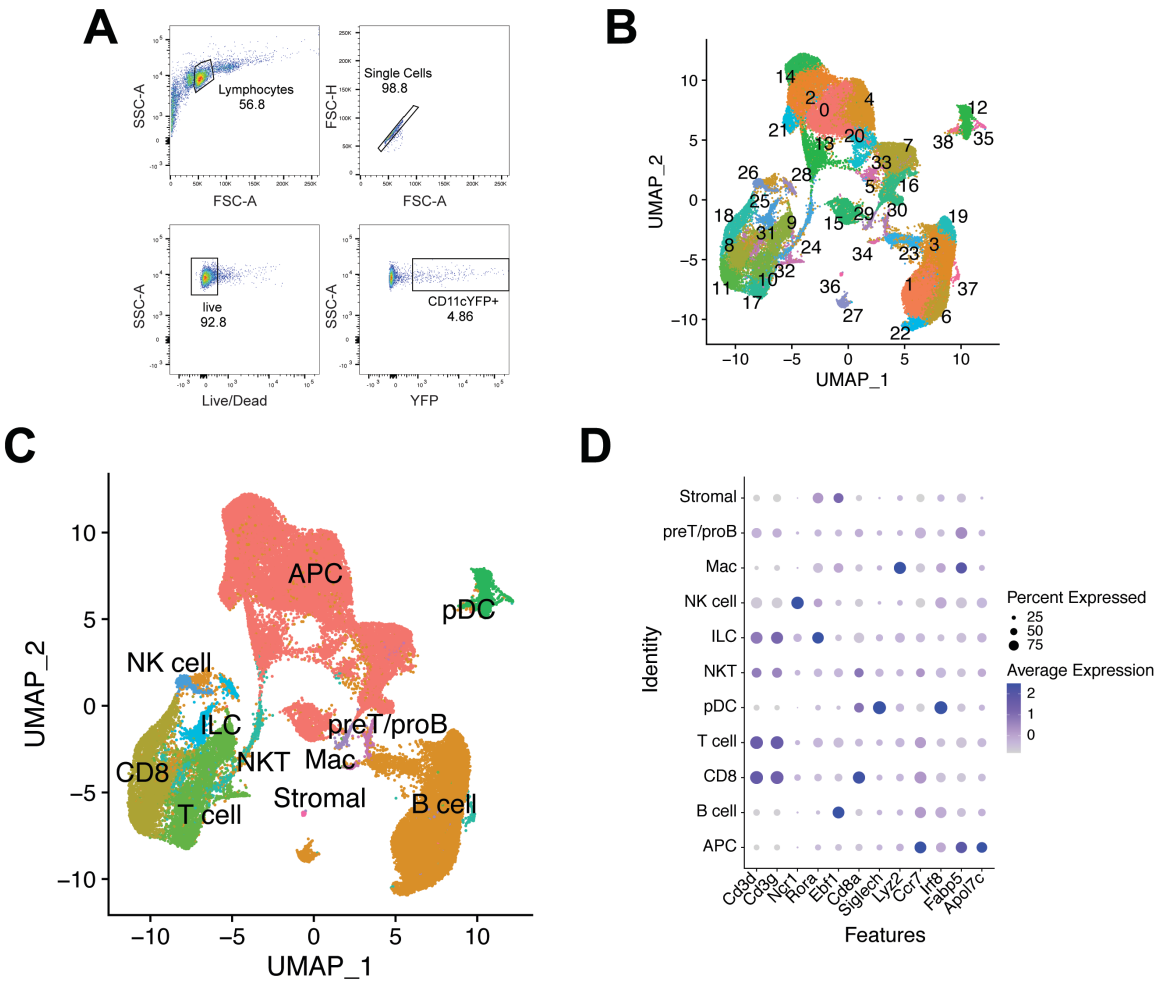

Figure 3.1.7 Dimensionality reduction of single cell sequencing of CD11cYFP+ cells sorted from pancreatic-duodenal LNs.

a) Representative flow plots demonstrating gating strategy of sorting live, YFP^{+} cells from liver, celiac, duodenal LNs of *CD11c*^{YFP} mice. n=3 per LN, (each sample is 10 mice pooled). **b)** Uniform manifold approximation and projection (UMAP) of 58,466 QC-filtered cells after single cell sequencing by 10x Genomics (Celiac: 15,852, Duodenal: 11,636, Liver: 30,978). In total 38 clusters were identified. **c)** Same UMAP as in **b** labeled according to cell type. **d)** Dot plot of gene expression of several cluster defining genes in the respective cluster cell type.

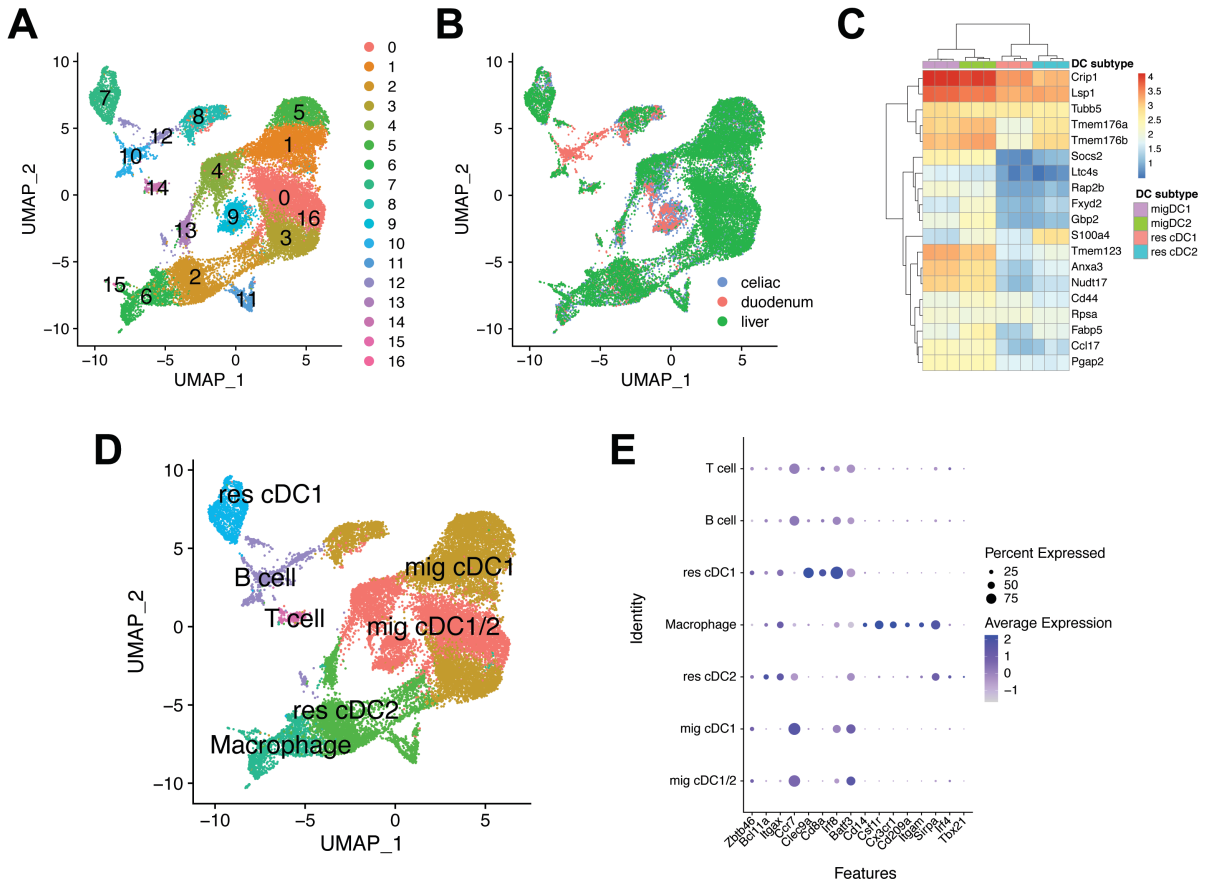

Figure 3.1.8 Main APC UMAP and cluster identification.

a) UMAP of re-clustered APC subset containing 23,704 cells yielding 16 clusters. **b)** UMAP of APC subset colored by LN sample. **c)** Representative heatmap displaying the top 10 defining genes of the respective cluster and their gene expression values from Esterhazy *et al*. DC RNAseq dataset. **d)** UMAP of APC subset relabeled by cell type. **e)** Dot plot of gene expression of several cluster defining genes in the respective cluster cell type. Mig = migratory, res = resident.

As previously mentioned, the migratory cDC1 population ($CD103^+CD11b^-$) is the major migratory DC population shared between the pancreas, liver and duodenum. Thus, to investigate possible subsets of this population, I subsetted the data again focusing only on the migratory cDC1 and cDC1/2 populations. Reclustering and dimensionality reduction produced a new UMAP with 7 clusters (Fig 3.1.9A). As with the APC UMAP, the migratory DC UMAP revealed an entire cluster (6) as well as parts of clusters (5 and 3) that were found only in celiac and duodenal LN samples, suggesting they may represent duodenal-derived DCs (Fig 3.1.9B). To account for differences in cell number across the different LN samples, each dataset was randomly downsampled to produce equal numbers of cells for each LN type. After downsampling, despite a significant decrease in cell number, the enrichment of cluster 6 in the celiac and duodenal LNs compared to the liver LN was evident (Fig 3.1.9C). Markers specific to each cluster were then identified and used to define each cluster resulting in clusters of *Il12b*$^+$ cells, *Ccl5*$^+$ cells, *Cd40*$^+$ cells, *Anxa2*$^+$ cells, *Bhlhe40*$^+$ cells, *Il1b*$^+$ cells, *Ftl1*$^+$ cells and a group of metabolically activated cells (Fig 3.1.9D). *Il12b*$^+$ cells were characterized by expression of *Il12b*, *Ncoa7*, and *Fgfbp3*; *Ccl5*$^+$ cells by *Gas5*, *Ccl5*, and *Txndc17*; *Cd40*$^+$ cells by *Csf1*, *Cd40*, and *Ccl22*; *Anxa2*$^+$ cells by *S100a6*, *S100a4*, *Anxa2*, and *Fabp5*; *Bhlhe40*$^+$ cells by *Cdkn1a*, *Nfkbia*, and *Fos*; *Il1b*$^+$ cells by *Il1b*, *Apol7c*, and *H2-Ab1*; *Ftl1*$^+$ cells by *Ftl1*, AW112010, and *Uba52*; metabolically activated cells by *mt-Atp6*, *mt-Co3*, and *Malat1* (Fig 3.1.9E).

To better understand how the migratory DC subsets relate back to the tissue of origin, I generated tissue specific gene expression signatures for each tissue type and projected the score of each signature onto the migratory DC UMAP. The duodenal tissue signature derived of *Aldh1a2*, *Il1b*, *Slc38a1*, *Ptp4a1*, *Ifitm6*, *Cybb*, *Stt3b*, *Dusp1*, *Hic1* showed distinct patterning, with a strong concentration of expression within the duodenal-specific *Il1b*$^+$ cell cluster (Fig 3.1.10A).

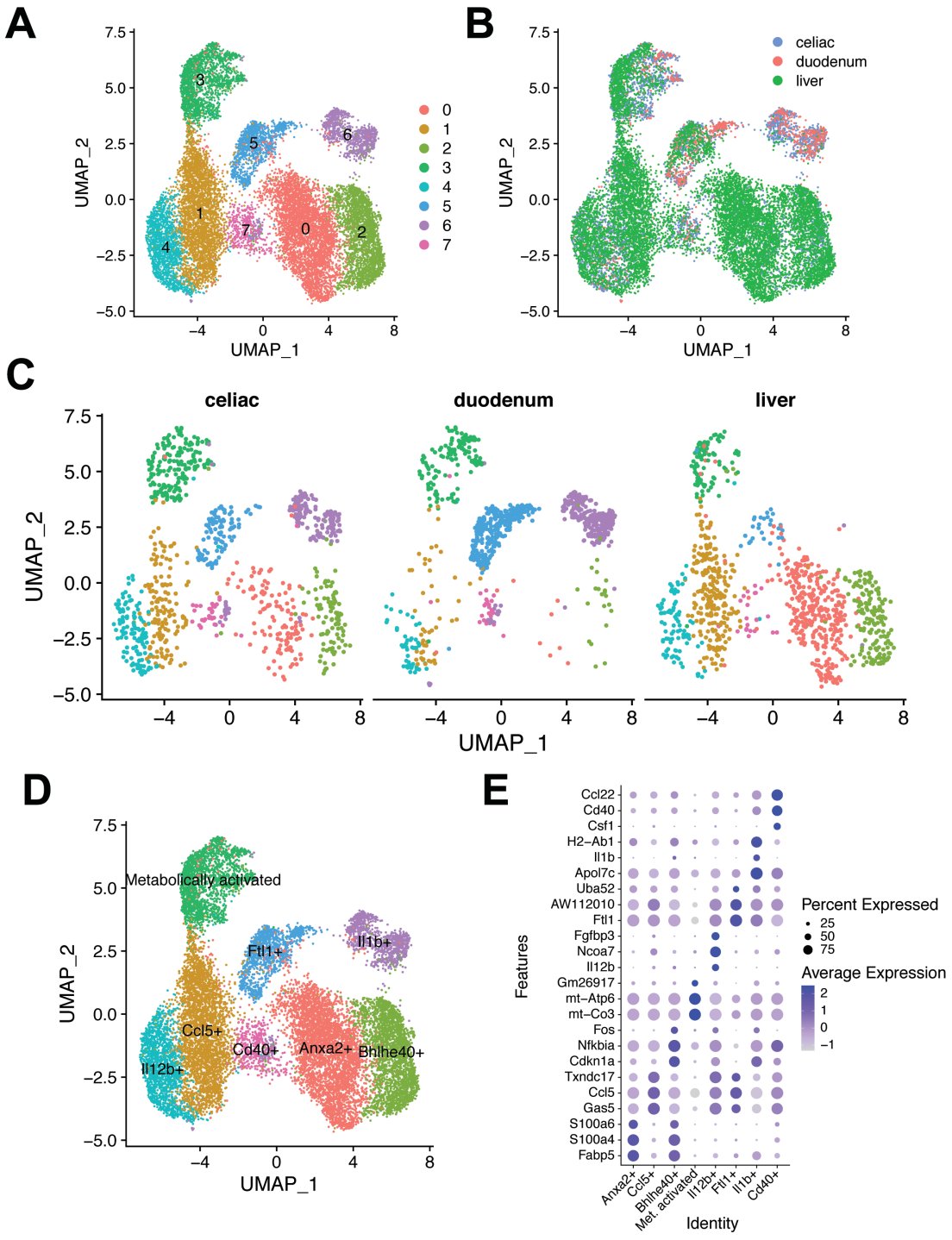

Figure 3.1.9 Subsets of migratory DC subsets unique to the duodenal-draining lymph nodes revealed by dimensionality reduction.

a) UMAP of migratory DC subset containing 15,631 cells across 7 clusters. **b)** UMAP of migratory DC subset colored by LN sample. **c)** UMAP of each LN sample downsampled to an

Figure 3.1.9 (continued) Subsets of migratory DC subsets unique to the duodenal-draining lymph nodes revealed by dimensionality reduction.

equivalent 962 cells each. **d)** UMAP of migratory DC subset relabeled with by defining genes. **e)** Dot plot of gene expression of several cluster defining genes in the respective cluster cell type.

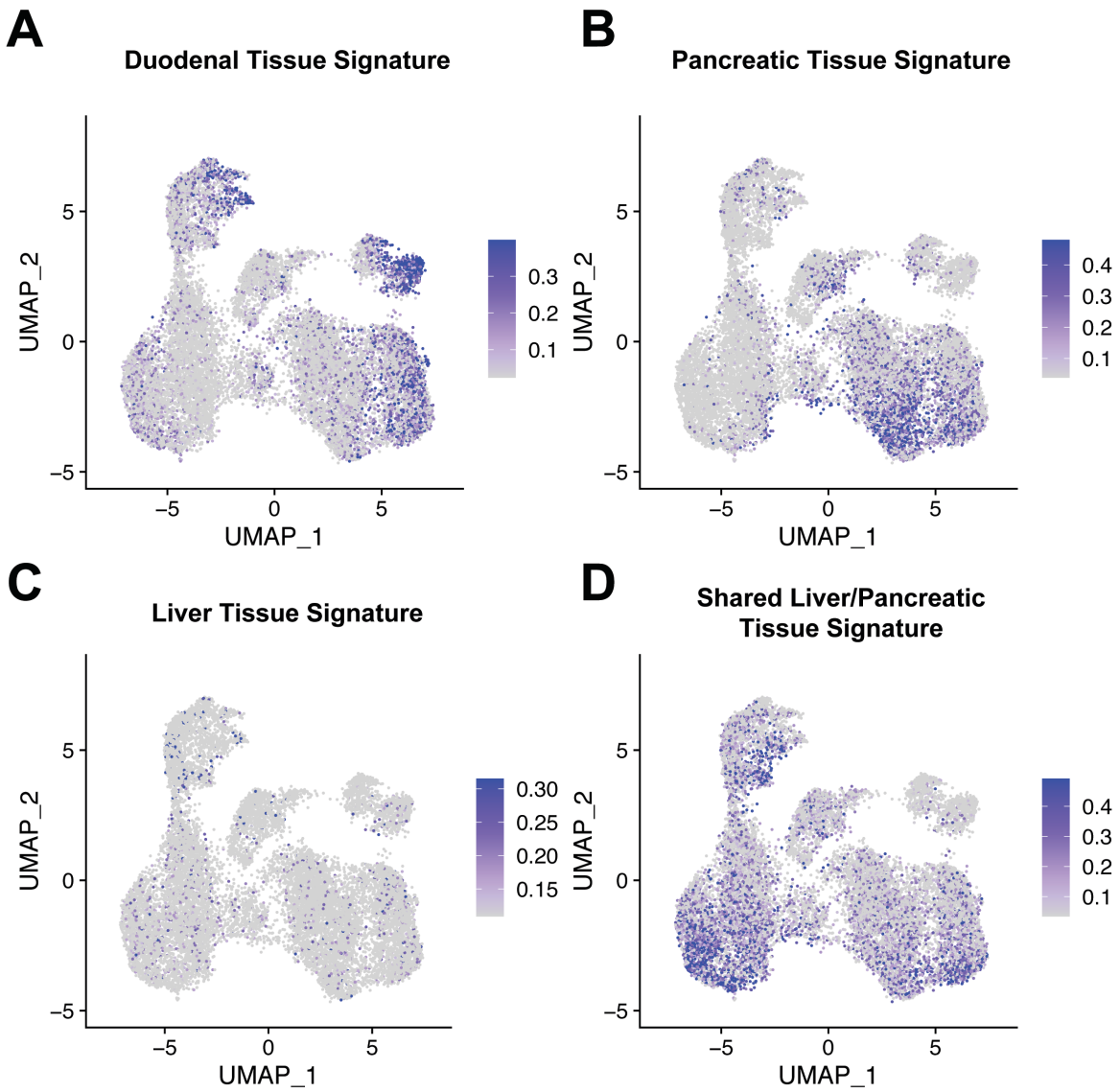

Figure 3.1.10 Tissue specific signatures distinguish migratory DCs within the shared lymph nodes.

a) Duodenal tissue signature (*Aldh1a2*, *Il1b*, *Slc38a1*, *Ptp4a1*, *Ifitm6*, *Cybb*, *Stt3b*, *Dusp1*, *Hic1*) projected onto migratory DC UMAP. **b)** Pancreatic tissue signature (*Anxa2*, *Fcer1g*, *Axl*, *Ccl6*, and *Klrb1b*) projected onto migratory DC UMAP. **c)** Liver tissue signature (*Id3*, *Ly6a*, *Cd34*, *Sema4c*, *Apoa1*, and *Fabp1*) projected onto migratory DC UMAP. **d)** Shared liver pancreatic tissue signature (S*ema4a*, *Il15ra*, *Cd63*, *Fcgr2b*, *Il12b*, *Alox5ap*, and *Emp3*) projected onto migratory DC UMAP.

Interestingly, the pancreatic tissue signature comprising *Anxa2*, *Fcer1g*, *Axl*, *Ccl6*, and *Klrb1b* did not overlap with the duodenal signature, instead showing an enrichment for the *Anxa2*$^{+}$ and *Bhlhe40*$^{+}$ clusters (Fig 3.1.10B). Surprisingly, the liver tissue signature made up of *Id3*, *Ly6a*, *Cd34*, *Sema4c*, *Apoa1*, and *Fabp1* was very weak and did not show any patterning (Fig 3.1.10C), however a shared liver/pancreatic signature composed of *Sema4a*, *Il15ra*, *Cd63*, *Fcgr2b*, *Il12b*, *Alox5ap*, and *Emp3* displayed strong expression across almost all clusters except the duodenal-specific *Il1b*$^{+}$ cell cluster (Fig 3.1.10D). However, upon closer inspection, the majority of these tissue signatures are driven by only one or two genes (*Il1b*$^{+}$ or *Anxa2*$^{+}$) within the gene set. Individual mapping of a number of these genes onto the UMAP reveals three patterns of gene expression within the shared LNs: tissue specific genes that are strongly expressed but with a ubiquitous pattern across all clusters (Fig 3.1.11A), tissue specific genes that are no longer expressed in the LN (Fig 3.1.11B), and tissue specific genes that are maintained within the LN in a site-selective way (Fig 3.1.11C). To confirm these results, I sorted CD103^{+}CD11b^{-} DCs from the liver, pancreas, duodenum and from the liver, celiac, and duodenal LNs and performed qPCR on several of the tissue specific genes highlighted in Fig 3.1.11. Consistent with the 10x data, the qPCR showed a similar patterning of gene expression into three major groups. Genes identified in the 10x dataset that showed high expression across many migratory DC clusters were similarly highly expressed in the LNs but displayed very minimal expression in the tissue (Fig 3.1.12A), suggesting that these genes were upregulated upon migration to or entry to the LN. In contrast, the second set of genes that showed poor migratory DC expression in the 10x dataset had the opposite pattern; this set of genes was highly expressed in its respective tissue but was barely expressed within the LNs (Fig 3.1.12B). Finally, the third group of genes showed somewhat comparable

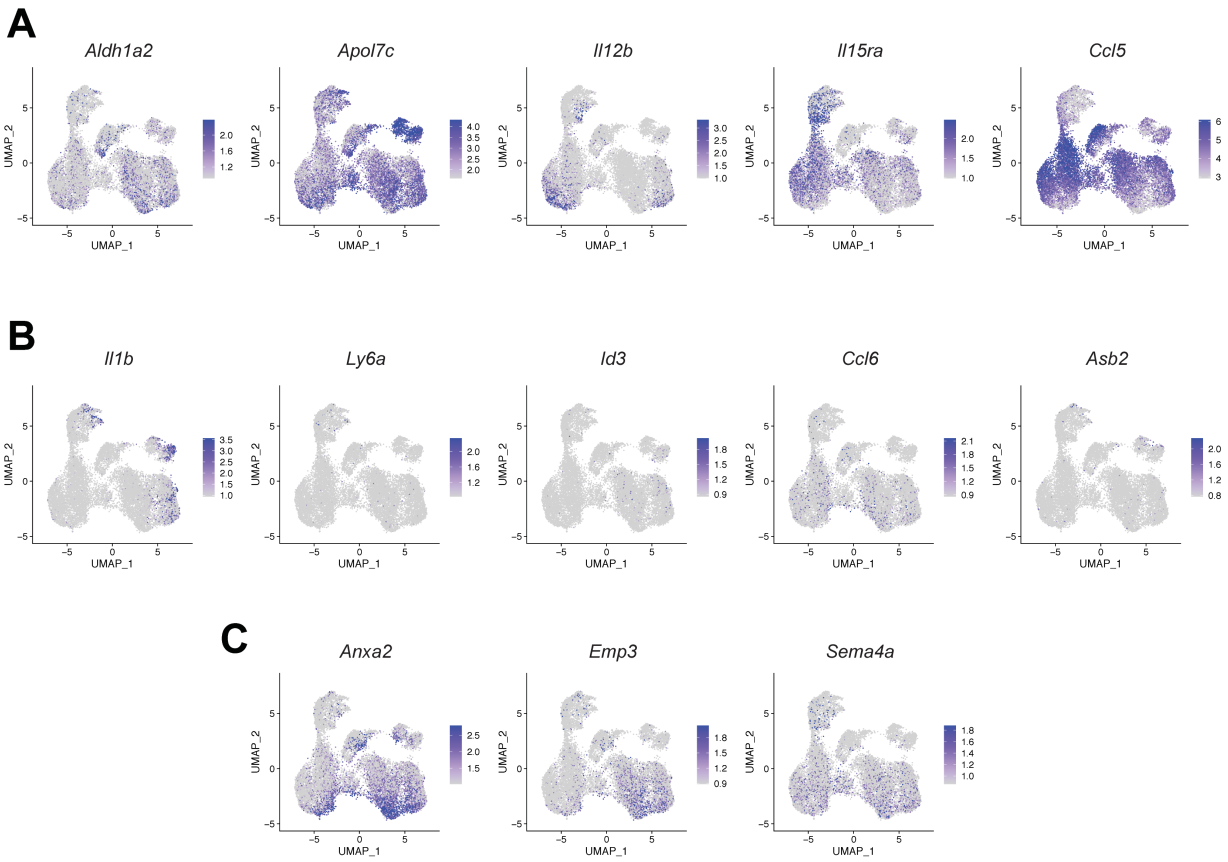

Figure 3.1.11 Distinct patterns of tissue specific gene expression within migratory DC subsets.

Feature plots displaying gene expression of indicated genes within the migratory DC UMAP. **a)** Genes that display high expression across multiple clusters within the LNs. **b)** Genes that display very minimal expression

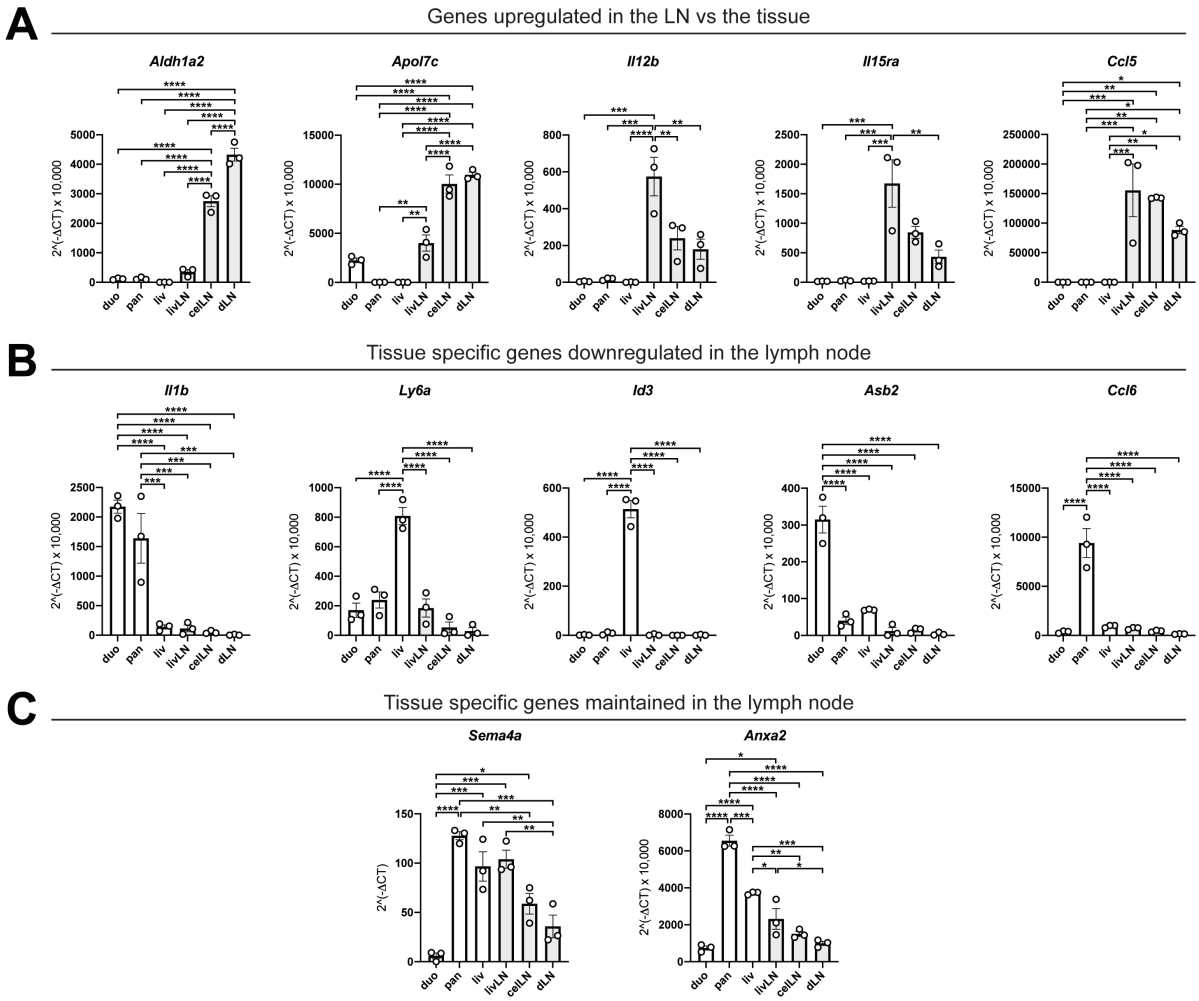

Figure 3.1.12 Distinct patterns of gene expression between migratory DCs from the tissue versus the lymph node.

qPCR was performed on sorted CD103^{+}CD11b^{-} DCs from the indicated tissues and LNs of B6 mice. Cells were defined as live, Dump^{-}(NK1.1, TCRβ, B220, CD90), CD11c^{int}, MHC^{+}, F4/80^{-}, CD103^{+}, CD11b^{-}. **a)** Relative expression of indicated genes that display an upregulation in the lymph node compared to the tissue. **b)** Relative expression of indicated genes that display a downregulation in the lymph node compared to the tissue. **c)** Relative expression of tissue specific genes in the tissue that show a corroborating expression pattern in the lymph nodes. Expression is displayed as 2^ΔCTx10,000 relative to the housekeeping gene 36B4, n=3 for all groups. Duo = duodenum, pan = pancreas, liv = liver, livLN = liver LN, celLN = celiac LN, dLN = duodenal LN. *p < 0.05, **p < 0.01, ***p < 0.001,****p < 0.0001 (ANOVA).

levels of gene expression in the tissue and the corresponding LNs (Fig 3.1.12C), indicating the expression of these genes is in the LNs. **c)** Genes with cluster specific expression patterns maintained during migration to the LN. Collectively, the differences in gene expression of migratory DCs from the tissue vs the LN point to a stronger role of the LN environment, rather than the tissue of origin in setting the expression profile of these DCs. It is also possible that this expression profile is initiated concomitantly with the triggering of migration to the LN.

Although the sequencing results are in line with an influence of the LN tone rather than tissue of origin effects on migratory DC gene expression, I reasoned that some of these markers may still be able to be used as a proxy for tissue of origin. One such gene was *Ly6a* which encodes the protein Sca-1. *Ly6a* is specifically expressed in liver derived DCs compared to pancreatic and duodenal DCs (Fig 3.1.13B) and consistent with this a high frequency of Sca-1^+ migratory DCs was observed in the liver but not the pancreas or duodenum (Fig 3.1.13C). Despite its low expression in the shared LNs (Fig 3.1.12B), Sca-1 protein expression was still observable, albeit at a lower frequency and MFI, in the main LNs of the liver (liver and celiac LNs), but as expected was not observed in the duodenal LN (Fig 3.1.12A, C). The decrease in Sca-1 expression in the LNs compared to the tissue DCs suggests that either cells lose expression of Sca-1 upon migration to the LN or that only Sca-1^- cells are the main cell type that migrates to the LN.

Another tissue specific marker, *Aldh1a2* was uniquely expressed in duodenal DCs compared to pancreatic and liver DCs by RNAseq (Fig 3.1.14B). Accordingly, RALDH activity as a proxy of *Aldh1a2* expression, measured by cleavage of fluorescein isothiocyanate–positive boron-dipyrromethene–tagged aminoacetate (ALDEFLUOR), was highest by frequency and MFI within the duodenal LN (Fig 3.1.14A-C). The celiac LN which also drains the duodenum had a

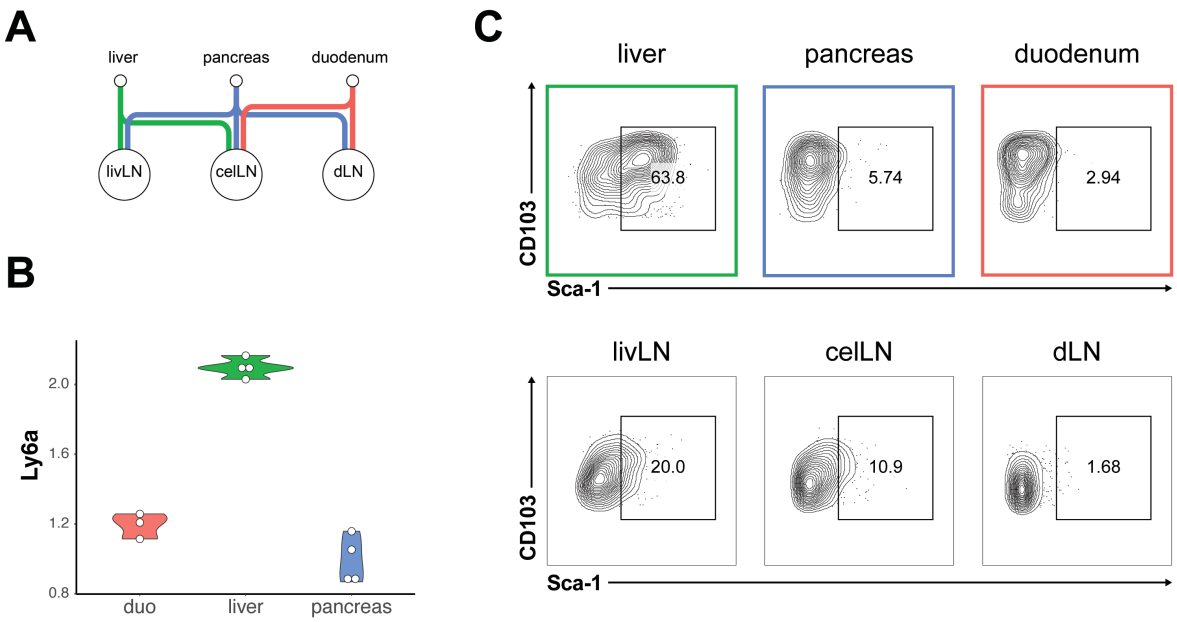

Figure 3.1.13 Liver DCs express Sca-1 in the tissue and the lymph node.

a) Schematic of tissue drainage to indicated lymph nodes. Liver LN (LivLN) receives lymph from the liver and the pancreas, celiac LN (celLN) receives lymph from the liver, pancreas and duodenum, duodenal LN (dLN) receives lymph from the pancreas and the duodenum. **b)** Log(transcripts per million) of *Ly6a* from bulk RNA sequencing of $CD103^{+}CD11b^{-}$ migratory DCs from indicated tissues. **c)** Representative flow cytometry plots of CD103 and Sca-1 expression within $CD103^{+}CD11b^{-}$ migratory DCs in indicated tissues and LNs. LivLN = liver LN, celLN = celiac LN, dLN = duodenal LN.

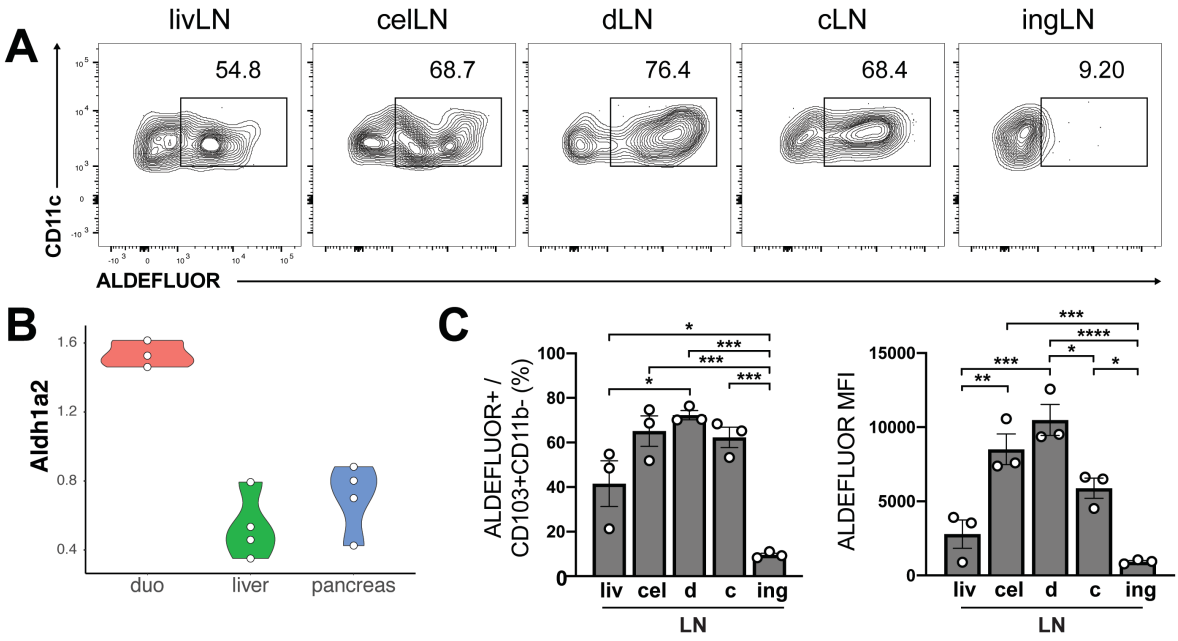

Figure 3.1.14 RALDH activity is enriched in duodenal draining lymph nodes.

a) Representative flow cytometry plots of fluorescein isothiocyanate–positive boron-dipyrromethene–tagged aminoacetate (ALDEFLUOR) within $CD103^{+}CD11b^{-}$ DCs in indicated lymph nodes. **b)** Log(transcripts per million) values for *Aldh1a2* expression levels in indicated tissues. **c)** Frequency and mean fluorescent intensity (MFI) of $ALDEFLUOR^{+}$ $CD103^{+}CD11b^{-}$ DCs in indicated LNs. Liv = Liver LN, cel = celiac LN, d = duodenal LN, c = cecal-colonic LN, ing = inguinal LN.

similar frequency of ALDEFLUOR$^+$ cells but was lower in MFI (Fig 3.1.14B, C). Importantly, the liver LN which does not drain the duodenum had the lowest frequency and MFI of the pancreatic LNs (Fig 3.1.14B, C). These data are consistent with qPCR data showing higher expression of *Aldh1a2* in the celiac and duodenal LNs than the liver LN (Fig 3.1.12A). However, the low expression of *Aldh1a2* in all tissue derived DCs speaks to the influence of specific LN environments in regulating its expression.

While a number of genes displayed tissue specific expression patterns, the differences in expression levels between the tissue and the LN preclude many of their use as tissue of origin markers once DCs are in the LN. Instead, alternative approaches utilizing reporter mice or fate mapping with some of the identified tissue specific genes may be necessary to carefully distinguish migratory DCs in the LN. In an effort to fate map cells from one location I took advantage of *Rosa26*$^{\text{LSL-Tdtomato/wt}}$ *Villin*$^{\text{CreERT}}$ mice which upon tamoxifen administration express Tdtomato within the intestinal epithelial cells. Thus, DCs that have taken up gut-derived antigen can be visualized as Tdtomato$^+$ within the draining LNs (Fig 3.1.15A). It is important to note that this system cannot distinguish whether cells took up antigen in the tissue vs if antigen reached the LN acellularly and was then picked up by DCs. However, a large majority of Tomato$^+$ cells within the pancreatic-duodenal LNs are CD103$^+$CD11b$^-$ DCs (Fig 3.1.15B), suggestive of antigen uptake within the tissue, though this cannot be stated conclusively. Since Tdtomato expression is confined to the gut, I utilized these mice to explore whether the Tdtomato$^+$ cells in the LN that are likely enriched for duodenal origin most closely resembled the DC gene expression profiles of duodenum, pancreas, or liver derived DCs. I sorted CD103$^+$CD11b$^-$ Tdtomato$^+$ DCs from the pooled liver, celiac and duodenal LNs of *Rosa26*$^{\text{LSL-Tdtomato/wt}}$ *Villin*$^{\text{CreERT}}$ mice as well as the CD103$^+$CD11b$^-$ Tdtomato$^-$ DCs from the duodenum, pancreas

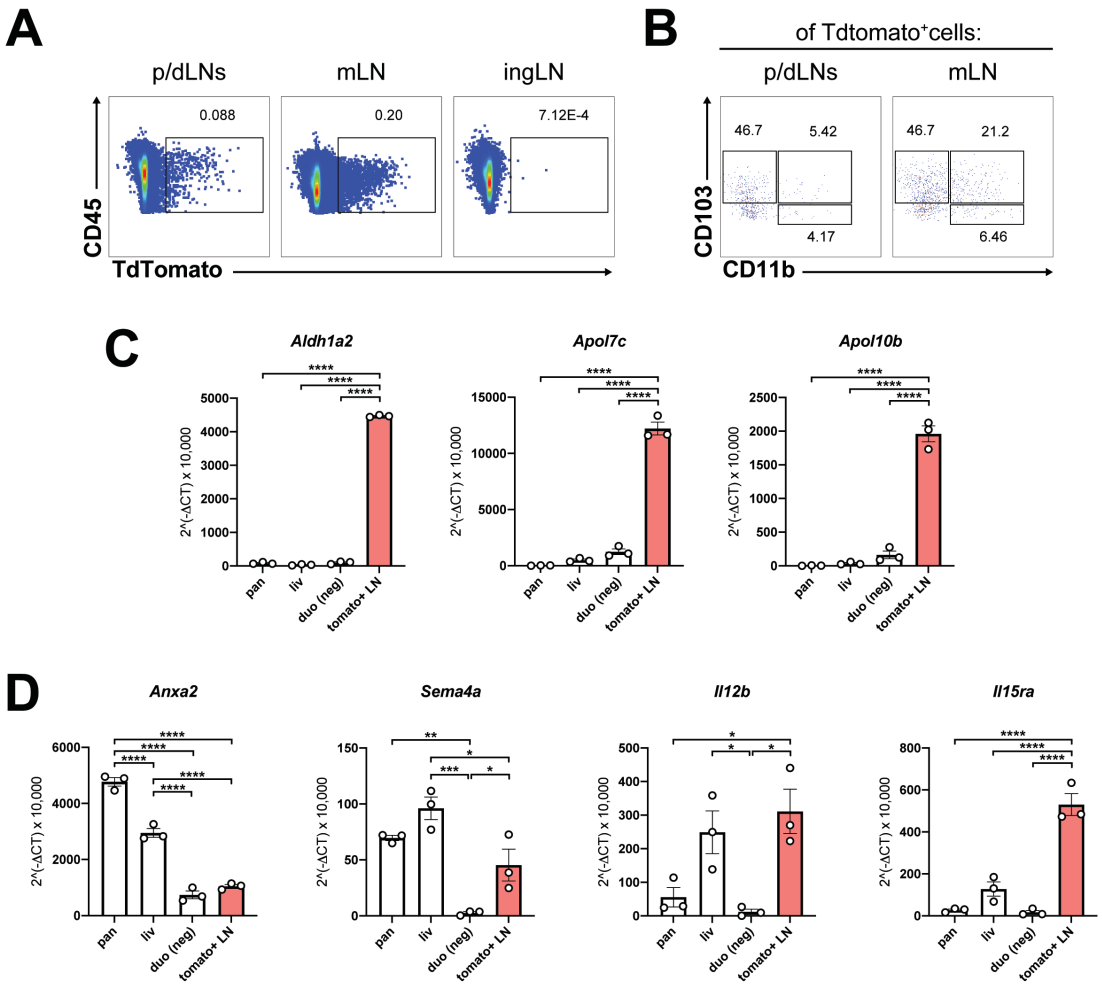

Figure 3.1.15 CD103+CD11b- DCs are the major DC subset that acquires gut-derived TdTomato and display a gene expression profile consistent with predominantly duodenal origin.

a) Representative flow cytometry plots displaying TdTomato uptake and CD45 expression of live cells from indicated LNs of *VillinCreERT2*$^{+/-}$*Rosa26*$^{LSL\text{-}tdTomato/wt}$ mice. **b)** Representative flow cytometry plots showing distribution of CD103^{+}CD11b^{-} DCs among Tdtomato^{+} cells in indicated LNs. **c-d)** qPCR was performed on sorted Tomato^{+}CD103^{+}CD11b^{-} DCs from pooled liver, celiac and duodenal LNs or sorted Tomato^{-}CD103^{+}CD11b^{-} DCs from indicated tissues (n=3, each a pool of two mice). Cells were defined as live, Dump^{-}(NK1.1, TCRβ, B220, CD90), CD11c^{int}, MHC^{+}, F4/80^{-}, CD103^{+}, CD11b^{-}. Expression is displayed as 2^ΔCTx10,000 relative to the housekeeping gene 36B4. Duo (neg) = duodenum Tdtomato^{-}, pan = pancreas, liv = liver. *p < 0.05, **p < 0.01, ***p < 0.001, ****p < 0.0001 (ANOVA).

and liver and performed qPCR for several tissue specific genes. Based on the RNA sequencing results and the qPCR validation, a number of duodenal DC specific genes are enriched in the duodenal LN compared to the celiac and liver LNs including *Aldh1a2*, *Apol7c*, *Apol10b*. These genes were highly expressed in the Tdtomato^{+} subset while expression of the pancreas-specific gene *Anxa2* was very lowly expressed, consistent with a predominant duodenal origin (Fig 3.1.15C,D). Other LN upregulated genes such as *Il12b*, *Il15ra* and *Sema4a* were also expressed by Tdtomato^{+} cells (Fig 3.1.15D). Since Tomato^{-} cells within the LNs also contain gut derived DCs (only about 10% of migratory DCs were Tomato^{+}, even in more distal strictly gut draining LNs) I did not collect them for comparison, as they cannot be used as a reliable indicator of non-duodenal DCs.

In sum, the sequencing based approach taken here demonstrates that migratory DCs from the pancreas, duodenum and liver express distinct tissue specific signatures when present in their respective tissue. However, once in the shared LNs, migratory DCs become much more homogenous, expressing only remnants of the tissue of origin signature. These data support the concept that LN environment rather than tissue of origin is the major influencing factor on DC gene expression. Therefore, the tone of each LN may be the most important factor in determining how antigen is handled within the shared LNs. The implication of this data is that tissue specific stressors that result in alterations to the LN environment may have important consequences on other tissue specific immunity as a result of shared LNs.

3.2 Influence of the duodenum on pancreatic immunity

Concomitant intestinal infection and dietary antigen feeding results in a measurable change to the tolerogenic properties of the duodenal LNs with respect to the response to dietary antigen. If and how the response to self-antigen derived from the pancreas is similarly influenced by

infection is unknown. I hypothesized that intestinal perturbation in the form of infection may be able to reshape the pancreatic immune system by virtue of the shared lymph node drainage with the duodenum. In the case of T1D, infection may result in triggering of diabetes through activation of autoreactive diabetogenic T cells. To test the impact of intestinal infection on pancreas-reactive T cells I utilized several infectious agents known to compromise oral tolerance[15,48–50]. Importantly, none of the pathogens used have been demonstrated to infect the pancreas, allowing evaluation of indirect effects on pancreatic adaptive immunity via shared lymph nodes rather than infection of the pancreas itself. To do so, I developed a general infection and T cell transfer system in which fluorescently labeled T cells (either CFSE or CTV) were transferred into mice previously infected with the pathogen of interest such that the T cells would be expected to be present in the gLNs at the peak of infection. This meant that each infection and T cell transfer had slightly different timing for each respective infection. Additionally, when possible, multiple doses of infection were used to generate a range of effects.

The prior studies utilizing infection induced disruptions in oral tolerance focused exclusively on the $CD4^+$ T cell phenotypes. Thus, I initially began by testing pancreas reactive $CD4^+$ T cells. Knowing the peak of T1L reovirus infection in the small intestine is between 2-3 days post infection in B6 mice, NOD mice were infected with 10^8, 10^9, and 10^{10} PFU of T1L reovirus and 6 hours later given an adoptive transfer of β cell specific $CD4^+$ BDC2.5 T cells. On the day of T cell transfer and every subsequent day of the experiment mice received a 40mg/kg dose of STZ to boost the amount of antigen present in the LNs. After three days, cell proliferation and differentiation were evaluated within the shared pancreatic-duodenal LNs, other gLNs and a peripheral control the inguinal LN. As expected, BDC2.5 cells mainly homed to and divided within the pancreatic LNs, reflecting their antigen specificity. Infection did not result in changes in cell

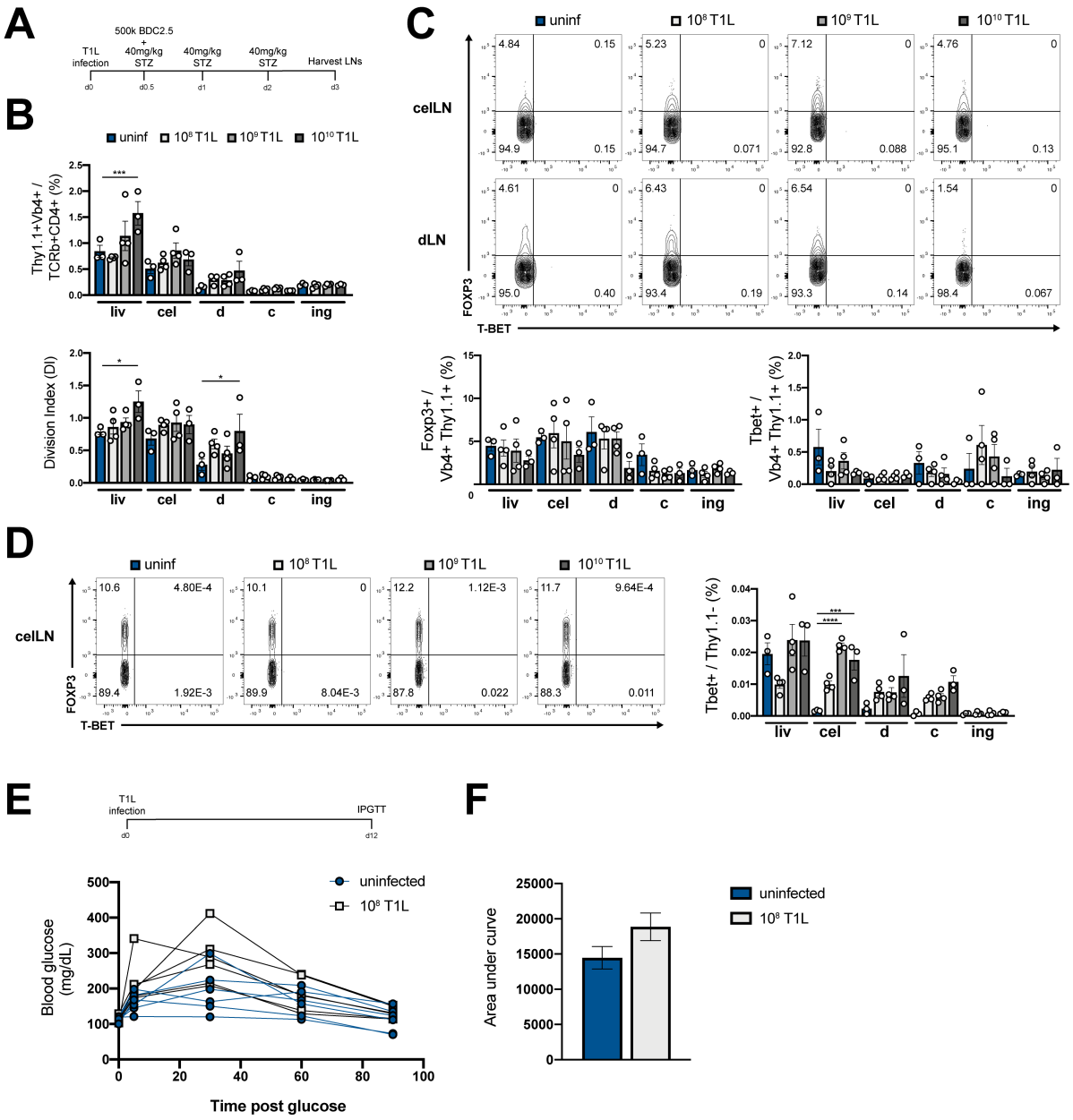

Figure 3.2.1 T1L reovirus infection does not induce inflammatory pancreas-specific BDC2.5 CD4+ T cells.

a) Schematic of experimental timing. **b)** Frequency of Thy1.1$^+$Vβ4$^+$ among TCRβ$^+$CD4$^+$ cells and division index in indicated lymph nodes 3 days post adoptive transfer of 500k Thy1.1$^+$ BDC2.5 cells into NOD mice infected or not with indicated doses of T1L reovirus: 10^8, 10^9, or 10^{10} PFU. Mice were additionally treated with 40mg/kg STZ daily, n=3 per group. **c)** Representative flow cytometry plots and frequency of FOXP3 and T-BET expression among Thy1.1$^+$ BDC2.5 cells in celiac and duodenal LNs as in **b**. **d)** Representative flow cytometry plots and frequency of FOXP3 and T-BET expression among endogenous CD4$^+$Thy1.1$^-$ cells as in **b**. **e)** Intraperitoneal glucose tolerance test (IPGTT) of mice infected or not with 10^8 PFU of T1L reovirus 12 days prior (n=10). **f)** Area under the curve of blood glucose after glucose

Figure 3.2.1 (continued) T1L reovirus infection does not induce inflammatory pancreas-specific BDC2.5 CD4$^+$ T cells.

(2 g/kg) administration. Liv = liver LN, cel = celiac LN, d = duodenal LN, c = cecal-colonic LN, ing = inguinal LN.

retention within the LNs or changes in division except at the 10^{10} PFU dose, a dose not feasible to reliably prepare for experiments (Fig 3.2.1A,B). Furthermore, when T cell differentiation was assessed, I found that BDC2.5 cells from infected mice did not show any differences in expression levels of Foxp3 and T-bet, marking pTreg and Th1 differentiation respectively (Fig 3.2.1C). This was unexpected given that oral tolerance experiments utilizing similar infectious doses but oral antigen-specific T cells results in decreased pTreg frequencies and increased Th1 cells. To confirm the infection was truly affecting the LN, I checked the endogenous T cell response and found slightly elevated levels of T-bet expression, indicating successful infection and the induction of an anti-viral immune response-though lower than observed in B6 mice[48] (Fig 3.2.1D). These experiments focused solely on $CD4^+$ T cell differentiation but didn't investigate any potential effect of infection on diabetes progression. To investigate whether T1L infection alters diabetes onset, 6 week old NOD mice were infected with T1L and blood glucose levels were monitored for two weeks. At 12 days post infection, an intraperitoneal glucose tolerance test (IPGTT) was performed to assess β cell insulin production capacity. In this assay, mice are injected with a large dose of glucose and blood glucose levels are monitored as glucose levels are cleared. Mice with severely decreased functional β cell mass will show defects in glucose clearance which can be measured by the differences in blood glucose levels and the area under the curve representing the estimated total rise in blood glucose over the entire assay. T1L infected mice did not show any significant differences compared to uninfected mice in both blood glucose levels and area under the curve (Fig 3.2.1E, F), indicating T1L infection did not alter acute β cell function.

Viral infections typically generate a type 1 immune response, characterized by an interferon (IFN) response and Th1 cells. Thus, to test whether a different type of infection altered pancreas-reactive T cell fates, I focused on the type 2 inducing helminth *Strongyloides*

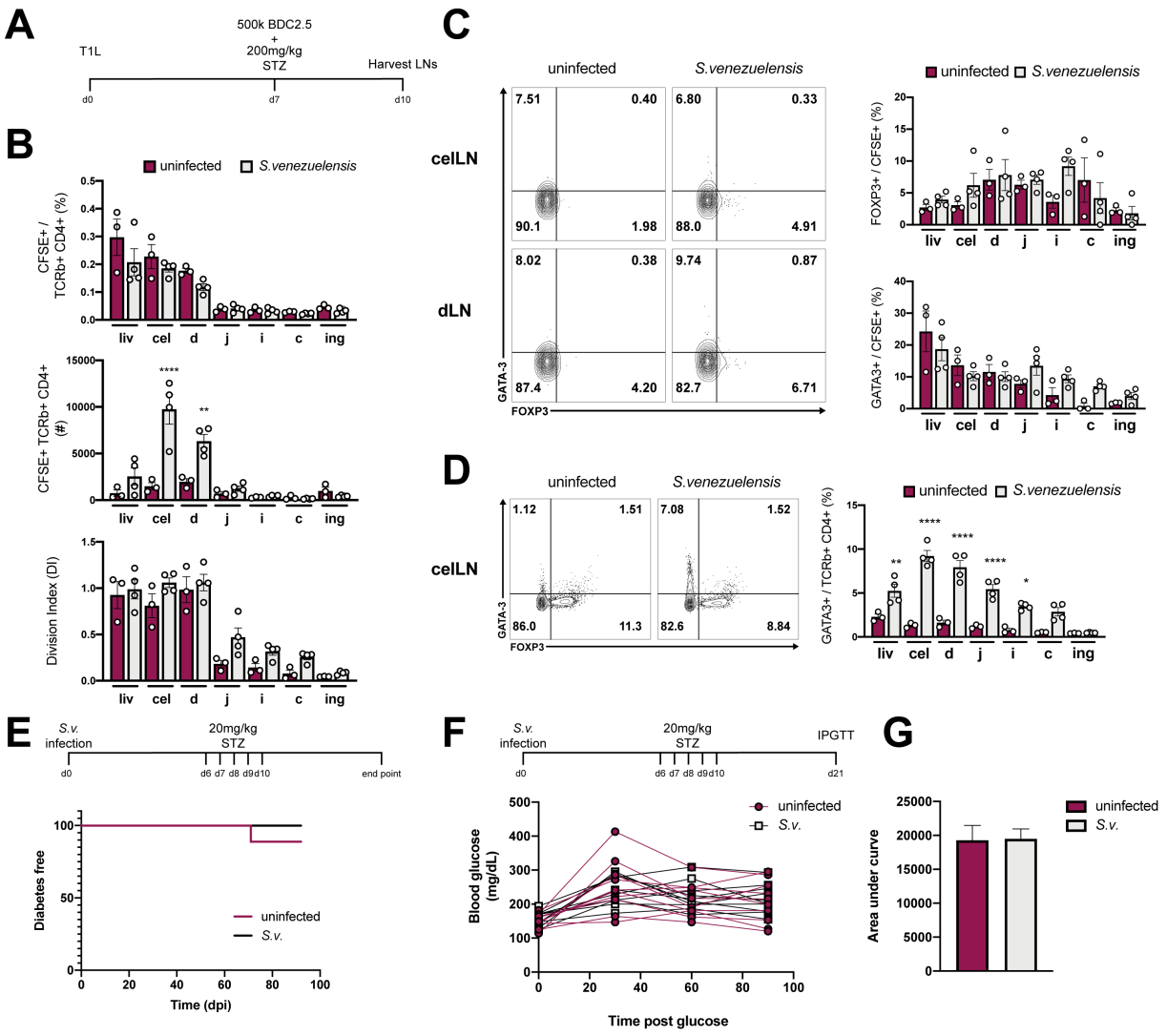

Figure 3.2.2 Duodenal-tropic helminth S. venezuelensis infection does not impact pancreas-specific BDC2.5 T cell differentiation.

a) Schematic of experimental timing. **b)** Frequency of CFSE$^+$ Vβ4$^+$ among TCRβ$^+$CD4$^+$ cells and division index in indicated lymph nodes 3 days post adoptive transfer of 500k CFSE-labeled BDC2.5 cells into NOD mice infected or not with *S. venezuelensis* larvae 7 days prior. Mice were treated with a single 200mg/kg dose of STZ on the day of T cell transfer, n=3. **c)** Representative flow cytometry plots and frequency of FOXP3 and GATA-3 expression among CFSE$^+$ BDC2.5 cells in celiac and duodenal LNs as in **b**. **d)** Representative flow cytometry plots and frequency of FOXP3 and GATA-3 expression among endogenous TCRβ$^+$CD4$^+$ cells as in **a**. **e)** Diabetes incidence of NOD mice infected with *S. venezuelensis* larvae at 3 weeks of age and treated with 20mg/kg STZ for 4 consecutive days at 6 days post infection. Random fed blood glucose was checked weekly, n=10. **f)** Intraperitoneal glucose tolerance test (IPGTT) of mice infected or not with *S. venezuelensis* larvae and treated with 20mg/kg STZ as in **e** three weeks prior. **g)** Area under the curve of blood glucose after glucose (2 g/kg) administration. Liv = liver

Figure 3.2.2 (continued) Duodenal-tropic helminth *S. venezuelensis* infection does not impact pancreas-specific BDC2.5 T cell differentiation.

LN, cel = celiac LN, d = duodenal LN, j=jejunal LN, i = ileal LN, c = cecal-colonic LN, ing = inguinal LN. *p < 0.05, **p < 0.01, ***p < 0.001,****p < 0.0001 (ANOVA).

venezuelensis (*S.v.*). Unlike T1L which is delivered orally, *S.v.* is administered subcutaneously through the injection of larvae. Over the course of several days, larvae travel to the lungs where they are coughed up and swallowed, finally reaching the intestine where they develop into adult worms. An important distinction about *S.v.* is that unlike intestinal viral infection helminths do not travel from the gut to the LN. Therefore, changes to the LN environment may be reflective of inflammatory cytokines or migrating worm products but not the worm itself. Since the peak of infection for *S.v.* is around 7 days post infection, CFSE labeled BDC2.5 T cells were transferred one week after infection and mice were treated with 200mg/kg STZ. Three days later BDC2.5 LNs were dissected and BDC2.5 T cells were phenotyped. Much like the T1L infections, BDC2.5 T cells did not show major changes in LN retention or division index (Fig 3.2.2A,B). The absolute number of BDC2.5 T cells as measured by the number of CFSE labeled cells was significantly increased, but this likely reflects the massive swelling of the celiac and duodenal LNs rather than a specific increase in BDC2.5 T cell division in LNs of infected mice. The frequency of Th2 skewed BDC2.5 T cells was assessed by flow cytometry for the expression of the type 2 transcription factor Gata3. BDC2.5 cells from *S.v.* infected mice expressed similar levels of Gata3 and Foxp3 as uninfected mice, indicating minimal Th2 differentiation of pancreas reactive T cells (Fig 3.2.2C). This was despite a robust endogenous Gata3 response within the same LNs that was similar to the response observed in B6 mice[15] (Fig 3.2.2D). Consistent with minimal changes to pancreas-reactive T cells, *S.v.* infection did not cause any acceleration of diabetes progression in when NOD mice were infected at 4 weeks of age (Fig 3.2.2E). Moreover, an IPGTT at 6 weeks showed no measurable differences between infected and uninfected mice (Fig 3.2.2F,G).

Prior experiments demonstrating alterations to oral tolerance upon *S.v.* and T1L infections were all performed in B6 mice, unlike the previously described BDC2.5 T cells experiments. In

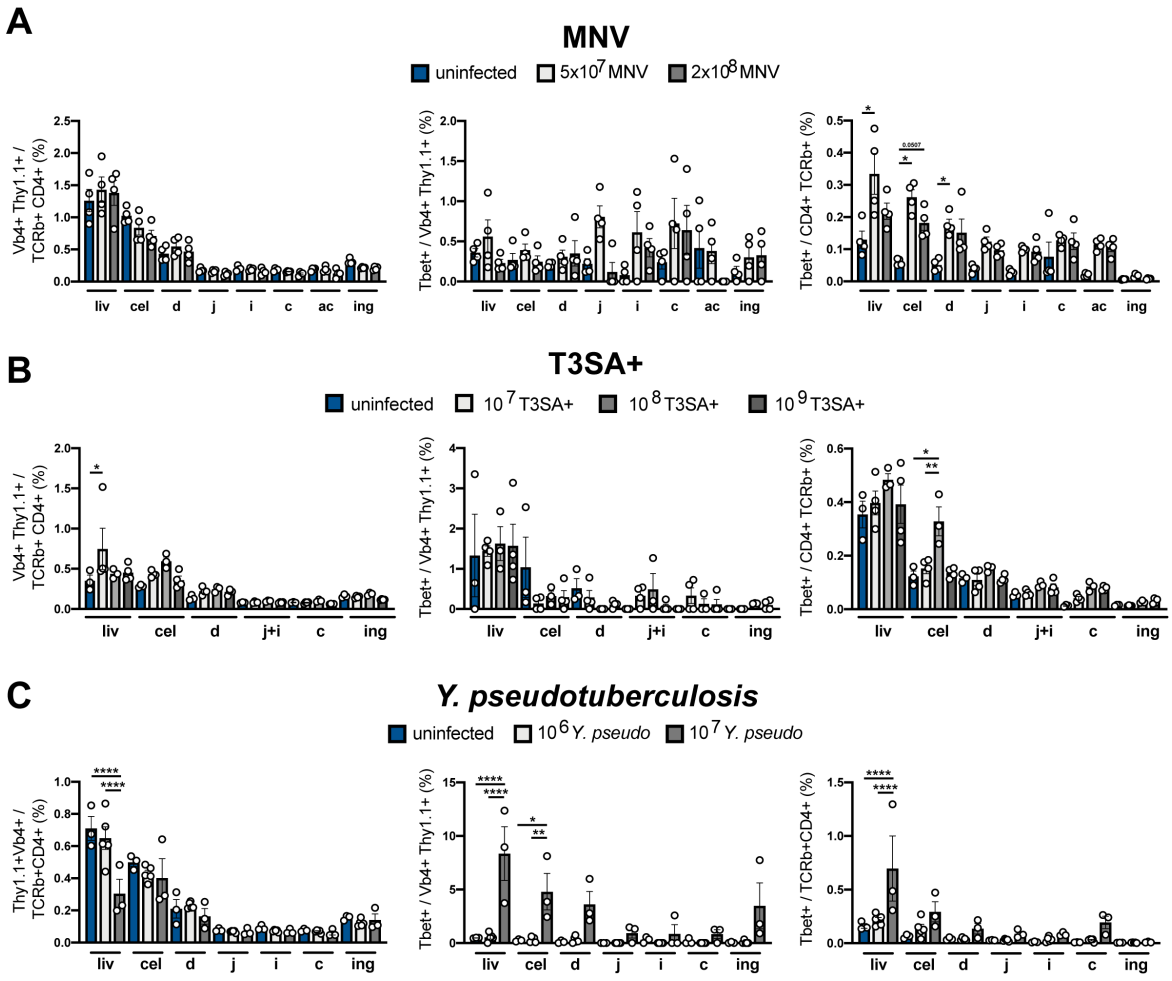

Figure 3.2.3 Pancreas-specific CD4+ BDC2.5 T cell differentiation is unperturbed across several types and doses of intestinal infection.

Frequency of Vβ4$^+$Thy1.1$^+$ among TCRβ$^+$CD4$^+$ cells, Tbet$^+$ among Vβ4$^+$Thy1.1$^+$ cells, and Tbet$^+$ among endogenous TCRβ$^+$CD4$^+$ cells in indicated lymph nodes: **a)** 4 days post adoptive transfer of 500k BDC2.5 cells into NOD mice infected or not with 5x10^7 or 2x10^8 TCID50 units of murine norovirus CW3 5 days prior and treated with 40mg/kg STZ daily, n=4. **b)** 5 days post adoptive transfer of 500k BDC2.5 cells into NOD mice infected or not with 10^7, 10^8, or 10^9 PFU T3SA+ reovirus 6 days prior and treated with 40mg/kg STZ daily, n=3 (uninfected, 10^8), n=4 (10^7, 10^9). **c)** 4 days post adoptive transfer of 375k BDC2.5 cells into NOD mice infected or not with 10^6 or 10^7 CFU 7 days prior and treated with 40mg/kg STZ daily, n= 3 (uninfected, 10^7), n=4 (10^6).

order to overcome potential differences in infectious dose or tropism of T1L or *S.v.* based on mouse strain, additional infectious agents were utilized including other viral infections and bacterial infection. Figure 3.2.3 shows the summarized results from these infection experiments. Similar to the T1L results, infection with the pan intestinal virus MNV did not alter BDC2.5 T cell fate. BDC2.5 T cells did not display any increased frequency of T-bet expressing cells at two different infectious doses (Fig 3.2.3A). A second type of reovirus, T3SA+, which primarily infects the bile duct epithelium rather than the intestine, was also tested. BDC2.5 T cells transferred into NOD mice infected with T3SA+ likewise did not display any differences in LN retention or T-bet expression (Fig 3.2.3B). Lastly, infection of NOD mice with a sublethal dose of *Yersinia pseudotuberculosis* had no measurable effect on BDC2.5 T cell differentiation (Fig 3.2.3C). However, a high, lethal dose of *Y. pseudotuberculosis* did result in increased frequencies of T-bet$^+$ BDC2.5 cells, likely as a result of systemic dissemination of the bacteria (Fig 3.2.3C).

Collectively, these results show that across multiple types of intestinal infections, there were no changes in cell division or T cell fates of pancreas-specific CD4$^+$ BDC2.5 cells within infected mice compared to uninfected. These results suggest that intestinal infection does not alter the fate of pancreas-reactive CD4$^+$ T cells. This stands in contrast to the response to oral antigen in similar circumstances, whereby intestinal infection causes a reduction of oral antigen specific pTreg differentiation and increased Th1 differentiation within the same lymph nodes. Whether differences in the response lies in the difference between oral neoantigens vs (pancreatic) autoantigens with a pre-existing, antigen experienced CD4$^+$ T cell pool, or if it can be attributed to nuances in the T cell clone or mouse strain used cannot be excluded at this time.

The majority of the infections tested in these experiments have been shown to exert substantial changes to the CD103$^+$CD11b$^-$ DC population both at the level of gene expression and

their subsequent T cell priming capabilities[15,48,49,98]. Although this DC subset is thought to be the most potent pTreg inducing DC subset, their classical function is the activation of $CD8^+$ T cells. Given the profound changes to this DC subset in the relevant intestinal infections, I hypothesized that pancreas-reactive $CD8^+$ T cells may be more strongly influenced by LN changes resulting from infection. Since previous studies had only considered the effect of intestinal infection on oral antigen specific $CD4^+$ T cells, I first tested what happens to oral antigen specific $CD8^+$ T cells during intestinal infection. Mice were infected with either T1L or MNV and given an adoptive transfer of $CD8^+$ OVA specific OT-I T cells. Mice were then given a gavage of OVA and kept on OVA containing drinking water for the duration of the experiment. Consistent with previous $CD4^+$ T cell data, in both T1L and MNV infection but not uninfected controls, OT-I T cells became activated, showing increased frequencies of $GranzymeB^+$ cells, either single positive or double positive for TNFα or $IFN\gamma^+$ (Fig 3.2.4A-E).

To investigate the impact of intestinal infection on pancreas-reactive $CD8^+$ T cells, similar experiments were performed in T1L infected mice, except that NY8.3 $CD8^+$ T cells were transferred instead of BDC2.5 $CD4^+$ T cells. As before, mice were treated daily with 40mg/kg STZ. NY8.3 cells from infected mice showed little difference in LN retention, and only exhibited minor changes in division rates that were not statistically significant (Fig 3.2.5A, B). Interestingly, NY8.3 cells had increased frequencies of $GranzymeB^+$ and $GranzymeB^+/IFN\gamma^+$ double-positive cells, marking differentiation of cytolytic T cells (Fig 3.2.5C). This effect was limited to the celiac and duodenal LNs, but not the liver LN consistent with the fact that the liver LN is not connected to the duodenum. To test the universality of this phenomenon, an additional virus, MNV was tested in the same conditions. Just as in T1L infected mice, NY8.3 cells from MNV infected mice did not appear different from uninfected controls with respect to LN retention, absolute number, or

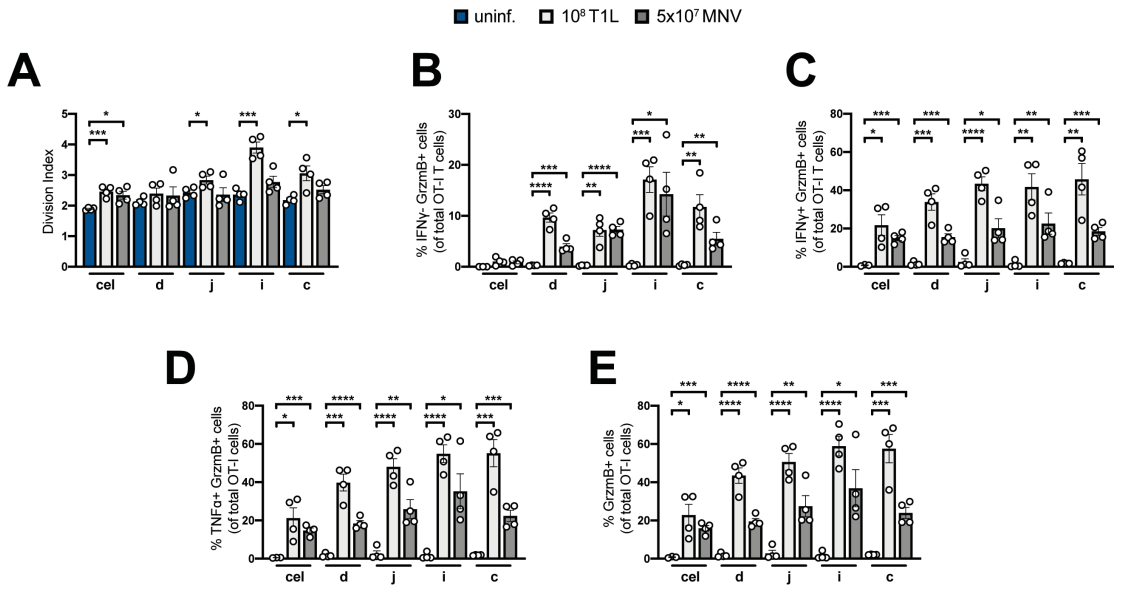

Figure 3.2.4 Oral antigen specific CD8+ T cells become activated upon T1L and MNV infection.

a) Division index of OT-I T cells in indicated lymph nodes 3 days post adoptive transfer of 750k OT-I T cells into B6 mice infected or not with 10^8 PFU T1L or $5x10^7$ MNV 3 days prior and gavaged with OVA and kept on OVA containing drinking water for the duration of the experiment. Frequency of $IFN\gamma^-GranzymeB^+$ (**b**), $IFN\gamma^+GranzymeB^+$ (**c**), $TNF\alpha^+GranzymeB^+$ (**d**), total $GranzymeB^+$ cells in the indicated LNs of uninfected, T1L and MNV infected mice as in **a**. Cel = celiac LN, d = duodenal LN, j = jejunal, i = ileal, c = cecal-colonic LN. *p < 0.05, **p < 0.01, ***p < 0.001,****p < 0.0001 (Student's t test).

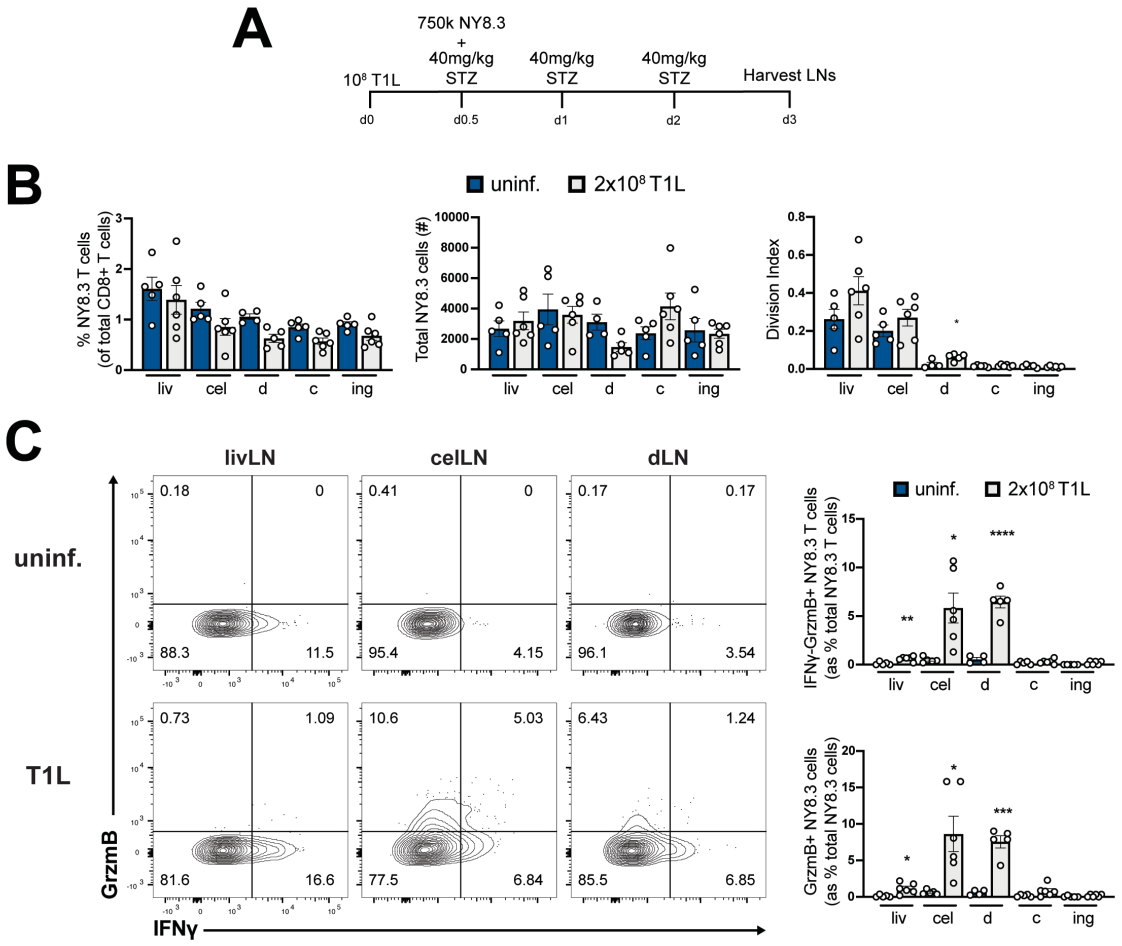

Figure 3.2.5 Pancreas-specific CD8+ NY8.3 cells become activated upon intestinal T1L reovirus infection.

a) Schematic of experimental timing. **b)** Frequency, absolute number, and division index of NY8.3 T cells among TCRβ^{+}CD8^{+} cells in indicated lymph nodes 3 days post adoptive transfer of 750k NY8.3 cells into NOD mice infected or not with 2x10^{8} PFU T1L 3 days prior and treated with 40mg/kg STZ daily, n=4 uninfected, n=5 infected. **c)** Representative flow cytometry plots and frequency of expression (out of total NY8.3 cells) of GranzymeB and IFNγ in the indicated LNs of uninfected and T1L infected mice as in **b**. Liv = liver LN, cel = celiac LN, d = duodenal LN, c = cecal-colonic LN, ing = inguinal LN. *p < 0.05, **p < 0.01, ***p < 0.001,****p < 0.0001 (Student's t test).

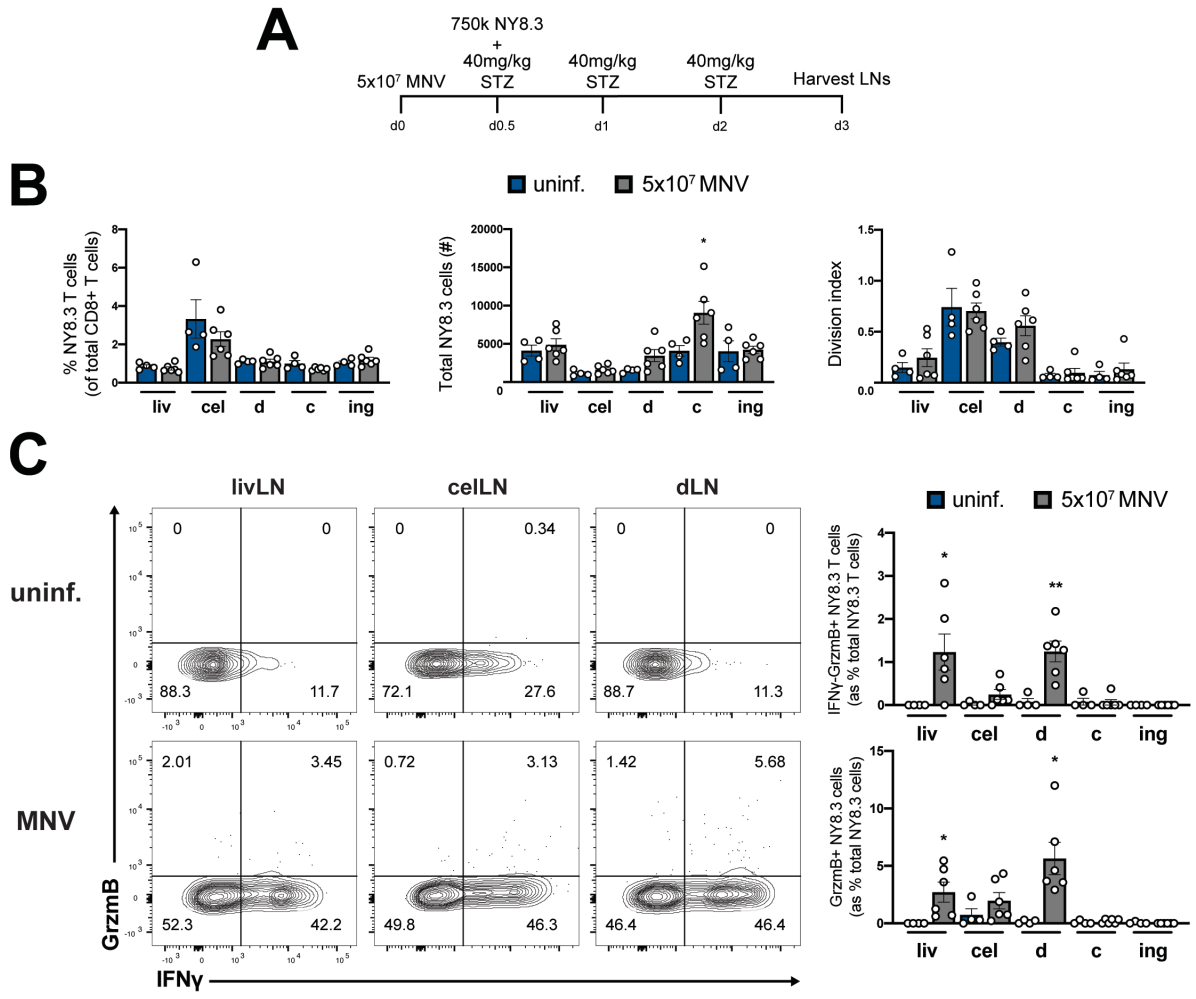

Figure 3.2.6 MNV CW3 infection leads to increased frequency of cytolytic pancreas-specific CD8+ NY8.3 T cells.

a) Schematic of experimental timeline. **b)** Frequency, absolute number, and division index of NY8.3 T cells among TCRβ$^+$CD8$^+$ cells in indicated lymph nodes 3 days post adoptive transfer of 750k NY8.3 cells into NOD mice infected or not with 5x10^7 TCDI50 units of MNV CW3 3 days prior and treated with 40mg/kg STZ daily, n=4 uninfected, n=6 infected. **c)** Representative flow cytometry plots and frequency of expression (out of total NY8.3 cells) of GranzymeB and IFNγ in the indicated LNs of uninfected and T1L infected mice as in **a**. Liv = liver LN, cel = celiac LN, d = duodenal LN, c = cecal-colonic LN, ing = inguinal LN. *p < 0.05, **p < 0.01 (Student's t test).

division index (Fig 3.2.6A,B). The frequency of cytolytic T cells, measured by GranzymeB and IFNγ expression was increased in the pancreatic LNs but not other LNs, consistent with the T1L results (Fig 3.2.6C). One noticeable distinction between the MNV and T1L results was that an increased frequency of cytolytic NY8.3 cells was observed within the liver LN in MNV infected animals. As previously mentioned, the liver LN does not drain the duodenum, so whether the effect of MNV on this LN is due to secondary effects of the infection or some other mechanism is not known at this time.

In light of evidence that STZ treatment can lead to gut microbiome translocation[99], as well as the fact that microbial antigens from NY8.3 *Myd88*$^{-/-}$ mice can mimic the NY8.3 IGRP epitope and lead to the promotion of diabetes[100], it was critical to rule out the possibility that STZ treatment had an effect on the phenotype observed. As before, mice infected with T1L were given an adoptive transfer of NY8.3 T cells but were not treated with STZ. NY8.3 cells from T1L infected mice had increased frequencies of TNFα^{+} and GranzymeB^{+}/TNFα^{+} cells mirroring the results found in STZ treated mice (Fig 3.2.7A, B). Thus, the increased activation of CD8^{+} T cells seen from T1L infected mice is not due to STZ treatment.

Taken together, these data using pancreas-reactive CD8^{+} T cells indicate that intestinal infection, and therefore disruption of the LN, has the power to alter pancreas-reactive T cell responses. These results support the idea that the local LN milieu shapes the immune response to any antigen that enters the LN, complementing the DC gene expression data demonstrating that DC tissue of origin is secondary to the LN to which the DC drains. How only CD8^{+}, but not CD4^{+}, T cell fate is affected remains unclear and is discussed in more detail below.

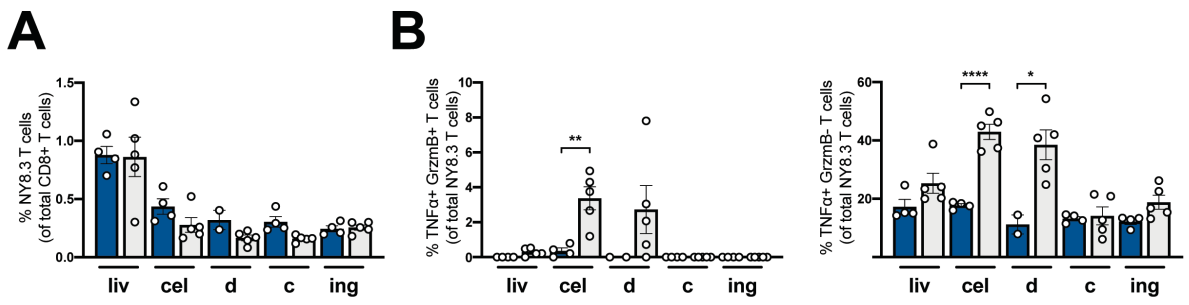

Figure 3.2.7 STZ treatment is dispensable for the generation of cytolytic pancreas-reactive CD8+ T cells during T1L infection.

a) Frequency of NY8.3 T cells among TCRβ^{+}CD8^{+} cells in indicated lymph nodes 3 days post adoptive transfer of 750k NY8.3 cells into NOD mice infected or not with 2x10^{8} PFU of T1L 3 days prior, n=4 uninfected, n=5 infected. **b)** Frequency of expression (out of total NY8.3 cells) of GranzymeB and TNFα in the indicated LNs of uninfected and T1L infected mice as in **a**. Liv = liver LN, cel = celiac LN, d = duodenal LN, c = cecal-colonic LN, ing = inguinal LN. *p < 0.05, **p < 0.01, ****p < 0.0001 (Student's t test).

3.3 Novel tool generation for controlling and tracking antigen origin

Previous attempts to investigate how the source of antigen, whether that be from different tissues or subcellular localization of antigens, impacts immune responses have been limited in many cases by the current set of tools available. In order to address this gap in technology I sought to generate a suite of new mouse lines that would enable more accessible tracking of antigen. The first set of tools focused on generating mice that would enable tissue specific expression of a model antigen: ovalbumin.

Our results demonstrating that intestinal infection can alter pancreas-reactive $CD8^+$ T cell differentiation stands in contrast to the effect we observe for pancreas-reactive $CD4^+$ T cells in which no differences are found. The $CD8^+$ T cell data fit well with the original hypothesis that the local LN milieu shapes the immune response to any antigen that enters the LN, however it cannot be ruled out that technical differences between the two T cell clones may be contributing to experimental differences. It is known that concomitant intestinal infection during oral antigen administration leads to inflammatory T cell differentiation of $CD4^+$ and $CD8^+$ T cells specific to the oral antigen. However, these experiments were performed on the B6 background and utilized different T cell clones (OT-II and OT-I). Therefore, to address whether there are technical differences responsible for discrepancies between the NOD BDC2.5 experiments and the B6 oral tolerance experiments, I sought to generate mice with conditional expression of OVA by knocking in a lox-stop-lox OVA construct into the *Rosa26* locus (Figure 3.3.1A). These mice enable induction of OVA expression in a tissue-specific manner when crossed to different Cre-driver mouse lines. In this way, I have standardized the antigen and T cell clones (OT-II and OT-I) making it straightforward to compare the fate of $CD4^+$ and $CD8^+$ T cells when antigen is confined to the pancreas, the gut or when it is a dietary antigen by feeding OVA. Furthermore, to refine our

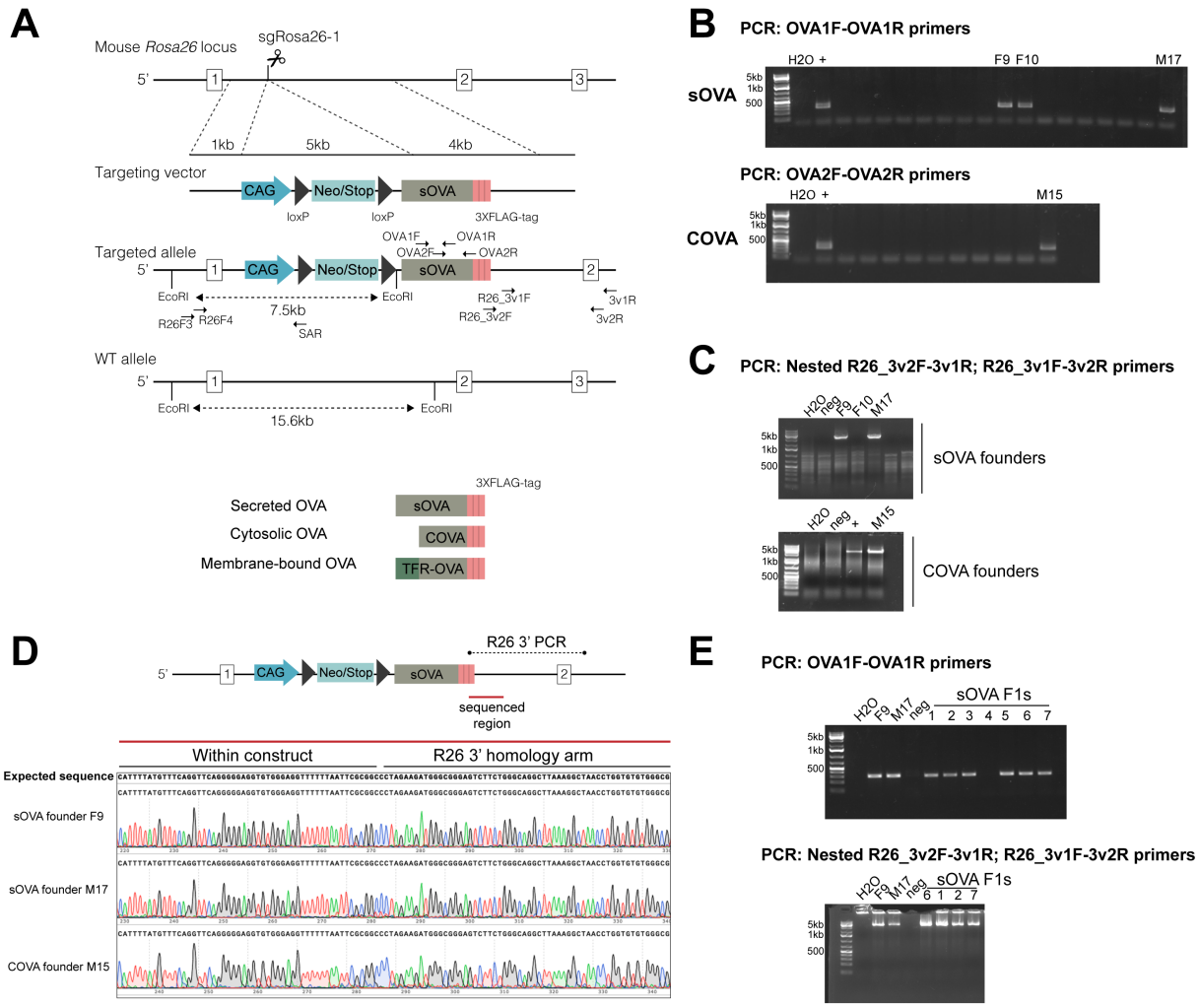

Figure 3.3.1 Generation of novel knock-in mouse lines with tissue restricted expression of OVA subtypes.

a) General schematic of mouse generation via Cas9 Ribonucleoprotein (RNP) delivery. Targeting constructs are designed with asymmetric homology arms that flank a single guide RNA site within the *Rosa26* locus. Secreted OVA (sOVA) is shown as a general example. Arrow heads indicate primer binding sites within the locus. Three different subcellular localizations of OVA were generated: sOVA, cytosolic OVA (COVA), and membrane bound (TFR-OVA). **b)** PCR detection of the presence of OVA in pups derived from microinjection using primers OVA1F and OVA1R. Labels indicate potential founders for either sOVA or COVA as indicated. **c)** OVA positive mice were tested for proper insertion of the knock-in construct by PCR using a nested reaction utilizing primers R26_3v2F and R26_3v1R, followed by R26_3v1F and R26_3v2R. Band of interest is ~5kb. **d)** Sequencing chromatograms of products yielded in **c**, confirming sequence identity of amplified PCR product. **e)** Genotyping to detect OVA presence (top) and proper insertion (bottom) in F1 pups derived from crossing OVA founders to B6 mice.

understanding of how subcellular antigen localization affects T cell outcomes, I have generated multiple versions of OVA confined to different subcellular compartments, placing OVA strictly in the secretory pathway (secreted OVA, sOVA), cytosol (cytosolic OVA, COVA), or cell surface (transferrin-OVA, TFR-OVA) (Figure 3.3.1A). Expression of each OVA version was tested *in vitro* in 293T cells and Ins1 cells by transfection with pcDNA expression constructs containing OVA fused to a 3x FLAG tag driven by a CMV promoter. Each type of OVA was then cloned into *Rosa26* targeting vectors, consisting of a CAG promoter followed by a loxP flanked puromycin cassette (lox-STOP-lox) and then the respective OVA subtype coding region fused with a 3x FLAG epitope tag, flanked by asymmetric homology arms (Figure 3.3.1A)[101].

Pups derived from Cas9/RNP microinjections were genotyped for the presence of OVA using primer sets within the coding sequence of OVA (Figure 3.3.1B), identifying potential founder mice. To confirm insertion of the knock in construct within the correct region, targeting PCR was done to amplify a band spanning from within the construct to outside of the homology arm in the endogenous locus, a novel band that is only present in a correctly knocked in mouse (Figure 3.3.1C). Though three sOVA mice were positive for the presence of OVA, only two of the mice had the presence of targeting bands, highlighting the importance of this control. Sequencing of the PCR products from targeting reactions confirmed the identity of the band, identifying bona fide founder mice (Figure 3.3.1D). For the sOVA mice, 2/22 mice were considered founders, for COVA mice 1/10 were founders and for TFR-OVA mice 3/13 were founders. Founder mice were then backcrossed to B6 mice for one generation, resulting in F1 mice. All founders successfully passed on the knock-in allele to their progeny (Figure 3.3.1E) based on PCR for the presence of OVA and proper targeting of the inserted construct.

Confirmed F1 mice were then used to cross to tissue specific Cre driver lines. Since the mice express a lox-stop-lox version of OVA, protein expression could only be interrogated after mice have been crossed to a Cre line. I am particularly interested in pancreas and gut derived antigens so I focused my efforts on crossing the mice to *Ptf1a*^{CreERT}, *Ins1*^{Cre}, *Ins1*^{CreERT2}, and *Villin*^{CreERT} mice. To check protein expression, CFSE labeled OT-II T cells were adoptively transferred into *Rosa26*$^{LSL\text{-}sOVA/wt}$ *Ptf1a*^{CreERT} mice previously treated with tamoxifen and proliferation was assessed in the various LNs four days later. Consistent with tissue specific expression, robust proliferation was observed in the pancreatic LNs but not in the cecal-colonic or inguinal LNs (Figure 3.3.2A).

In parallel, I wanted to generate a system in which I could visually track the origin of antigen within the shared pancreatic duodenal LNs. Such a system would allow for identification of the different types of DCs that uptake antigen and whether the subtype of DC or localization of antigen loaded DCs differs depending on the tissue source. My initial efforts focused on utilization of tissue specific expression of fluorescent proteins, thereby generating a source of fluorescent antigen that could be taken up by DCs within the tissue or the draining LNs. While these kinds of systems have worked for exogenous proteins[102], continued fluorescence is dependent on the tertiary structure of the fluorescent protein remaining intact. Using *Rosa26*$^{LSL\text{-}Tdtomato/wt}$ *Villin*^{CreERT} I found that 10% of the CD103^{+}CD11b^{-} DCs within the gLNs were Tdtomato^{+} as early as 48 hours after tamoxifen treatment (see Fig 3.1.16B,C). However, in *Rosa26*$^{LSL\text{-}Tdtomato/wt}$ *Ins1*^{CreERT2} and *Rosa26*$^{LSL\text{-}Tdtomato/wt}$ *Ptf1a*^{CreERT} mice treated with tamoxifen I did not observe any Tdtomato^{+} cells within the pancreatic LNs, likely due to intact antigen levels falling below the limit of detection in this assay.

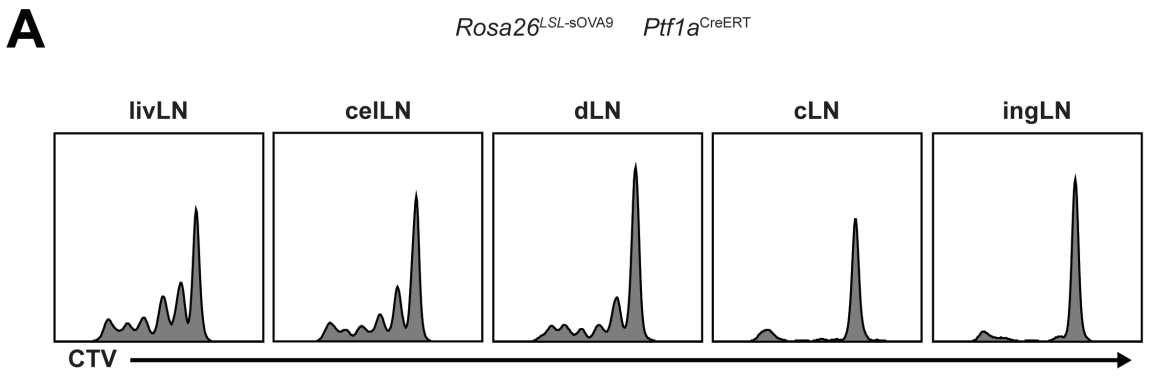

Figure 3.3.2 Validation of OVA knock in mice.

a) Flow cytometry plots displaying CTV dilution of 400k labelled OT-II T cells 5 days after transfer into *Rosa26*$^{\text{LSL-sOVA/wt}}$ *Ptf1a*$^{\text{CreERT}}$ mice previously treated with five consecutive doses of tamoxifen ending 5 days prior.

To overcome this problem, I have generated a new mouse which would label and therefore track a much larger range of pancreatic antigen. To do this, I generated a new mouse line containing a floxed-stop promiscuous biotin ligase that allows for nonspecific labeling of pancreatic proteins with biotin. Unlike natural BirA, the mutant BirA-R118G, hereby referred to as BirA*, indiscriminatingly biotinylates proteins in close proximity[103]. This approach has been classically used fused to a protein of interest to identify potential binding partners, though a cytosolic version has been demonstrated *in vivo* to nonspecifically biotinylate cytosolic proteins in the presence of supplemented biotin[104]. I confirmed through *in vitro* expression experiments that cytosolic BirA* expresses and is capable of biotinylating cytosolic proteins (Fig 3.3.4B). Using a very similar approach to the OVA knock in mice described above, a construct containing a CAG promoter, followed by a loxP flanked puromycin cassette (lox-STOP-lox) and then the HA-tagged BirA* coding sequence, flanked by asymmetric homology arms (Fig 3.3.3A). Pups from the BirA* microinjection were genotyped for the presence of BirA* using two primer sets within the BirA* coding region (Fig 3.3.3B). Positive pups will be checked for the proper targeting of the knock-in construct into the locus by PCR and sequencing. At the time of writing, these mice were in the process of breeding to B6 mice for F1 generation. These mice will then be crossed to the aforementioned Cre driver lines to generate tissue specific expression of BirA*. Upon tamoxifen administration, any APCs in the pancreas or lymph node that have acquired antigen should stain positive by streptavidin staining. This model overcomes the potential sensitivity issues and degradation issues of the tdTomato mouse since significantly more antigen will be biotin-labeled and protein cleavage is less likely to disrupt biotinylation status once inside the APC.

Given the importance of secretory antigens in autoimmunity, I wanted to generate an additional model in which BirA* is restricted to the secretory compartment by fusing BirA* to the

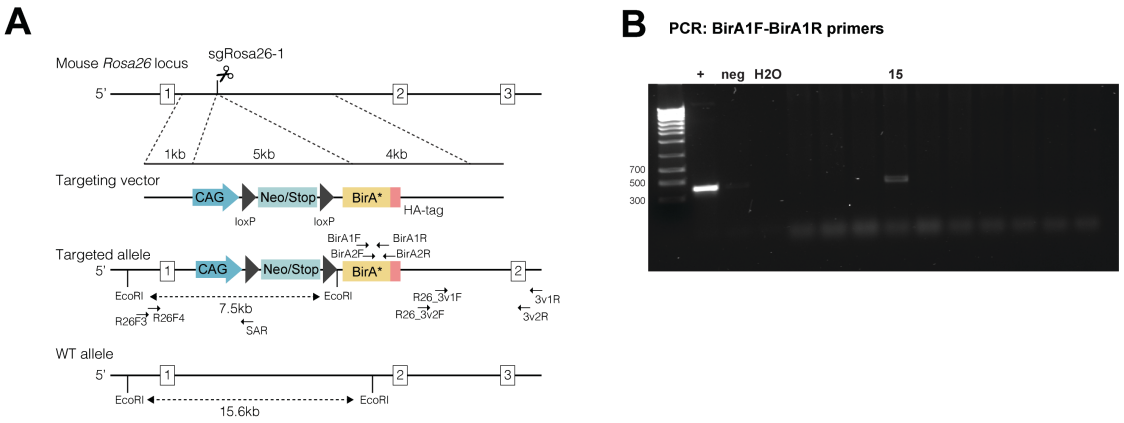

Figure 3.3.3 Generation of BirA* mice.

a) General schematic of mouse generation via Cas9 Ribonucleoprotein (RNP) delivery. Targeting constructs are designed with asymmetric homology arms that flank a single guide RNA site within the *Rosa26* locus. Arrow heads indicate primer binding sites within the locus. **b)** PCR detection of the presence of OVA in pups derived from microinjection using primers BirA1F and BirA1R. Labels indicate potential founders for BirA*.

transmembrane domain (TMD) of a secretory granule resident protein. In this way, secreted proteins could be biotinylated but BirA* itself would not be secreted, confining the biotinylation to secreted proteins only from the cell expressing BirA* rather than any antigen in the proximal extracellular region. Based on a previous report that the putative TMD of prohormone convertase (PC1/3) was sufficient to localize a fusion protein to the secretory granule, I generated a BirA* fusion protein (Fig 3.3.4A). The first iteration of this construct utilized the insulin signal peptide, and the rat prohormone convertase TMD coding sequence. The expression of this construct *in vitro* in 293T and Ins1 cells did not reach the levels of the cytosolic protein, especially noticeable in Ins1 cells (Fig 3.3.4B). Furthermore, the fusion protein did not localize to the secretory granules as expected (Fig 3.3.4C). In order to address these issues, I generated several different versions of the construct, adding in a linker between BirA* and the TMD, switching out the signal peptide to the mouse PC1/3 signal peptide, and exchanging the TMD for C-terminal regions of mPC1/3 that have been previously shown to mediate granule localization. In all cases, the expression of these constructs was still suboptimal (Fig 3.3.4B), and the localization never appeared granular (data not shown). Future work will focus on generating additional BirA* fusion proteins, focusing on the TMD of Vamp2. Once a construct has been optimized *in vitro*, it will be then knocked into the *Rosa26* locus exactly as the cytosolic BirA* was. This system would allow for sensitive tracking of secreted antigens and permit comparisons of which type of APCs uptake cytosolic vs secreted antigens and how the type of antigen may affect APC localization within the LN.

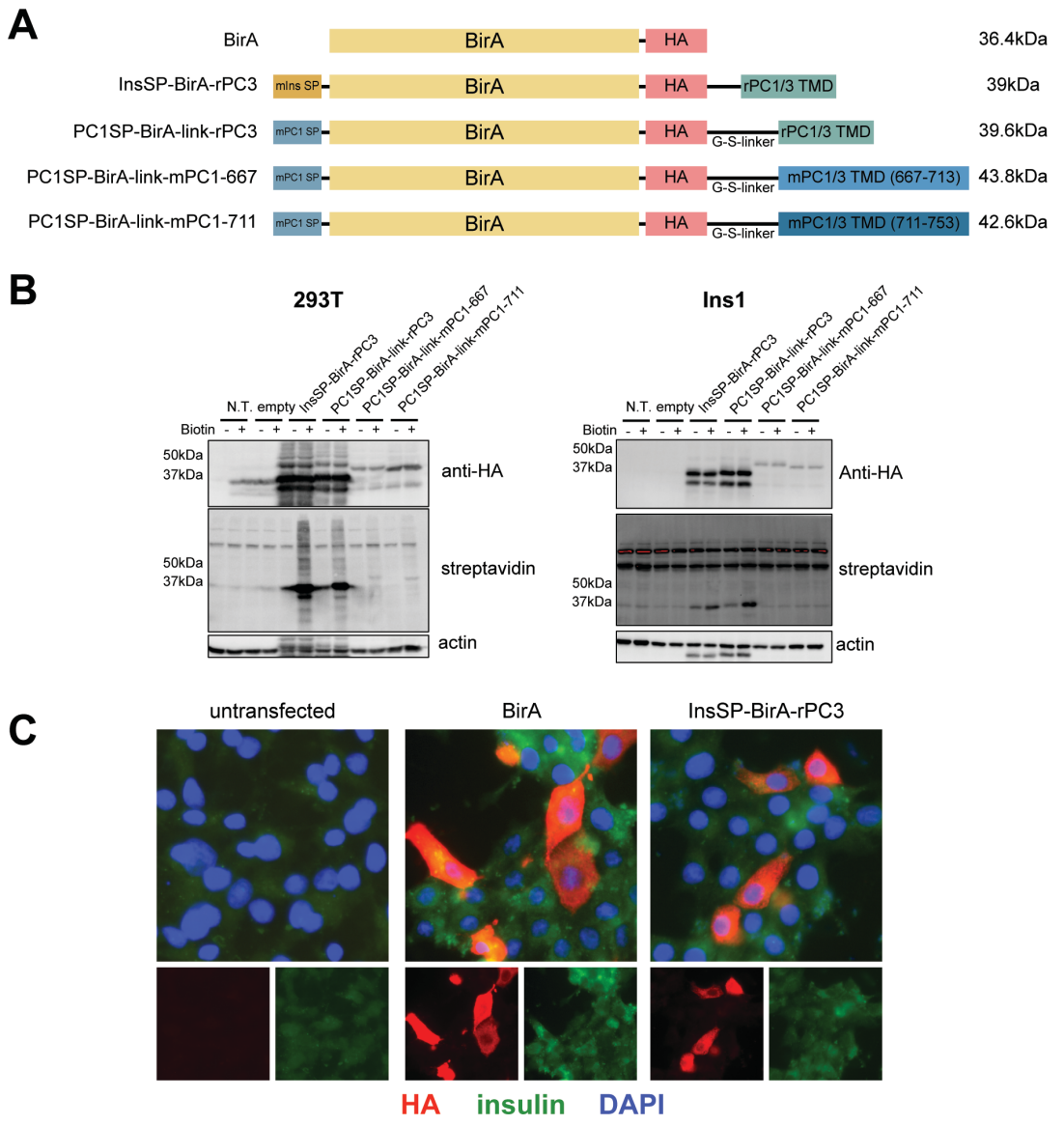

Figure 3.3.4 Optimization of secretory granule restricted BirA*.

a) Schematic of various BirA* fusion constructs to target BirA* to the secretory granule. **b)** Protein expression and biotinylation measured by western blot from 293T and Ins1 cells transfected with indicated constructs with or without 50uM biotin supplementation. Fusion proteins were probed by rabbit anti-HA followed by anti-rabbit HRP while biotinylation was probed by streptavidin-HRP. Anti-actin as a loading control. **c)** Immunofluorescence of indicated constructs transfected in Ins1 cells. Constructs were visualized by anti-HA staining and co-stained with anti-insulin and DAPI.

4. DISCUSSION

4.1 Characterization of effects of tissue of origin on migratory DCs in shared lymph nodes

4.1.1 Tissue specific signatures of migratory DCs

While it has been appreciated LNs are shared between the pancreas and the duodenum in both mouse and human, the immunological consequences and mechanisms that enable this functionally are not well understood. This phenomenon is quite prevalent in the human lymphatic system, where a number of LNs are shared across the digestive system including the stomach, gallbladder and even the lower limb system[105]. The concept of common lymph nodes between multiple organs contrasts heavily with the fact that the lymph nodes draining the intestine are compartmentalized by intestinal segment, though why this is the case remains unclear. Given the importance of LNs and specifically APCs in the induction of adaptive immunity, I took a DC-centric approach to evaluate how DC function may differ according to tissue of origin, if at all. Prior to this thesis, an in-depth characterization of the relative contribution of DCs from each organ within these shared LNs had not been performed. The experiments taken here aimed to address whether there was compartmentalization within a LN, such that DCs from each organ were kept separate, either by location or gene expression or if DCs were more or less equivalent once in the shared LNs. From previous data comparing migratory DCs across different gLNs, it is known that DCs express distinct profiles in the duodenal LNs versus the cecal-colonic LNs[15]. Furthermore, DCs from different tissues, as well as in different contexts such as infection and cancer are known to have unique profiles[48,106,107]. However, in the context of shared LNs whether DC imprinting at the level of the originating tissue is more important versus the LN environment is not well understood. The experiments

performed here attempt to track the tissue signature of DCs within shared pancreatic-duodenal LNs to understand how gene expression profiles in the LN as well as localization are informed by their tissue of origin. The approach focused on establishing a DC tissue of origin signature for the pancreas, liver and duodenum using bulk RNA sequencing and then comparing these signatures to migratory DC subsets identified by single cell sequencing (scRNAseq) of the shared LNs. The expectation was that there would be a strong correlation between the tissue of origin signature and the various migratory DC clusters in the LN.

Using differential gene expression analysis and compilation of the pairwise comparisons, I generated sets of genes specific to each tissue, representing the tissue signature. It is important to note that since only the pancreas, liver and duodenum were profiled, genes may not be truly specific to one of these tissues when assessed globally to all other tissues in the host, but within the three tissues these genes can distinguish DCs from each tissue relative to the other two tissues. Certain genes identified in the tissue signatures were expected such as *Aldh1a2* which is known to be expressed in gut derived DCs and important for tolerogenic immune responses in the duodenal LN. On the other hand, some genes were very surprising to see expressed in DCs such as *Ly6a* expression in liver-derived DCs. *Ly6a* encodes the protein Sca-1, which is classically used as a marker of tissue resident stem cells and is also expressed during lymphocyte development. Interestingly, liver-derived DCs expressed two other stem cell related genes *Id3* and *Cd34*, though the function of these stem cell related genes in liver migratory DCs is unclear. Expression of *Id3* has been shown to prevent plasmacytoid DC development, instead pushing cells toward a cDC fate[108]. Since plasmacytoid DCs are the dominant DC population within the liver[109], it is possible that expression of *Id3, Cd34* and *Ly6a* somehow contributes to the maintenance of the cDC1 fate by $CD103^{+}CD11b^{-}$ DCs in this tissue, or that these are markers of

immature DCs within the liver. The latter can be tested by flow cytometry by looking at expression of other markers of DC activation such as CCR7 and CD80/86. The pancreas derived DCs had a very limited number of tissue specific genes, the highest expressing being *Anxa2* and *Ccl6*, though a role for these genes in DCs is not well characterized. In contrast, the duodenal-derived DCs had over 40 genes that were unique to its DCs compared to the liver and pancreas. Gene ontology (GO) analysis on the list of duodenal-enriched genes did not return any significant GO terms, making it difficult to ascribe a function to these genes. Notably, a large number of genes were enriched in both pancreatic DCs and liver DCs compared to duodenal DCs such as *Ccl5*. Whether this is biased due to the sampling of only these three tissues, or truly reflects a strong similarity between the pancreas and the liver DCs cannot be determined at this time.

4.1.2 Single cell sequencing of migratory DCs in shared LNs

Interestingly, when I performed the complementary experiment of scRNA of the migratory DCs within the LN, I found that many of the tissue specific signatures of DCs are dampened in the LN. While some marks of the tissue of origin remain, the majority of the DCs seem to lose expression of many of the genes identified in the tissue, instead upregulating a number of genes across the three assayed LNs. This could be due to two major possibilities. First, the tone of the LN overrides the DC tissue imprint such that DCs that enter the LN become much more homogenous regardless of their tissue of origin. In this case, the LN exerts a LN specific gene expression profile. Alternatively, it is possible that the DCs that migrate to the LN are a specific subset of DCs from the tissue that do not express the same tissue signature as the total population. This could be due to the fact that these DCs took up antigen and therefore undergo another step of maturation. Since the tissue signature was determined using bulk RNA

sequencing the expression profiles of the genes may actually be heterogeneous amongst DCs, meaning it is possible that the cells that migrate to the LN did not express those genes in the first place. Without single cell sequencing of the DCs from the tissue this is difficult to rule out entirely. One other caveat of these experiments is that some of the tissue specific genes identified by bulk RNAseq are similar to well described non hematopoietic genes such as *Alb* expression in the liver DCs. The expression level of many of these genes is quite low, which may reflect engulfment of tissue cells like a hepatocyte rather than true DC expression. This could be in part caused by the digestion process used to analyze the cells, but would not be a true concern *in vivo*. Therefore, the loss of expression in the LN compared to the tissue would reflect degradation of engulfed material rather than true downregulation of gene expression. To prove these genes are specifically expressed by DCs and are not due to engulfed debris, it will be important to stain each tissue in the absence of digestion, which can artificially enrich for this kind of phenomenon. Additionally, epigenetic profiling such as Assay for Transposase-Accessible Chromatin using sequencing (ATAC-seq) could be used to confirm chromatin accessibility at the promoters of each tissue specific gene. Ultimately, the goal of these studies is to identify markers that can be used for staining or use in a fate mapping/reporter mouse to distinguish DCs of multiple origins within the LNs. Therefore, it will be very important to clarify whether DCs truly express all of the identified tissue specific genes.

Nonetheless, the scRNAseq identified multiple clusters of migratory DCs within the LNs and some of the defining genes of these clusters correlate with a tissue of origin, such as the *Anxa2*$^{+}$ cluster potentially being derived from the pancreas (expressing both *Anxa2* and *Fcer1g*) and the *Il1b*$^{+}$ cluster originating from the duodenum (expressing both *Il1b* and *Apol7c*). The remaining clusters are not easily traceable to a specific tissue of origin. Rather, these clusters

may reflect unique states in the LN, such as the time spent in the LN. It is known that DCs, once in the LN only survive for 3-4 days before dying. Therefore, if the tissue signature is being lost during either exit from the tissue or entrance to the LN then the clusters of DCs in the LNs may each represent different states of cells in that process, including clusters that are recently arrived to the LN and may still contain a mark of their origin, or cells that have been in the LN for days and no longer express tissue distinguishing genes. To address this question, it may be necessary to generate fate mapper or reporter mice for tissue specific genes within the pancreas, liver and duodenum. Reporter mice have the caveat that if the expression of the gene declines between the tissue and the LN, the level of reporter may mirror this and then become difficult to assess reporter positive cells once in the LN. The fate mapping approach would overcome this by permanently labeling any cell that expresses the tissue specific gene, thereby allowing visualization of those cells in the LN regardless of if they are still expressing the gene. It is unlikely that the genes I have identified are unique to DCs, and may be expressed in multiple cell types and even at different stages of development. Thus, designing the fate map mouse such that expression of the tissue specific gene drives the expression of an inducible Cre such as CreERT2 may be the most useful. Until true fate map mice can be generated, the *Rosa26*$^{\text{LSL-Tdtomato/wt}}$ mice can be used as the best proxy for fate mapping. One marker that is maintained at the protein level in the LN is Sca-1 which is highest in the liver and can be detected in the liver LNs. *Ly6a* expression is significantly decreased in the LN and this is reflected in a decreased MFI of Sca-1 staining in the LN, likely indicative of downregulation. Using *Rosa26*$^{\text{LSL-Tdtomato/wt}}$ mice transduced with Adenovirus-Cre, or B6 mice transduced with Adenovirus-GFP, thereby turning on Tdtomato or GFP expression in the liver, respectively, Tdtomato^{+} or GFP^{+} cells in the LN could be stained for Sca-1 to see how the signals overlap. If the LN environment is leading to

downregulation of tissue specific markers, one would expect the remaining Sca-1^{lo} cells in the LN to also be Tdtomato^{+}.

The tone of the LN is likely set by a number of factors, ranging from the tissues it drains to the resident cells that make up the LN structure, in particular the stromal cells. The tolerogenic potential of the duodenal LN has been demonstrated to be heavily dependent on the stromal cells that contribute to the LN structure[15,20]. Even after transplant of the LN to the popliteal fossa, effectively eliminating the effect of lymphatic drainage to the LN, the tolerogenic properties are still maintained[20]. Future directions in the lab will evaluate which factors are most dominant in setting the LN tone.

4.1.3 Validation of RNA sequencing data

Despite all of the sequencing, there is still a lack of readily available markers that can distinguish DCs by their tissue of origin. This has hampered my ability to visualize where DCs from each tissue localize once they reach the LN by microscopy. While the sequencing data indicate that the DCs lose a large part of their tissue of origin signatures, it is still possible that the afferent lymphatics that bring the DCs from the tissue to the LN results in distinct distribution of cells throughout the LN. In general, studies have shown that specific subsets of DCs such as cDC1s vs cDC2s localize to unique niches within the LN, with the cDC1s favoring a location deeper within the T cell zone while cDC2s localize to the interfollicular region. However, whether pancreas-derived and duodenal-derived DCs are found clustered in specific regions or randomly spread throughout the LN is currently unknown. Ongoing experiments in the lab utilizing the *Rosa26*$^{\text{LSL-Tdtomato/wt}}$ *Villin*$^{\text{CreERT}}$ mice, thereby labeling cells that have taken up duodenal antigen will help us clarify whether DC localization is distinct. Though this only looks at one tissue derived subset, if the Tdtomato^{+} cells from this experiment are found to be

distributed throughout the LN, this supports a model in which DCs are not sub-compartmentalized within the LN according to tissue of origin.

A major arm of the project that has not yet been addressed is to understand the dynamics of the DCs in shared LN during times of tissue specific stress. I am most interested in the effect of duodenal infection on DCs derived from the pancreas and the liver. Based on the DC sequencing data and the pancreas-specific $CD8^+$ T cell data (discussed more below), the overall LN environment seems to play a critical role in shaping DC expression profiles, and therefore T cell outcomes. However, the evidence that DCs from each tissue in the LN are equally affected by intestinal infection is currently missing. Ideally, DCs that correspond to each tissue of origin could be sorted after intestinal viral infection to compare expression of IFN-stimulated genes (ISGs). However, since the expression data indicates a homogenization in the LN, a fate map approach will need to be taken. Again, in the meantime until fate-mapping mice can be generated, ongoing experiments using *Rosa26*$^{\text{LSL-Tdtomato/wt}}$ *Villin*$^{\text{CreERT}}$ mice will test whether $Tdtomato^+$ and $Tdtomato^-$ in the shared LNs express similar levels of ISGs after T1L and MNV infection. If the level of ISG expression is equivalent between $Tdtomato^+$ and $Tdtomato^-$, it would suggest the inflammation of the LN equally affects all the DCs, regardless of their origin, further supporting the role of the LN environment rather than tissue origin in shaping DC function. These results could be complemented by microscopy and flow cytometry approaches to see if $Tdtomato^+$ and $Tdtomato^-$ cells differ by localization or expression activation markers such as CD80/86 after viral infection.

In sum, these results support a model in which the tone of the LN offsets the tissue of origin signature of migrating DCs, generating a more homogenous pool of DCs. In the case of shared LNs, this may enable one tissue to influence a connected tissue in a more direct way by

altering the tone of the common LN. While the tissue signature seems downregulated across the liver, celiac and duodenal LNs in a similar manner, the LN specific environment is not identical. Differences in lymph node tone are likely still informed by the tissues from which each LN receives lymph in addition to other factors such as resident cells of each LN. Assuming all DC subtypes would be similarly influenced by the lymph node tone, we have preliminarily investigated differences in gene expression of the resident cDC2s. Utilizing the same scRNAseq dataset, after subsetting on the resident cDC2s, we find there are some differences in the cell concentration within clusters among each LN type, where cluster 3 is enriched in the celiac and duodenal LNs, while cluster 2 appears to be more enriched within the liver LN (Figure 4.2.1A). Furthermore, using the defining genes of the migratory DC *Il1b*$^{+}$ cluster to generate a signature score (*Apol7c*, *Pla2g7*, *Cd1d1*, *Car2*, *Dnah2*, *Ccnd2*, *Pou2f2*, *Fndc5*, *Rnase6*, *Apol10b*, *Herpud1*, *Nr4a2*) we find this is enriched within cluster 3, the same cluster that shows an enrichment within duodenal draining LNs (Figure 4.2.1B). While these results are still very preliminary, they speak to the potential influence of the LN tone on multiple DC subtypes and not exclusive to the migratory populations. Future experiments in the lab will expand upon these observations and additionally investigate the contribution of various components to the LN tone which may clarify how each shared LN arrives at a set point.

4.2 Influence of the duodenum on pancreatic immunity

4.2.1 Consequences of duodenal infection on pancreas-reactive CD4^{+} and CD8^{+} T cells

A key aim of this thesis was to explore the consequences of shared LNs between the pancreas and duodenum on tissue specific immune responses, particularly T cell responses. The fact that the pancreas also drains to the tolerogenic LNs of the duodenum raised the question of whether the tendency to induce tolerance in these LNs also applied to other antigens in the LN

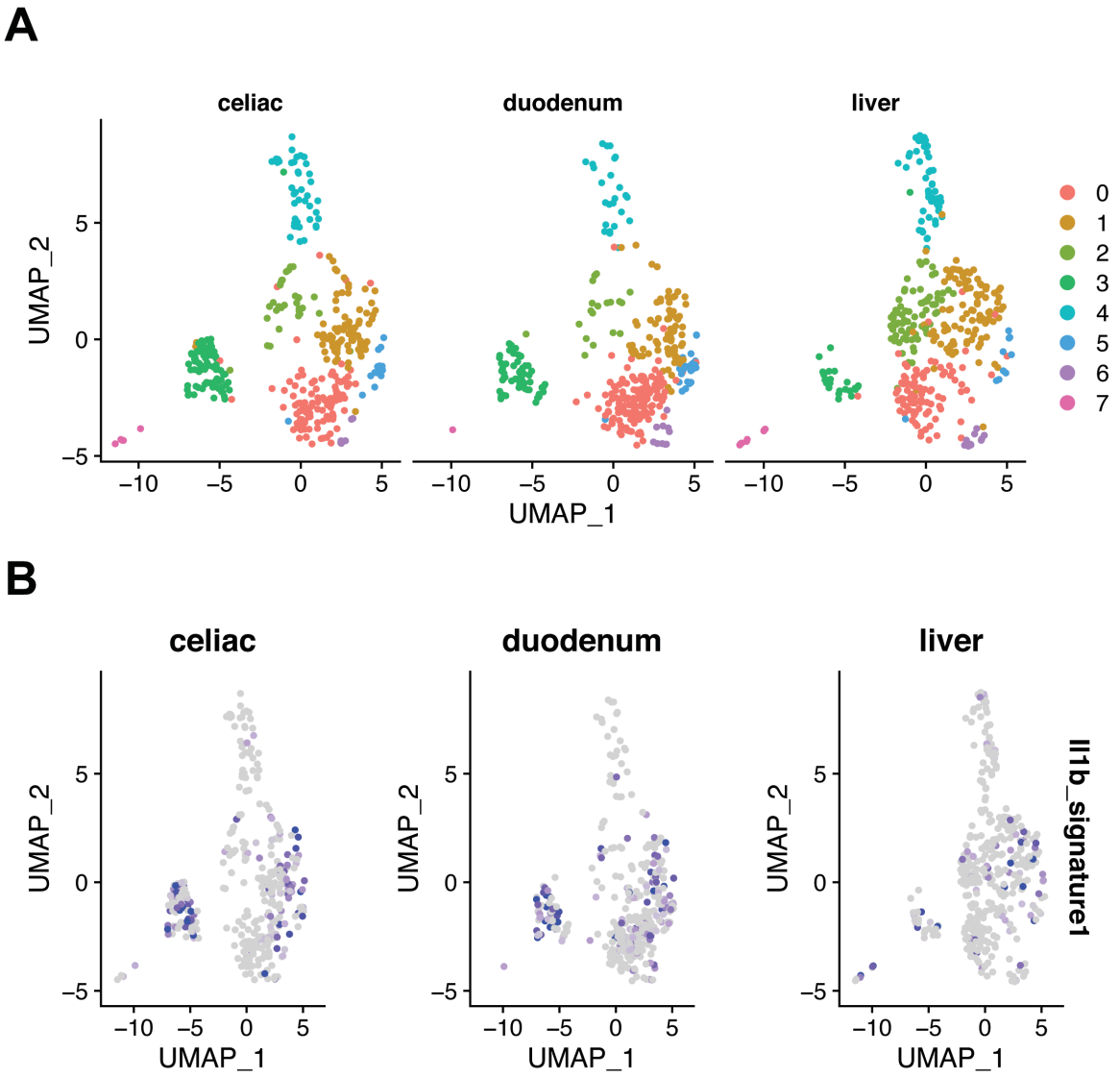

Figure 4.2.1 Dimensionality reduction of resident cDC2s by lymph node.

a) UMAP of resident cDC2s within each LN sample downsampled to an equivalent of 377 cells. **b)** Migratory DC *Il1b*$^{+}$ cluster signature (*Apol7c*, *Pla2g7*, *Cd1d1*, *Car2*, *Dnah2*, *Ccnd2*, *Pou2f2*, *Fndc5*, *Rnase6*, *Apol10b*, *Herpud1*, *Nr4a2*) projected onto resident cDC2 UMAP.

such as pancreatic antigens. Evolutionarily, it would make sense to coordinate immune responses across both tissues given the functional and physical connections of the pancreas and the duodenum. However, during times of tissue specific stress such as an intestinal infection, linkage of immunity between multiple tissues raises the possibility of unintended immune responses towards the unaffected tissue, posing a potential threat to homeostasis.

Previous data from our lab and others has demonstrated that intestinal infection during oral antigen introduction led to impaired oral tolerance induction, often accompanied by significant changes to the LN environment[15,48,49,98]. I utilized the same infections to test whether pancreas-specific immunity was altered by intestinal infection as a result of sharing LNs with the duodenum. My initial experiments focused on pancreas-specific $CD4^+$ T cells using the BDC2.5 clone since the oral tolerance experiments showed phenotypic changes to oral antigen specific $CD4^+$ T cells. Surprisingly, across many different types of infection, the BDC2.5 T cells did not show any alterations in activation or differentiation. In all cases, an endogenous T cell response, albeit lower than what is seen in B6 mice, to the infection was produced, indicating the lack of pancreas-specific $CD4^+$ T cell responses was unlikely due to lack of infection. These results were not consistent with the hypothesis that the LN environment influences any response to antigen regardless of the antigenic origin. Unfortunately, however, the oral tolerance experiments and BDC2.5 experiments are performed in different mouse strains, B6 and NOD respectively. Thus, it is very difficult to compare the LN environments in an exact way since tools to investigate oral antigen specific T cells are lacking on the NOD background. One way this could be addressed is using B6.g7 mice which express the MHC class II allele I-A^{g7} from NOD mice but otherwise are on a B6 background. In this way, the response to oral antigen and pancreatic antigen could be compared at the same time by infecting mice with the desired pathogen, feeding OVA and

transferring both BDC2.5 cells and OT-II cells. Alternatively, to eliminate potential differences in infection potency between mouse strains, I have generated B6 mice that have pancreas specific expression of a model antigen (discussed more below). Additionally, cognate peptides for BDC2.5 of NY8.3 T cells can be fed to NOD mice to evaluate what the response is to peptides when introduced through an oral setting to compare to the natural source of the pancreas.

The infections previously demonstrated to interfere with the induction of oral tolerance were hypothesized to do via disruption of the pTreg generating properties of the cDC1 population $CD103^{+}CD11b^{-}$ DCs. Despite these pTreg inducing properties, the cDC1s have classically been viewed as the prominent $CD8^{+}$ T cell priming DC subset. The fact that this DC subset is the main migratory population in the pancreas and the liver prompted us to check whether pancreas-specific $CD8^{+}$ T cell priming was impacted by duodenal infection. Using NY8.3 IGRP-reactive $CD8^{+}$ T cells, I found that duodenal infection led to increased activation and cytolytic potential of pancreas-reactive $CD8^{+}$ T cells. These results indicated that duodenal infection did indeed have the capability to influence pancreas-specific immune responses. Since T1L and MNV are not reported to infect the pancreas or liver, these data point to a critical role in the shared LNs in mediating this cross-talk.

Collectively, the results of the pancreas-specific $CD8^{+}$ and $CD4^{+}$ T cell transfers during intestinal infection raise very important questions about the mechanisms of duodenal influence on pancreatic immunity. If the LN tone is truly responsible for imparting the effect from the duodenum onto pancreas specific responses, why would this effect be limited to only $CD8^{+}$ T cells? Is this a reflection of differential imprinting on DC subsets (cDC1 vs cDC2) or is this an

artifact of using transgenic T cells? Additionally, what is the physiological consequence of this duodenal influence? How does this impact disease progression?

4.2.2 Discordance between pancreas-reactive CD4$^+$ and CD8$^+$ T cell phenotypes

First, I will focus on the discordance between CD4$^+$ and CD8$^+$ phenotypes within the pancreatic-duodenal LNs. The cDC1 sequencing discussed in Section 4.1 supported an active role of the LN environment in shaping DC gene expression profiles such that migratory cells from each tissue converged on a similar profile once inside the shared LNs. While we do not yet know about how DC expression profiles change during infection, the hypothesis would be that since the tone of the LN would be altered by duodenal infection, all DCs would be similarly affected. This idea would be consistent with the NY8.3 CD8$^+$ T cell responses that were found in response to T1L and MNV infection. These results point to a model in which intestinal infection leads to an inflammatory tone within the draining LNs, thereby altering DC expression profiles and leading to activation of CD8$^+$ T cells to both pancreas and duodenal derived antigen even though the infection is only present within one tissue (Figure 4.2.2). What this model cannot account for is the difference in phenotype between pancreas reactive CD4$^+$ and CD8$^+$ T cells. Presumably, if the LN tone is affecting cDC1s of each origin, it is likely that the other DC subsets within the LN are similarly affected. Studies have demonstrated that cDC2s are the primary CD4$^+$ T cell priming subset[110], which then allows CD4$^+$ T cells to license cDC1s to activate CD8$^+$ T cells[111,112]. A recent study by Murphy and colleagues has shown that in the context of tumor antigens, it is actually cDC1s that prime early CD4$^+$ T cell responses[113]. These observations coupled with the DC profiling of this thesis would therefore predict alterations to CD4$^+$ BDC2.5 T cell fate during intestinal infection. At this time, the reasons for this discrepancy are not clear. One possibility is that this is due to technical issues either as a result of

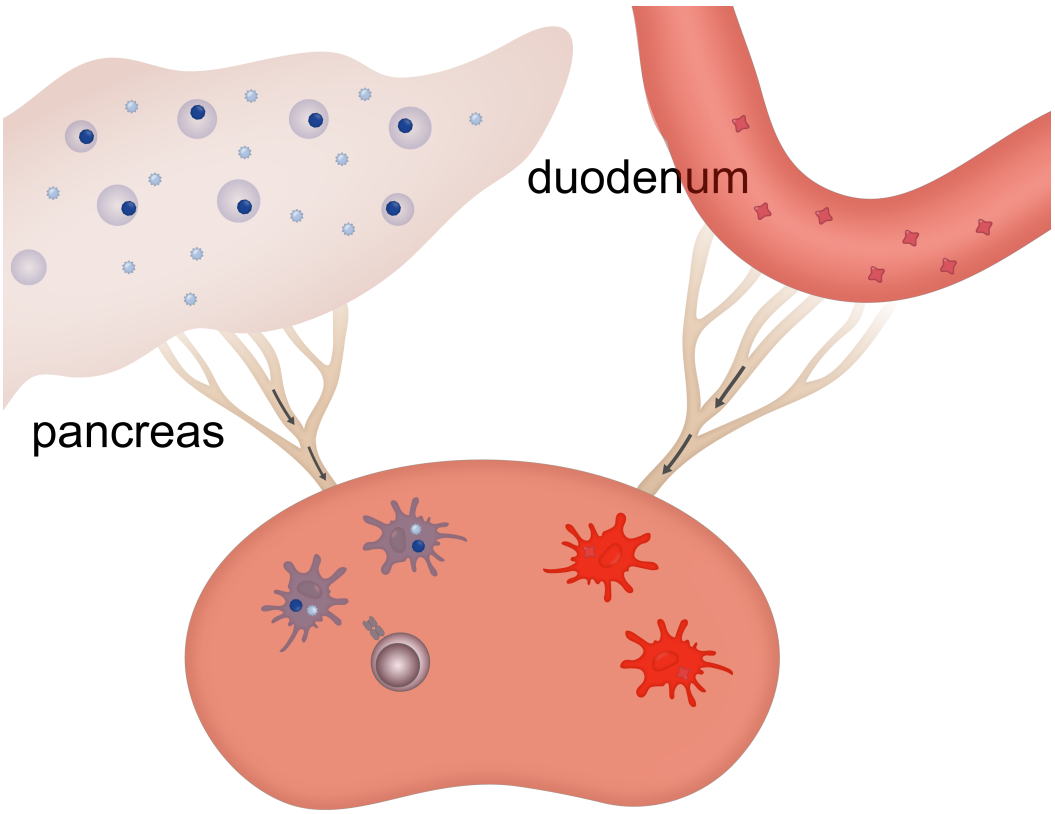

Figure 4.2.2 Model of pancreatic-duodenal immune axis.

Model depicting duodenal influence on pancreatic immunity. Intestinal infection (affecting duodenum) generates an inflammatory environment within the lymph node, characterized by activated DCs. Although the pancreas remains uninfected, activated DCs (either from the pancreas or duodenum) within the LN can present pancreatic antigen leading to induction of activated pancreas-specific T cells.

the mouse strain, or some nuances of the transgenic T cell that prevent its activation towards Th1 fates. The latter scenario is unlikely, given that transfer of T-bet deficient (*Tbx21*$^{-/-}$) BDC2.5 T cells does not lead to diabetes unlike their WT counterparts, indicating that BDC2.5 T cells are capable and in fact dependent on T-bet expression for pathology[114]. Future experiments discussed in more detail below using the novel model antigen expressing mice will aim to address whether technical issues explain this phenotype.

Biologically, the lack of changes to pancreas-reactive CD4$^+$ T cells could be due to differences in CD4 and CD8 T cell activation processes. The time required to initiate the activation of CD8$^+$ T cells seems to be lower than that of CD4$^+$ T cells[36]. Furthermore, CD8$^+$ cells are more flexible in the requirement for continuous antigen stimulation. After an initial strong antigenic encounter CD8+ but not CD4+ T cells can continue to divide with discontinuous antigen[115]. Since BDC2.5 T cells and NY8.3 T cells respond to unique antigens, it is possible that variability in antigen availability may influence the phenotypes observed. It is interesting to note that the actual stimulating peptide for BDC2.5 T cells is a very controversial subject. While it is clear that the peptide comes from the protein chromogranin A (ChgA)[68], native peptides derived from ChgA are only weakly stimulatory. Studies have reported that hybrid peptides formed by the fusion of insulin c-peptide and ChgA, or peptides modified by transglutaminase are significantly more antigenic[116,117]. Whether this has any consequence on duodenal influence of T cell priming will need to be resolved by further experiments.

The difference in cognate antigen between NY8.3 and BDC2.5 T cells may also contribute to a differential susceptibility to suppression by the endogenous Treg cell pool. CD25$^+$ cells are depleted during the negative selection of T cells for adoptive transfer, however, whether the endogenous frequencies of Treg cells that may suppress either T cell clone are equivalent is

not known. At least for the discrepancy between the oral tolerance experiments and BDC2.5 infection results, this would be very relevant. In the case of the oral tolerance experiments, the antigen is completely novel and thus would not already have preexisting Treg cells specific to that antigen. In contrast, the NOD mice receiving BDC2.5 T cells likely already have specific Treg cells that would be able to limit T cell activation. It is puzzling that BDC2.5 T cells still divide in the LN, but effector differentiation does not occur. Even in naïve mice, the cells divide but do not differentiate strongly towards a particular Th or the Treg fate. It is possible the cells are homeostatically proliferating but it is abortive. To test whether Treg cells are interfering with the ability of duodenal infection to activate BDC2.5 T cells, the same transfer and infection experiments can be confirmed in *Rag1*$^{-/-}$ NOD mice.

Generally, CD4^{+} T cells are thought to give help to CD8^{+} T cells by licensing cDC1s to activate CD8^{+} T cells. The current results indicate pancreas-specific CD8^{+} T cell activation in response to duodenal infection but not CD4^{+} T cell activation. It will be important to test whether the CD8^{+} activation seen here is dependent on CD4^{+} T cells by transferring NY8.3 T cells into *Rag1*$^{-/-}$ NOD mice infected with T1L or MNV to see if the CD8^{+} T cell activation occurs in the absence of polyclonal CD4^{+} T cells. Most of the experiments I performed were harvested at a similar time point, roughly 3-4 days post T cell transfer. It is noteworthy that at the time points tested there was not a significant difference in cell division of the CD8^{+} T cells despite the changes to their activation status. Gain of effector function of CD8^{+} T cells is tightly linked with cell division[118]. Thus, future experiments will need to test additional time points post transfer to see if differences in division become significant and to confirm the robustness of CD8^{+} T cell activation.

4.2.3 Physiological consequences of duodenal perturbation on pancreatic immunity

While the results presented here demonstrate the impact of shared LNs in imparting the effect of duodenal infection onto pancreas-specific T cells, the broader physiological consequences of this increased T cell activation are not yet established. So far, our results infecting younger mice (6 weeks and under) with T1L or *S.v*. showed no measurable changes in acute diabetes outcomes between infected and naïve mice. This is consistent with the overwhelming evidence in NOD mice indicates that infection with various pathogens either has no effect or actually prevents diabetes progression[80], despite links between viral infection and diabetes progression in humans. However, it has been shown that infection of NOD mice with pre-existing insulitis (>12 weeks old) with the intestinally confined rhesus rotavirus (RRV) develop diabetes at a faster rate than uninfected mice[82]. It was later shown that this is dependent on type I IFNs as increased levels of ISGs are found in the pancreatic LNs of infected mice and diabetes progression is not modulated by RRV infection in *Ifnar*$^{-/-}$ NOD mice[119]. Ongoing experiments will test whether T1L infection of older mice leads to increased levels of insulitis or acceleration of diabetes. Additionally, to more directly link NY8.3 activation and diabetes progression, future experiments will involve transferring splenocytes from NY8.3 T cells to *Rag1*$^{-/-}$ NOD mice and infect with T1L. The expectation is that infected mice will develop diabetes at a faster rate than naïve mice.

4.2.4 Future directions: Beyond the LN and other pancreatic diseases

Taken together, these results demonstrate a pathway of immunological crosstalk between the pancreas and the duodenum as a result of shared LNs. These data may give mechanistic insight into links between enteric infection and T1D, and provide a basis for targeting the pancreatic immune system via manipulation of the duodenal LN milieu. While this thesis focused primarily

on consequences of shared LN on T1D, other serious diseases of the pancreas including pancreatic ductal adenocarcinoma (PDAC) and pancreatitis have been associated with intestinal changes and may similarly be influenced by common LNs. PDAC is a particularly aggressive cancer that is highly unresponsive to chemotherapy and immunotherapy, resulting in a 5-year survival rate of less than 10%[120]. PDAC has recently been appreciated to be associated with changes in the commensal microbiota, though the mechanism or causal link is not fully understood[121,122]. As the major draining lymph nodes of the pancreas, the tolerogenic pancreatic-duodenal LNs may actually facilitate the immunosuppressive nature of PDAC, thereby promoting tumor progression. Future experiments in the lab will explore whether duodenal perturbations and resulting LN changes can affect PDAC development. These experiments will utilize a genetic model of PDAC in which mice harbor a genotype consisting of *Ptf1a*^{CreERT}, *p53*$^{fl/wt}$, for haploinsufficiency of p53 expression, and *Kras*$^{LSL\text{-}G12D/wt}$, which expresses a dominant negative oncogenic form of Kras upon Cre excision[123].

Beyond the LNs, the pancreas and duodenum share other connection points besides the LNs and these may contribute to the ability of the intestine to influence pancreatic immunity. Many studies have focused on the contribution of the gut microbiome to disease susceptibility, however, it has been recently appreciated that the pancreas harbors a unique microbiome. Initially considered a sterile organ, it is now clear that bacteria exist within the pancreas and may influence disease outcomes in the case of pancreatic cancer[121,122]. Whether the pancreatic microbiome is related to the intestinal microbiome or how it develops is not well understood. Given the intimate connection of the duodenum and the pancreas, it is possible microbes could enter the pancreas through a number of mechanisms. Duodenal reflux into the common bile duct may create an access point for microbes. Bacteria that successfully translocate across the

epithelium could travel to and colonize the pancreas via hepatic circulation or pancreatic-duodenal LNs[3]. These possibilities are currently addressed by others in the lab.

In a reciprocal manner, the shared LNs may be equally affected by pancreatic stressors, thereby influencing duodenal immunity. Shared vasculature between the pancreas and the gut serves as a first pass sensing route for the pancreas to react to nutrients and postprandial gut hormones but may also induce pancreatic stress via molecules absorbed in the gut. The pancreatic duct may similarly be important in the relationship of the organs as it could serve a reflux route for duodenal microbiome to access the pancreas. Previous unpublished work in the lab has already established changes in pancreatic gene expression of antimicrobial peptides, a typical pancreatic stress response, correlating with colonization status or infection. Thus, a number of interesting questions remain regarding the complex relationship between the pancreas and the duodenum.

4.3 Novel tool generation for controlling and tracking antigen origin

4.3.1 Generation of lox-stop-lox OVA mice

Prior to this thesis, the ability to track tissue specific antigens at internal tissues was severely hampered by the lack of available tools. Many approaches currently used to do so rely on the injection of antigen into the desired tissue such as the skin or footpad and tracking of responses in the draining LN, but for internal tissues that are normally inaccessible this would require surgery. Moreover, despite the existence of readily available T cell transgenic mice, the ability to selectively express cognate model antigens in a specific tissue did not exist. The tools generated here address this critical need by generating novel mouse lines containing lox-stop-lox versions of OVA, thereby enabling expression of OVA in any tissue that has a corresponding Cre driver, and the comparison to its well established natural, dietary version.

Given the discrepancies between the $CD4^+$ and $CD8^+$ phenotypes in the pancreas-specific but not oral antigen specific T cell transfer experiments, the generation of the *Rosa26*$^{LSL\text{-}sOVA}$ mice expressing a secreted form of OVA will be instrumental in clarifying the phenotype. These mice will offer additional utility by allowing model antigen expression in the liver as well. By introducing a model antigen in the pancreas on the B6 background, the antigen is standardized across the oral tolerance and pancreatic experiments, thereby allowing more precise comparisons of the effect of shared LNs on T cell outcomes. Future experiments will investigate how OT-II and OT-I cells respond in the shared LNs in *Rosa26*$^{LSL\text{-}sOVA}$ *Ins1*^{Cre} mice which will express OVA selectively in the β cells in the context of duodenal infection. Since both the CD4 and CD8 T cell clone will now be reactive to the same antigen, the question of antigen availability influencing the activation will no longer be an issue. Similarly, potential differences in tropism or infection efficiency between NOD and B6 mice will be remedied, since all infections tested in this thesis have been well characterized in B6 mice. Since *Ins1*^{Cre} exists in both a constitutive and inducible form (*Ins1*^{CreERT2}), future experiments can test how timing of antigen expression and therefore generation of a neo antigen affects T cell responses in the same system compared to a natural antigen. This may help answer whether the endogenous Treg cell pool, which would be absent in the case of a neoantigen, is interfering with the ability of BDC2.5 T cells to become activated by duodenal infection. Excitingly, the *Rosa26*$^{LSL\text{-}sOVA}$ mice also open up the ability to investigate T cell responses to exocrine pancreas antigens by crossing to the acinar cell specific Cre *Ptf1a*^{CreERT}. Whether duodenal infection also has the potential to influence exocrine specific T cell responses could have major implications on attempts to influence pancreatic cancer progression via intestinal manipulation. Since both the endocrine and exocrine pancreas likely

drain to the same LNs, I would hypothesize that responses to exocrine pancreatic antigen would appear very similar to endocrine responses.

Three different subcellular versions of OVA were generated all using the same knock-in strategy and with the same promoters, thereby ensuring comparable expression levels. These mice will be used to investigate how the cellular source of antigen impacts T cell responses in a tissue specific manner. The availability of antigen between the secreted, cytosolic and membrane bound forms of OVA will likely differ depending on the conditions of the experiment, and the cell type targeted by the Cre driver (secretory cell or not). We expect access to cytosolic and membrane bound forms of antigen to be more restricted as they potentially depend on cell death. Additionally, cell-associated antigens compared to soluble antigens may be taken up by DCs or other APCs through scavenging receptors rather than just phagocytosis and this may shape the subsequent T cell response generated.

4.3.2 Generation of lox-stop-lox BirA* mice

As a complementary approach to tracking T cell outcomes, I generated *Rosa26*$^{\text{LSL-BirA*}}$ mice to visualize antigen uptake by DCs, thereby allowing tissue specific biotinylation of antigens. This overcomes the sensitivity issues encountered in the *Rosa26*$^{\text{LSL-Tdtomato}}$ mice when crossed to *Ins1*$^{\text{CreERT2}}$ or *Ptf1a*$^{\text{CreERT}}$ mice. Though Tdtomato expression could be visualized in the respective cell type within the pancreas, there were next to no DCs that had taken up Tdtomato antigen in the LNs. This was in contrast to robust numbers of Tdtomato^{+} DCs in *Rosa26*$^{\text{LSL-Tdtomato}}$ *Villin*$^{\text{CreERT}}$ mice. The difference in Tdtomato^{+} DCs may be a reflection of differences in cell turnover between the intestinal epithelium (targeted by *Villin*$^{\text{CreERT}}$) and the β and acinar cells of the pancreas (targeted by *Ins1*$^{\text{CreERT2}}$ and *Ptf1a*$^{\text{CreERT}}$, respectively), as it is known that epithelial cells are shed from the top of villi every 4-5 days[124]. This contrasts with the

robust OT-II T cell proliferation found in *Rosa26*$^{LSL\text{-}sOVA}$ *Ptf1a*^{CreERT} mice, validating our approach using multiple forms of subcellularly localized antigen and multiple Cre drivers. Nonetheless, uncoupling antigen visualization from intact protein structure will greatly improve sensitivity and will allow interrogation of which APCs take up antigen from distinct tissues and if localization changes in the LN follow. Although these experiments focus only on cytosolic derived proteins, ongoing work to characterize a secretory granule resident version of BirA* will address the same questions except using secreted antigens. Upon successful generation of the mice, it will be very interesting to see if there are differences in APC uptake between secreted (soluble) antigens compared to cytosolic antigens which will be almost exclusively cell associated. Despite the fact that the mouse lines generated in this thesis were designed to answer specific questions about pancreatic and duodenal immunity, they have potential utility in a number of other tissue specific immunological questions.

In sum, the experiments presented here demonstrate the potential impact of the duodenum on pancreatic immunity via alterations to the common lymph nodes. Characterization of the migratory DCs from the liver, pancreas and duodenum revealed tissue specific signatures that were not maintained within the LNs; instead DCs expressed a different gene expression profile only reminiscent of the tissue signature within shared LNs. The consequences of this LN induced homogeneity were revealed during duodenal infection in which pancreas-specific $CD8^+$ T cells became activated despite an uninfected pancreas, illustrating the power of the duodenum to influence pancreatic immunity. Finally, the generation of new tools will help clarify existing results and expand the conclusions to additional tissues.

5. REFERENCES

1. Bastidas-Ponce, A., Scheibner, K., Lickert, H. & Bakhti, M. Cellular and molecular mechanisms coordinating pancreas development. *Development* **144**, 2873 (2017).

2. Mairose, U. B., Wurbs, D. & Classen, M. Santorini's Duct--an insignificant variant from normal or an important overflow valve? *Endoscopy* **10**, 24–29 (1978).

3. Thomas, R. M. & Jobin, C. Microbiota in pancreatic health and disease: the next frontier in microbiome research. *Nat. Rev. Gastroenterol. Hepatol.* **17**, 53–64 (2020).

4. Murtaugh, L. C. & Keefe, M. D. Regeneration and Repair of the Exocrine Pancreas. *Annu. Rev. Physiol.* **77**, 229–249 (2015).

5. Wang, B. J. & Cui, Z. J. How does cholecystokinin stimulate exocrine pancreatic secretion? From birds, rodents, to humans. *Am. J. Physiol. Integr. Comp. Physiol.* **292**, R666--R678 (2007).

6. Bakhti, M., Böttcher, A. & Lickert, H. Modelling the endocrine pancreas in health and disease. *Nat. Publ. Gr.* **15**, 155–171 (2019).

7. Fu, Z., Gilbert, E. R. & Liu, D. Regulation of insulin synthesis and secretion and pancreatic Beta-cell dysfunction in diabetes. *Curr. Diabetes Rev.* **9**, 25–53 (2013).

8. Röder, P. V, Wu, B., Liu, Y. & Han, W. Pancreatic regulation of glucose homeostasis. *Exp. Mol. Med.* **48**, e219--e219 (2016).

9. Michels, A. W. & Eisenbarth, G. S. Immunologic endocrine disorders. *J. Allergy Clin. Immunol.* **125**, S226–S237 (2010).

10. O'Morchoe, C. C. C. Lymphatic system of the pancreas. *Microsc. Res. Tech.* **37**, 456–477 (1997).

11. Turley, S. J., Lee, J.-W., Dutton-Swain, N., Mathis, D. & Benoist, C. Endocrine self and gut non-self intersect in the pancreatic lymph nodes. *Proc. Natl. Acad. Sci.* **102**, 17729–17733 (2005).

12. Grant, S. M., Lou, M., Yao, L., Germain, R. N. & Radtke, A. J. The lymph node at a glance {\textendash} how spatial organization optimizes the immune response. *J. Cell Sci.* **133**, jcs241828 (2020).

13. Rodda, L. B. *et al.* Single-Cell RNA Sequencing of Lymph Node Stromal Cells Reveals Niche-Associated Heterogeneity. *Immunity* **48**, 1014--1028.e6 (2018).

14. Carter, P. B. & Collins, F. M. The route of enteric infection in normal mice. *J. Exp. Med.* **139**, 1189–1203 (1974).

15. Esterhazy, D. *et al.* Compartmentalized lymph node drainage dictates intestinal adaptive

immune responses. *Nature* (2019) doi:10.1101/299628.

16. Veenbergen, S. *et al.* Colonic tolerance develops in the iliac lymph nodes and can be established independent of $CD103^+$ dendritic cells. *Mucosal Immunol.* **9**, 894–906 (2016).

17. Houston, S. A. *et al.* The lymph nodes draining the small intestine and colon are anatomically separate and immunologically distinct. *Mucosal Immunol.* **9**, 468–478 (2016).

18. Spahn, T. W. *et al.* Mesenteric lymph nodes are critical for the induction of high-dose oral tolerance in the absence of Peyer's patches. *Eur. J. Immunol.* **32**, 1109–1113 (2002).

19. Mucida, D. & Esterházy, D. SnapShot: Gut Immune Niches. *Cell* **174**, 1600--1600.e1 (2018).

20. Cording, S. *et al.* The intestinal micro-environment imprints stromal cells to promote efficient Treg induction in gut-draining lymph nodes. *Mucosal Immunol.* **7**, 359–368 (2014).

21. Pezoldt, J. *et al.* Neonatally imprinted stromal cell subsets induce tolerogenic dendritic cells in mesenteric lymph nodes. *Nat. Commun.* 1–14 (2018).

22. Eisenbarth, S. C. Dendritic cell subsets in T cell programming: location dictates function. *Nat. Rev. Immunol.* **19**, 1–15 (2019).

23. Durai, V. & Murphy, K. M. Functions of Murine Dendritic Cells. *Immunity* **45**, 719–736 (2016).

24. Esterházy, D. *et al.* Classical dendritic cells are required for dietary antigen–mediated induction of peripheral Treg cells and tolerance. *Nat. Immunol.* **17**, 505–513 (2016).

25. Ingulli, E., Ulman, D. R., Lucido, M. M. & Jenkins, M. K. In Situ Analysis Reveals Physical Interactions Between CD11b⁺ Dendritic Cells and Antigen-Specific CD4 T Cells After Subcutaneous Injection of Antigen. *J. Immunol.* **169**, 2247 LP – 2252 (2002).

26. Swartz, M. A. The physiology of the lymphatic system. *Adv. Drug Deliv. Rev.* **50**, 3–20 (2001).

27. Starr, T. K., Jameson, S. C. & Hogquist, K. A. Positive and Negative Selection of T Cells. *Annu. Rev. Immunol.* **21**, 139–176 (2003).

28. Hsieh, C.-S., Lee, H.-M. & Lio, C.-W. J. Selection of regulatory T cells in the thymus. *Nat. Rev. Immunol.* **12**, 157–167 (2012).

29. Josefowicz, S. Z., Lu, L.-F. & Rudensky, A. Y. Regulatory T Cells: Mechanisms of Differentiation and Function. *Annu. Rev. Immunol.* **30**, 531–564 (2012).

30. Mathis, D. & Benoist, C. Aire. *Annu. Rev. Immunol.* **27**, 287–312 (2009).

31. Mueller, D. L. Mechanisms maintaining peripheral tolerance. *Nat. Immunol.* **11**, 21–27 (2010).

32. Janeway, C. A. Approaching the Asymptote? Evolution and Revolution in Immunology. *Cold Spring Harb. Symp. Quant. Biol.* **54**, 1–13 (1989).

33. Steinman, R. M., Hawiger, D. & Nussenzweig, M. C. Tolerogenic Dendritic Cells. *Annu. Rev. Immunol.* **21**, 685–711 (2003).

34. Chen, W. *et al.* Conversion of Peripheral CD4+CD25− Naive T Cells to CD4+CD25+ Regulatory T Cells by TGF-β Induction of Transcription Factor Foxp3 . *J. Exp. Med.* **198**, 1875–1886 (2003).

35. Voskoboinik, I., Whisstock, J. C. & Trapani, J. A. Perforin and granzymes: function, dysfunction and human pathology. *Nat. Rev. Immunol.* **15**, 388–400 (2015).

36. Seder, R. A. & Ahmed, R. Similarities and differences in CD4+ and CD8+ effector and memory T cell generation. *Nat. Immunol.* **4**, 835–842 (2003).

37. Pabst, O. & Mowat, A. M. Oral tolerance to food protein. *Mucosal Immunol.* **5**, 232–239 (2012).

38. Walker, W. A. & Isselbacher, K. J. Uptake and Transport of Macromolecules by the Intestine: Possible role in clinical disorders. *Gastroenterology* **67**, 531–550 (1974).

39. Worbs, T. Oral tolerance originates in the intestinal immune system and relies on antigen carriage by dendritic cells. *J. Exp. Med.* **203**, 519–527 (2006).

40. Edelson, B. T. *et al.* Peripheral CD103+ dendritic cells form a unified subset developmentally related to CD8alpha+ conventional dendritic cells. *J. Exp. Med.* **207**, 823–836 (2010).

41. Jaensson-Gyllenbäck, E. *et al.* Bile retinoids imprint intestinal CD103+ dendritic cells with the ability to generate gut-tropic T cells. *Mucosal Immunol.* 1–10 (2019).

42. Sun, C.-M. *et al.* Small intestine lamina propria dendritic cells promote de novo generation of Foxp3 T reg cells via retinoic acid . *J. Exp. Med.* **204**, 1775–1785 (2007).

43. Hill, J. A. *et al.* Retinoic Acid Enhances Foxp3 Induction Indirectly by Relieving Inhibition from CD4+CD44hi Cells. *Immunity* **29**, 758–770 (2008).

44. Xiao, S. *et al.* Retinoic Acid Increases Foxp3+ Regulatory T Cells and Inhibits Development of Th17 Cells by Enhancing TGF-β-Driven Smad3 Signaling and Inhibiting IL-6 and IL-23 Receptor Expression. *J. Immunol.* **181**, 2277 LP – 2284 (2008).

45. Mora, J. R. *et al.* Selective imprinting of gut-homing T cells by Peyer's patch dendritic

cells. *Nature* **424**, 88–93 (2003).

46. Hadis, U. *et al.* Intestinal Tolerance Requires Gut Homing and Expansion of FoxP3+ Regulatory T Cells in the Lamina Propria. *Immunity* **34**, 237–246 (2011).

47. Dubois, B. *et al.* Innate CD4+CD25+ regulatory T cells are required for oral tolerance and inhibition of CD8+ T cells mediating skin inflammation. *Blood* **102**, 3295–3301 (2003).

48. Bouziat, R. *et al.* Reovirus infection triggers inflammatory responses to dietary antigens and development of celiac disease. *Science (80-.).* **356**, (2017).

49. Bouziat, R. *et al.* Murine Norovirus Infection Induces TH1 Inflammatory Responses to Dietary Antigens. *Cell Host Microbe* **24**, 677--688.e5 (2018).

50. Fonseca, D. M. da *et al.* Microbiota-Dependent Sequelae of Acute Infection Compromise Tissue-Specific Immunity. *Cell* **163**, 354–366 (2015).

51. Katsarou, A. *et al.* Type 1 diabetes mellitus. *Nat. Publ. Gr.* **3**, 1–18 (2017).

52. Pociot, F. & Lernmark, Å. Genetic risk factors for type 1 diabetes. *Lancet* 2331–2339 (2016).

53. Abadie, V., Sollid, L. M., Barreiro, L. B. & Jabri, B. Integration of genetic and immunological insights into a model of celiac disease pathogenesis. *Annu. Rev. Immunol.* **29**, 493–525 (2011).

54. Lee, K. H., Wucherpfennig, K. W. & Wiley, D. C. Structure of a human insulin peptide-HLA-DQ8 complex and susceptibility to type 1 diabetes. *Nat. Immunol.* **2**, 501–507 (2001).

55. Gioia, L. *et al.* Position $β$57 of I-Ag7 controls early anti-insulin responses in NOD mice, linking an MHC susceptibility allele to type 1 diabetes onset. *Sci. Immunol.* **4**, eaaw6329 (2019).

56. Ziegler, A. G. *et al.* Seroconversion to multiple islet autoantibodies and risk of progression to diabetes in children. *JAMA* **309**, 2473–2479 (2013).

57. Ilonen, J. *et al.* Patterns of β-cell autoantibody appearance and genetic associations during the first years of life. *Diabetes* **62**, 3636–3640 (2013).

58. Anderson, M. S. & Bluestone, J. A. The NOD mouse: a model of immune dysregulation. *Annu. Rev. Immunol.* **23**, 447–485 (2005).

59. Pozzilli, P., Signore, A., Williams, A. J. K. & Beales, P. E. NOD mouse colonies around the world- recent facts and figures. *Immunol. Today* **14**, 193–196 (1993).

60. Gagnerault, M.-C., Luan, J. J., Lotton, C. & Lepault, F. Pancreatic lymph nodes are required for priming of beta cell reactive T cells in NOD mice. *J. Exp. Med.* **196**, 369–377

(2002).

61. Wong, F. S. & Janeway, C. A. J. The role of CD4 and CD8 T cells in type I diabetes in the NOD mouse. *Res. Immunol.* **148**, 327–332 (1997).

62. Calderon, B. *et al.* The pancreas anatomy conditions the origin and properties of resident macrophages. *J. Exp. Med.* **212**, 1497–1512 (2015).

63. Ferris, S. T. *et al.* A Minor Subset of Batf3-Dependent Antigen-Presenting Cells in Islets of Langerhans Is Essential for the Development of Autoimmune Diabetes. *Immunity* **41**, 657–669 (2014).

64. Zheng, Y. *et al.* Role of conserved non-coding DNA elements in the Foxp3 gene in regulatory T-cell fate. *Nature* **463**, 808–812 (2010).

65. Holohan, D. R., Van Gool, F. & Bluestone, J. A. Thymically-derived Foxp3+ regulatory T cells are the primary regulators of type 1 diabetes in the non-obese diabetic mouse model. *PLoS One* **14**, e0217728 (2019).

66. Schuster, C., Jonas, F., Zhao, F. & Kissler, S. Peripherally induced regulatory T cells contribute to the control of autoimmune diabetes in the NOD mouse model. *Eur. J. Immunol.* **48**, 1211–1216 (2018).

67. Haskins, K., Portas, M., Bergman, B., Lafferty, K. & Bradley, B. Pancreatic islet-specific T-cell clones from nonobese diabetic mice. *Proc Natl Acad Sci USA* **86**, 8000 (1989).

68. Stadinski, B. D. *et al.* Chromogranin A is an autoantigen in type 1 diabetes. *Nat. Immunol.* **11**, 225–231 (2010).

69. Katz, J. D., Wang, B., Haskins, K., Benoist, C. & Mathis, D. Following a diabetogenic T cell from genesis through pathogenesis. *Cell* **74**, 1089–1100 (1993).

70. Gonzalez, A., Andre-Schmutz, I., Carnaud, C., Mathis, D. & Benoist, C. Damage control, rather than unresponsiveness, effected by protective DX5+ T cells in autoimmune diabetes. *Nat. Immunol.* **2**, 1117–1125 (2001).

71. Nagata, M., Santamaria, P., Kawamura, T., Utsugi, T. & Yoon, J. W. Evidence for the role of CD8+ cytotoxic T cells in the destruction of pancreatic beta-cells in nonobese diabetic mice. *J. Immunol.* **152**, 2042 (1994).

72. Lieberman, S. M. *et al.* Identification of the beta cell antigen targeted by a prevalent population of pathogenic CD8+ T cells in autoimmune diabetes. *Proc. Natl. Acad. Sci.* **100**, 8384–8388 (2003).

73. Verdaguer, J. *et al.* Spontaneous autoimmune diabetes in monoclonal T cell nonobese diabetic mice. *J. Exp. Med.* **186**, 1663–1676 (1997).

74. Rewers, M. & Ludvigsson, J. Environmental risk factors for type 1 diabetes. *Lancet*

(London, England) **387**, 2340–2348 (2016).

75. Bach, J.-F. The Effect of Infections on Susceptibility to Autoimmune and Allergic Diseases. *N. Engl. J. Med.* **347**, 911–920 (2002).

76. Filippi, C. M. & von Herrath, M. G. Viral Trigger for Type 1 Diabetes: Pros and Cons. *Diabetes* **57**, 2863–2871 (2008).

77. Yoon, J. W., Austin, M., Onodera, T. & Notkins, A. L. Isolation of a virus from the pancreas of a child with diabetic ketoacidosis. *N. Engl. J. Med.* **300**, 1173–1179 (1979).

78. Zipris, D. *et al.* TLR activation synergizes with Kilham rat virus infection to induce diabetes in BBDR rats. *J. Immunol.* **174**, 131–142 (2005).

79. Zaccone, P. & Cooke, A. Helminth mediated modulation of Type 1 diabetes (T1D). *Int. J. Parasitol.* **43**, 311–318 (2013).

80. Shoda, L. K. M. *et al.* A Comprehensive Review of Interventions in the NOD Mouse and Implications for Translation. *Immunity* **23**, 115–126 (2005).

81. Serreze, D. V, Ottendorfer, E. W., Ellis, T. M., Gauntt, C. J. & Atkinson, M. A. Acceleration of type 1 diabetes by a coxsackievirus infection requires a preexisting critical mass of autoreactive T-cells in pancreatic islets. *Diabetes* **49**, 708 (2000).

82. Graham, K. L. *et al.* Rotavirus Infection Accelerates Type 1 Diabetes in Mice with Established Insulitis. *J. Virol.* **82**, 6139 (2008).

83. Kushner, J. A. The role of aging upon $β$ cell turnover. *J. Clin. Invest.* **123**, 990–995 (2013).

84. Böber, E., Dündar, B. & Büyükgebiz, A. Partial remission phase and metabolic control in type 1 diabetes mellitus in children and adolescents. *J. Pediatr. Endocrinol. Metab.* **14**, 435–441 (2001).

85. Wen, L. *et al.* Innate immunity and intestinal microbiota in the development of Type 1 diabetes. *Nature* **455**, 1109–1113 (2008).

86. Bosi, E. *et al.* Increased intestinal permeability precedes clinical onset of type 1 diabetes. *Diabetologia* **49**, 2824–2827 (2006).

87. Vaarala, O. Leaking gut in type 1 diabetes. *Curr. Opin. Gastroenterol.* **24**, 701–706 (2008).

88. Sorini, C. *et al.* Loss of gut barrier integrity triggers activation of islet-reactive T cells and autoimmune diabetes. *Proc. Natl. Acad. Sci.* **116**, 15140 LP – 15149 (2019).

89. Vatanen, T. *et al.* The human gut microbiome in early-onset type 1 diabetes from the TEDDY study. *Nature* **562**, 589–594 (2018).

90. Furusawa, Y. *et al.* Commensal microbe-derived butyrate induces the differentiation of colonic regulatory T cells. *Nature* **504**, 446–450 (2013).

91. Mariño, E. *et al.* Gut microbial metabolites limit the frequency of autoimmune T cells and protect against type 1 diabetes. *Nat. Immunol.* **18**, 552–562 (2017).

92. Bray, N. L., Pimentel, H., Melsted, P. & Pachter, L. Near-optimal probabilistic RNA-seq quantification. *Nat. Biotechnol.* **34**, 525–527 (2016).

93. Love, M. I., Huber, W. & Anders, S. Moderated estimation of fold change and dispersion for RNA-seq data with DESeq2. *Genome Biol.* **15**, 550 (2014).

94. Zhu, A., Ibrahim, J. G. & Love, M. I. Heavy-tailed prior distributions for sequence count data: removing the noise and preserving large differences. *Bioinformatics* **35**, 2084–2092 (2019).

95. Hao, Y. *et al.* Integrated analysis of multimodal single-cell data. *bioRxiv* 2020.10.12.335331 (2020) doi:10.1101/2020.10.12.335331.

96. Choi, J. *et al.* The parasitophorous vacuole membrane of Toxoplasma gondii is targeted for disruption by ubiquitin-like conjugation systems of autophagy. *Immunity* **40**, 924–935 (2014).

97. Brown, C. C. *et al.* Transcriptional Basis of Mouse and Human Dendritic Cell Heterogeneity. *Cell* **179**, 846-863.e24 (2019).

98. Fonseca, D. M. da *et al.* Microbiota-Dependent Sequelae of Acute Infection Compromise Tissue-Specific Immunity. *Cell* **163**, 354–366 (2015).

99. Costa, F. R. C. *et al.* Gut microbiota translocation to the pancreatic lymph nodes triggers NOD2 activation and contributes to T1D onset. *J. Exp. Med.* **213**, 1223–1239 (2016).

100. Tai, N. *et al.* Microbial antigen mimics activate diabetogenic CD8 T cells in NOD mice. *J. Exp. Med.* **213**, 2129–2146 (2016).

101. Chu, V. T. *et al.* Efficient generation of Rosa26 knock-in mice using CRISPR/Cas9 in C57BL/6 zygotes. *BMC Biotechnol.* **16**, 4 (2016).

102. Itano, A. A. *et al.* Distinct Dendritic Cell Populations Sequentially Present Antigen to CD4 T Cells and Stimulate Different Aspects of Cell-Mediated Immunity. *Immunity* **19**, 47–57 (2003).

103. Roux, K. J., Kim, D. I., Raida, M. & Burke, B. A promiscuous biotin ligase fusion protein identifies proximal and interacting proteins in mammalian cells. *J. Cell Biol.* **196**, 801–810 (2012).

104. Uezu, A. *et al.* Identification of an elaborate complex mediating postsynaptic inhibition. *Science (80-.).* **353**, 1123 (2016).

105. Gray, H. *Anatomy of the Human Body*. (1918).

106. Miller, J. C. *et al.* Deciphering the transcriptional network of the dendritic cell lineage. *Nat. Immunol.* **13**, 888–899 (2012).

107. Maier, B. *et al.* A conserved dendritic-cell regulatory program limits antitumour immunity. *Nature* **580**, 257–262 (2020).

108. Spits, H., Couwenberg, F., Bakker, A. Q., Weijer, K. & Uittenbogaart, C. H. Id2 and Id3 Inhibit Development of Cd34+ Stem Cells into Predendritic Cell (Pre-Dc)2 but Not into Pre-Dc1: Evidence for a Lymphoid Origin of Pre-Dc2. *J. Exp. Med.* **192**, 1775–1784 (2000).

109. Rahman, A. H. & Aloman, C. Dendritic cells and liver fibrosis. *Biochim. Biophys. Acta - Mol. Basis Dis.* **1832**, 998–1004 (2013).

110. Vander Lugt, B. *et al.* Transcriptional programming of dendritic cells for enhanced MHC class II antigen presentation. *Nat. Immunol.* **15**, 161–167 (2014).

111. Eickhoff, S. *et al.* Robust Anti-viral Immunity Requires Multiple Distinct T Cell-Dendritic Cell Interactions. *Cell* **162**, 1322–1337 (2015).

112. Hor, J. L. *et al.* Spatiotemporally Distinct Interactions with Dendritic Cell Subsets Facilitates CD4+ and CD8+ T Cell Activation to Localized Viral Infection. *Immunity* **43**, 554–565 (2015).

113. Ferris, S. T. *et al.* cDC1 prime and are licensed by CD4+ T cells to induce anti-tumour immunity. *Nature* **584**, 624–629 (2020).

114. Esensten, J. H., Lee, M. R., Glimcher, L. H. & Bluestone, J. A. T-bet-Deficient NOD Mice Are Protected from Diabetes Due to Defects in Both T Cell and Innate Immune System Function. *J. Immunol.* **183**, 75 LP – 82 (2009).

115. Rabenstein, H. *et al.* Differential Kinetics of Antigen Dependency of CD4⁺ and CD8⁺ T Cells. *J. Immunol.* **192**, 3507 LP – 3517 (2014).

116. Liu, B. *et al.* A Hybrid Insulin Epitope Maintains High 2D Affinity for Diabetogenic T Cells in the Periphery. *Diabetes* **69**, 381 LP – 391 (2020).

117. Delong, T. *et al.* Diabetogenic T-Cell Clones Recognize an Altered Peptide of Chromogranin A. *Diabetes* **61**, 3239 LP – 3246 (2012).

118. Oehen, S. & Brduscha-Riem, K. Differentiation of Naive CTL to Effector and Memory CTL: Correlation of Effector Function with Phenotype and Cell Division. *J. Immunol.* **161**, 5338 LP – 5346 (1998).

119. Pane, J. A. *et al.* Rotavirus acceleration of type 1 diabetes in non-obese diabetic mice

depends on type I interferon signalling. *Sci. Rep.* **6**, 29697 (2016).

120. Ryan, D. P., Hong, T. S. & Bardeesy, N. Pancreatic Adenocarcinoma. *N. Engl. J. Med.* **371**, 1039–1049 (2014).

121. Pushalkar, S. *et al.* The Pancreatic Cancer Microbiome Promotes Oncogenesis by Induction of Innate and Adaptive Immune Suppression. *Cancer Discov.* **8**, 403–416 (2018).

122. Aykut, B. *et al.* The fungal mycobiome promotes pancreatic oncogenesis via activation of MBL. *Nature* **8**, 1–13 (2019).

123. Nolan-Stevaux, O. *et al.* GLI1 is regulated through Smoothened-independent mechanisms in neoplastic pancreatic ducts and mediates PDAC cell survival and transformation. *Genes Dev.* **23**, 24–36 (2009).

124. Mayhew, T. M., Myklebust, R., Whybrow, A. & Jenkins, R. Epithelial integrity, cell death and cell loss in mammalian small intestine. *Histol. Histopathol.* **14**, 257–267 (1999).